



Norwegian University of
Science and Technology

Parametric Design and Gradient-Free Optimization of Super Long-Span Suspension Bridges

Fredrik Giske

Eivind Aasrum Midtgarden

Master of Science in Engineering and ICT

Submission date: June 2018

Supervisor: Ole Andre Øiseth, KT

Norwegian University of Science and Technology
Department of Structural Engineering



MASTER THESIS 2018

SUBJECT AREA: Dynamics of structures	DATE: 11.06.2018	NO. OF PAGES: 141
---	---------------------	----------------------

TITLE:

Parametric Design and Gradient-Free Optimization of Super Long-Span Suspension Bridges

Parametrisk design og optimering av lange hengebroer

BY:

Eivind Aasrum Midtgarden and Fredrik Giske

SUMMARY:

This thesis demonstrates the feasibility of the application of using an optimizing process when designing long-span suspension bridges, using a parametric FE-model. The optimization process is tested on a proposed single span, twin-box suspension bridge of 2800m across Sulafjorden. In a case study, the parametric model is used to create an Abaqus model of a specific geometry. Multimodal flutter speed is computed for this design, where corresponding aerodynamic derivatives obtained by wind tunnel tests are used.

The objective of the optimization process is to minimize the total material cost of the structure. A gradient-free optimization algorithm is used to optimize the tower height and the girder gap, considering total material cost. Three girders with different plate thicknesses are analyzed in the optimization. The main code to perform the optimization process is written in MATLAB, which is connected to Abaqus to obtain the responses, sectional forces and modal properties.

In hand with the parametric model, the gradient-free optimization procedure provides essential information about the bridge structure, which is used to study structural behavior.

The optimizing process gives a proposed tower height of 391 meters and a girder gap of 22.6 meters, when the smallest girder is used. However, this proposal is highly dependent on the objective function, which has several uncertainties.

The case study evaluates the modifiability of the parametric model by creating a specific bridge design. The flutter speed is calculated to 67.23 m/s, which is less than the calculated criteria for flutter speed. By including flutter calculation into an optimization process and improving the objective function, the application of an optimizing process may be highly beneficial for complex bridge structures.

RESPONSIBLE TEACHER: Ole Øiseth

SUPERVISOR(S) Ole Øiseth, Øyvind Wiig Petersen

CARRIED OUT AT: NTNU Department of Structural Engineering

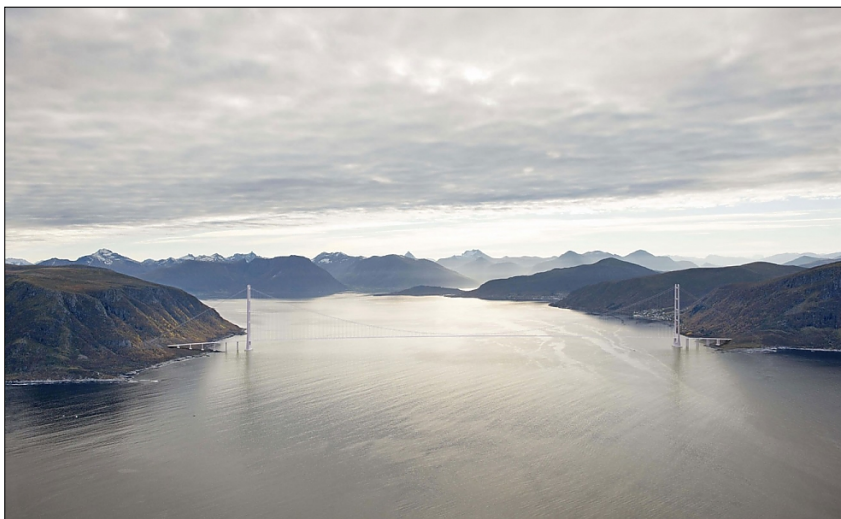
Master Thesis 2018

In order to realize the ambition to complete the E39 Coastal Highway Route as an improved and continuous route without ferries, new bridge technology needs to be developed for crossing the extreme fjords along the west coast. The Norwegian Public Road Administration is conducting a feasibility study regarding a bridge crossing of Sulafjorden. The narrowest part of the fjord is approximately 3000 meters wide and 420 meters deep. If built as a one-span suspension bridge, the Sulafjorden Bridge will be the longest suspension bridge ever built.

It has not been performed advanced calculations related to wind-induced dynamic response. It is therefore desirable to perform more detailed calculations of how this bridge will behave in strong winds.

The thesis should contain the following:

- Preliminary design of the Sulafjorden Bridge.
- Parametric modeling of the bridge in Abaqus.
- Calculation of dynamic response.
- Optimization of the bridge.
- Calculation of aerodynamic stability in a case study.



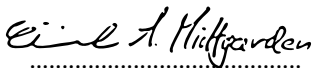
Preface

This master thesis is the final dissertation for the M.Sc. degree at the Department of Structural Engineering at the Norwegian University of Science and Technology (NTNU), completing the five-year study program in spring 2018.

We would like to thank our supervisor Professor Ole Andre Øiseth for his guidance throughout the semester, and to PhD Candidate Øyvind Wiig Petersen for helping with the modeling in Abaqus.

We would also like to thank Oddbjørn Kildal and Johannes Grongstad for providing us experimental results.

Trondheim, 07.06.2018



.....

Eivind Aasrum Midtgarden

Trondheim, 07.06.2018



.....

Fredrik Giske

Abstract

This thesis demonstrates the feasibility of the application of using an optimizing process when designing long-span suspension bridges, using a parametric FE-model. The optimization process is tested on a proposed single span, twin-box suspension bridge of 2800m across Sulafjorden. In a case study, the parametric model is used to create an Abaqus model of a specific geometry. Multimodal flutter speed is computed for this design, where corresponding aerodynamic derivatives obtained by wind tunnel tests are used.

The objective of the optimization process is to minimize the total material cost of the structure. A gradient-free optimization algorithm is used to optimize the tower height and the girder gap, considering total material cost. Three girders with different plate thicknesses are analyzed in the optimization. The main code to perform the optimization process is written in MATLAB, which is connected to Abaqus to obtain the responses, sectional forces and modal properties.

In hand with the parametric model, the gradient-free optimization procedure provides essential information about the bridge structure, which is used to study structural behavior.

The optimizing process gives a proposed tower height of 391 meters and a girder gap of 22.6 meters, when the smallest girder is used. However, this proposal is highly dependent on the objective function, which has several uncertainties.

The case study evaluates the modifiability of the parametric model by creating a specific bridge design. The flutter speed is calculated to $67.23 \frac{m}{s}$, which is less than the calculated criteria for flutter speed. By including flutter calculation into an optimization process and improving the objective function, the application of an optimizing process may be highly beneficial for complex bridge structures.

Sammendrag

Denne masteravhandlingen demonstrerer muligheten for å bruke en optimeringsprosess når superlange hengebroer skal designes. Optimeringsprosessen er testet på en hengebro over Sulafjorden med dobbel brokasse og et spenn på 2800 meter. Ved hjelp av MATLAB er en parametrisert elementmetodemodell er laget i Abaqus. Den kritiske flutterhastigheten er beregnet i et eksempelstudie hvor resultatene fra en vindtunneltest er brukt.

Objektivet til optimeringsprosessen er å minimere den totale materielle kostnaden til konstruksjonen. En gradient-free optimeringsalgoritme er brukt til å optimere høyden på tårnene og avstanden mellom brokassene. Tre brokasser med ulike platetykkelser er analysert i optimeringen. Koden til å utføre optimeringen er laget i MATLAB, som videre er koblet til Abaqus for å innhente responsen, seksjonskrefter og modale egenskaper.

Gradient-free optimering ved hjelp av en parametrisert modell gir verdifull informasjon som kan brukes til å analysere komplekse konstruksjoner.

Optimeringsprosessen foreslår en tårnhøyde på 391 meter og en avstand mellom brokassene på 22.6 meter, når den minste brukassen er valgt. Den foreslåtte geometrien er svært avhengig av objektivfunksjonen, som har flere usikkerhetsmomenter.

Eksempelstudiet viser modifiserbarheten til modellen og hvordan den kan brukes til å representere en bro med et spesifikt design. Flutterhastigheten er kalkulert til $67.23 \frac{m}{s}$, som er mindre enn det kalkulerte kravet for flutterhastighet. Ved å inkludere flutterberegninger i optimeringsprosessen og å forbedre objektivfunksjonen, kan bruken av optimeringsprosessen bli svært gunstig for komplekse konstruksjoner.

Contents

Preface	iv
Abstract	vi
Sammendrag	viii
Acronyms	xiv
1 Introduction	1
2 Suspension Bridges Fundamental Behaviour	3
2.1 Challenges of a Super Long Suspension Bridge	4
2.2 The Problem of Scale	5
2.2.1 Scale Issue one: Cable Steel Self Weight and Quantity	5
2.2.2 Scale Issue Two: Dynamic Properties and Aeroelastic Stability	8
3 Theory	13
3.1 Theory Used for Preliminary Design	13
3.1.1 Cable System	13
3.2 Dynamic Response	15
3.2.1 Background Theory	15
3.2.2 Buffeting Theory	15
3.2.3 Fourier Transform	19
3.2.4 Power spectral Density	19
3.2.5 PSD relations	19
3.2.6 Extreme Values	21
3.3 Motion Induced Instabilities	21
3.3.1 Aerodynamic Derivatives	22
3.3.2 Flutter	23
3.3.3 Multimodal Flutter Computation in MATLAB	24
4 Loads and Response	25
4.1 Loads	25
4.1.1 Permanent Loads	25
4.1.2 Traffic loads	26
4.1.3 Wind Loads	28
4.2 Static Response	31

4.3	Dynamic Response	31
5	Preliminary Design of the Bridge	33
5.1	Geometry	33
5.2	Materials	34
5.3	Cables and Hangers	34
5.3.1	General Design	34
5.3.2	Cable Variations in Parametrization	35
5.4	Cross Section of the Girder	35
5.4.1	General Design	35
5.4.2	Girder Variations in Parametrization	37
5.4.3	Ultimate Limit State (ULS)	37
5.5	Cross Beams	40
5.5.1	General design	40
5.5.2	Girder Variations in Parametrization	42
5.6	Pylons	42
5.6.1	Pylon Variations in Parametrization	43
5.6.2	Influence Lines	44
6	Parametric Modelling of the Sulafjorden Bridge	49
6.1	Simplification of the Model	49
6.1.1	Towers	50
6.1.2	Twin-Box Girder	51
6.1.3	Boundary Condition	51
6.2	Prestressing / Model Tensioning	52
6.3	Possible Improvements	54
7	Optimizing the Bridge Geometry	55
7.1	Objective Function and Design Variables	55
7.2	Types of Optimization Methods	56
7.2.1	Gradient Based Method	56
7.2.2	Derivative-Free	58
7.3	Constraints	60
7.4	Challenges	61
7.4.1	Objective Function	61
7.4.2	FE-Analysis	61
7.4.3	Aeroelastic Coefficients	62
7.4.4	Comparing Frequencies	63
8	Case Study	65
8.1	Bridge Design	65

8.2 Flutter Computations	67
8.2.1 Uncertainties in Computations	69
9 Results	71
9.1 The Optimizing Process	71
9.2 Case Study	76
9.2.1 Flutter	76
10 Discussion	79
10.1 Optimization Results	79
10.2 The Optimization Process	80
10.3 Case Study	81
11 Conclusion	83
11.1 Case Study	84
11.2 Recommendations for Further Work	84
Bibliography	85
Appendix	87
A Case Study	89
A.1 Wind Direction 1	89
A.1.1 Mode Illustrations	89
A.1.2 Aerodynamic Derivatives	92
A.2 Wind Direction 2	93
A.2.1 Flutter Results	93
A.2.2 Aerodynamic Derivatives	94
B Preliminary Design	95
C MATLAB Code	117

Acronyms

- AD** Aerodynamic Derivatives
- BC** Boundary Condition
- CAE** Complete Abaqus Environment
- FE** Finite Element
- FEA** Finite Element Analysis
- FRF** Frequency Response Function
- MAC** Modal Assurance Criterion
- MCC** Mode Correlation Coefficient
- PSD** Power Spectral Density
- SDOF** Single Degree of Freedom
- ULS** Ultimate Limit State

Nomenclature

Notations

\dot{r}	Time derivative of r
\mathbf{Z}	Matrix
\mathbf{z}	Vector
$Im[-]$	Imaginary part of the variable within the brackets
$Re[-]$	Real part of the variable within the brackets
σ_X	Standard deviation of X
$Cov[X]$	Covariance of X
$Det(\mathbf{X})$	Determinant of matrix \mathbf{X}
$E[X]$	Expectancy of X
R_{xy}	Cross-correlation between x and y
S_{xy}	Cross-spectral density of x and y
z, Z	Scalar
$Z_{i,j}$	Element in row i and column j of matrix Z

Variable

α	Angle of incidence
$\eta_i(t)$	Generalized coordinate
$\bar{\mathbf{q}}$	Static wind force
ϕ_i	Mode shape
\mathbf{B}_q	Buffeting dynamic load coefficient matrix
\mathbf{C}_{ae}	Aerodynamic damping matrix
\mathbf{K}_{ae}	aerodynamic stiffness matrix
$\mathbf{Q}(t)$	Load vector
$\mathbf{r}(t)$	Response vector
\mathbf{v}	Turbulence wind velocity

ω_i	Eigenfrequencies
ρ	Density
M, C, K	Mass, damping and stiffness matrices
$\tilde{\mathbf{H}}(\omega)$	Frequency response function
ζ	Damping ratio
ζ_{ae}	Aerodynamic damping ratio
B, D	Width and height of the girder section
c_0	Terrain factor
C_i	Drag, Lift and Moment coefficient, i=D,L,M
C'_i	Slopes of load coefficient curve
c_r	Roughness factor
f_{cbd}	Design cable stress
I	Identity matrix
l_{cb}	Cable length
m, c, k	Mass, damping and stiffness coefficients
P_i^*, H_i^*, A_i^*	Dimensionless ADs, i=1,2..6
Q_{cb}	Quantity of cable steel
R	Return period [year]
V	Mean wind velocity

1 Introduction

The Norwegian Public Road Administration is conducting a feasibility study regarding a bridge crossing of Sulafjorden. Sulafjorden is located on the border of Sula municipality and Hareid municipality in Møre og Romsdal. The narrowest part of the fjord is approximately 3000 meters wide and 420 meters deep. Because of the depth of the fjord, one of the suggested bridge types is a single-span suspension bridge. If built as a one-span bridge, the Sulafjorden Bridge will be the longest suspension bridge ever built, breaking the previous record of 1991 meters belonging to the Akashi Kaikyo Bridge in Japan. By building the Sulafjorden bridge, the travel time across the fjord may be reduced by 30 minutes.

Today, several very large scale bridges are built with success. In order to accomplish building even larger bridges, innovative design solutions are essential. A large number of bridge projects in this scale are now in progress. However, a great deal of research is still required. Super long-span suspension bridges are very complex structures and require extensive research and design development. These types of bridges have great technical difficulty due to their slender shape. It is essential to investigate how the enlarged span influences the behavior, properties, and response of the bridge, to find the best design solution related to, e.g., material cost, quality or stress-state. A parametric model is an efficient tool for investigating effects due to structural changes, and possible design solutions can be tested.

The characteristics of the conventional design process, implying repeated analysis of a structure and resizing of its members until a satisfactory design is obtained. In this process, it is implicitly assumed that by satisfying as closely as possible all requirements placed on the design this will lead to the 'best' design. Regarding the maximum stress in the members, this is the well-known principle of the fully stressed design. Effective as this method often is, common situations are identified where this does not lead to an optimum. Furthermore, the process may be very slowly convergent. For more complex structures, such as large suspension bridges, this conventional design method may not be the best alternative[17].

To find a possible optimal bridge design, optimization methods can be a very efficient tool. Design optimization in engineering has been used from around 1960. As the computational capacity has developed, optimization tools have been more commonly used. Today, several types of optimization procedures are in use in structural design, also for bridges. Optimization methods provide a final design of better quality, in less

time, which is very cost efficient. After the design process, the designer should observe which parameters that affects the final design, and learn [8].

Advantages of the application of an optimizing method in civil engineering:

- Time and cost saving.
- Better quality structures.
- Better understanding of structural properties.
- Re-usability of parametric models.
- Faster to test different structural concepts.

The objective of this thesis is to establish a parameterized FE-model of a one-span suspension bridge across Sulafjorden, which is used it to optimize the bridge design related to the total material costs. A gradient-free optimization procedure is used, where the chosen design variables are tower height, gap between the girders and girder plate thickness. The constraints included are displacements and accelerations.

In a case study, the parametric model is used to create an FE-model of a specific bridge design, provided by Multiconsult. Due to available experimental obtained aerodynamic derivatives, multimodal flutter computations are carried out, and the flutter stability is evaluated in the case study.

This thesis starts with an introduction to suspension bridges fundamental behavior and challenges with super long span suspension bridges. Then the theory used throughout this thesis is presented. In chapter four, the loads are defined, and the approach of response calculations are presented. Based on the determined loads, a preliminary bridge design is chosen. Here, bridge geometry and design of main construction parts are presented, in addition to simplifications. How the design of structural parts varies along with the parametrization are also described. Based on the initial design, MATLAB is used to create the parameterized model, which is the underlying engine behind the bridge optimization. The optimization process is coded in MATLAB, which is connected to Abaqus to run multiple FE-analysis and to gather the output information which is of interest. The optimization method and challenges are presented in chapter seven. In chapter eight, the case study is described. The geometry of the bridge used in the case study is presented, and the method for flutter computations are shown. Next, the optimization and flutter results are presented and discussed. At last, a conclusion and suggested further work is given.

2 Suspension Bridges Fundamental Behaviour

Construction of the modern suspension bridge is complex and challenging. But the underlying physical principle is relatively simple. The idea is that the cables which are anchored to the ground carry the bridge deck. Towers are the first step in the building process. Steel cables (made of thousands of smaller strands) are strung from shore to shore, resting on big saddles on top of each tower. These main cables will form a parabola and support a series of vertical suspender cables (the hangers), which in turn support the road deck. At each shore, huge anchorages keep the main cables in place. Figure 2.1 and 2.2 presents the force flow in a suspension bridge [6].



Figure 2.1: Force flow in a suspension bridge [1].

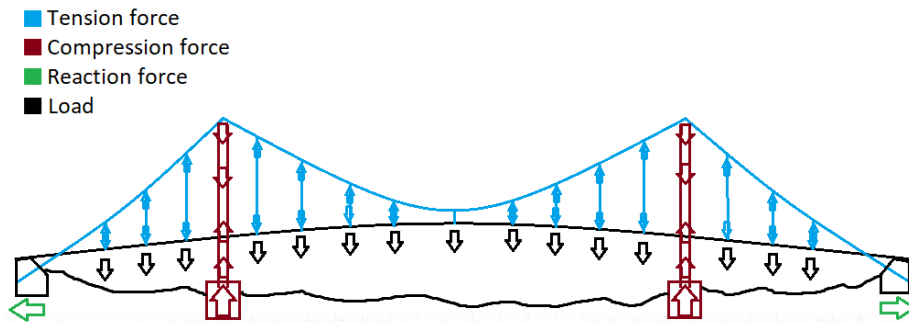


Figure 2.2: Force flow in a suspension bridge.

2.1 Challenges of a Super Long Suspension Bridge

The longest span of a suspension bridge today is the Akashi Kaikyō Bridge with its incredible main span of 1991 meters. The last decades it has been made lots of research on cable-supported bridges. The planned Messina Strait Bridge has not been built, but the project has led to lots of research on large-scale suspension bridges. This chapter discusses some of the dominant factors affecting the design of a super long suspension bridge.

When a suspension bridge is subject to traffic loads, the forces are carried through the structure depending on the relative stiffness of the different elements involved. The deck, whose stiffness is mainly related to flexure, and the main cables, whose stiffness is instead primarily geometric. For short span bridges, the two stiffnesses are comparable and both the deck and the cables carry significant shares of the traffic loads: the deck is viewed as the “stiffening girder.” For increasing spans, as the deck size does not depend directly on the span length, the relative deck stiffness decreases rapidly, and any significant stiffening role by the deck for global loads is lost. The deck acts merely as the element collecting live loads and distributing them between the hangers. This trend is illustrated in Figure 2.3, which shows the proportion of the total applied load carried by the deck as a function of span length for two different bridge deck girders. The Akashi Bridge has a truss type of deck, and the Messina Bridge has a box girder type of deck. The solution for The Sulafjorden Bridge in this thesis has a box girder type of deck [1].

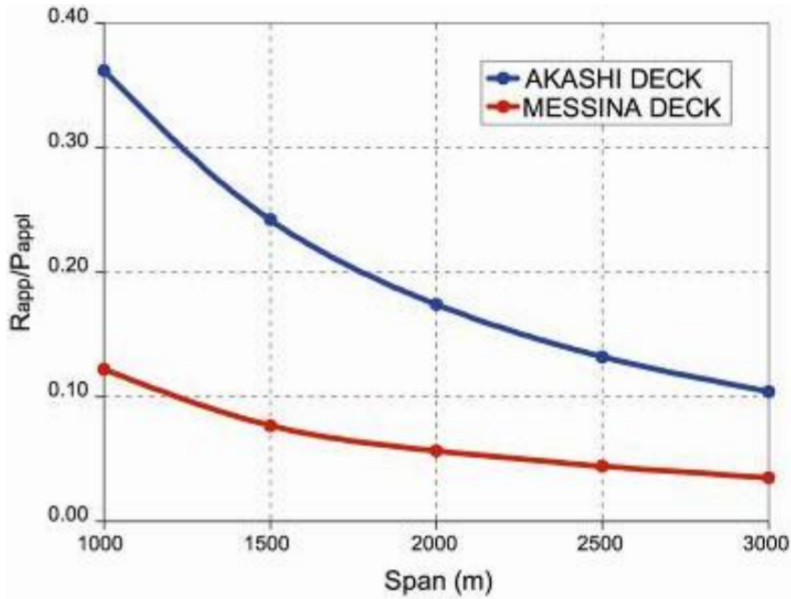


Figure 2.3: Proportion of load carried by deck girder as a function of span for two different girder types. Akashi = truss, Messina = twin-box [1].

2.2 The Problem of Scale

For a span between 2000 and 3000 meters the cables carries most of the loads and dominates the behaviour of the structure. From Figure 2.3 it can be seen that load carried by the girder is almost constant when the span length reaches 2000 meters. Although the transfer of stiffness towards the main cables is the most obvious consequence of span increase, it is not the only one.

2.2.1 Scale Issue one: Cable Steel Self Weight and Quantity

It has already been proved that the cable area increases significantly with the span. Figure 2.4 show the variation in cable tension with span due to the different loading types: road live load, deck self-weight and cable self-weight.

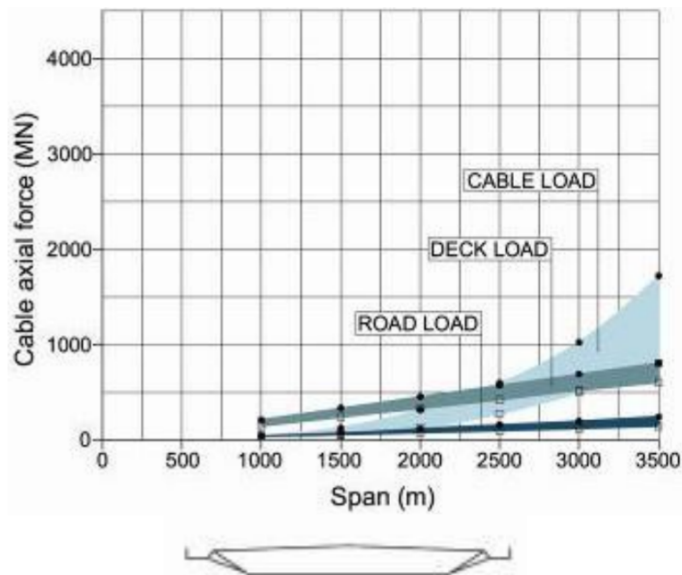


Figure 2.4: Cable axial forces related to the span for a single box girder suspension bridge [1].

For bridges with a span of 1000 meters it can be seen from Figure 2.4 that the self-weight of the deck is the largest contributor to the cable tension. For growing spans the increase in the deck contribution is, as expected, proportional to the span. The road load contribution is less than proportional, as for very large spans average live load intensities decrease, due to standard probability considerations. By contrast, the cable self weight contribution increases more than proportionally with increasing span. For spans over 2000 metres, the contribution of cable self weight to cable tension surpasses the effect of road loads, between 2000 and 2500 metres it equals the contribution of the deck, and it becomes clearly the largest contribution for spans over 2500 metres.

The theoretical curve for the cable area approaches the maximum possible achievable span for a suspension bridge asymptotically. One such curve, derived for the Sulafjorden Bridge is pictured in figure 2.5, and show the maximum theoretical span length of approximately 8800 meters. For comparison, this limit is about 7000 meters for the Messina Bridge (because of the larger deck of the Messina Bridge). Limiting the cable weight is thus the most fundamental design target to be achieved to deal with the first large-scale issue, to allow the overall sustainability and financial feasibility of a very large span bridge.

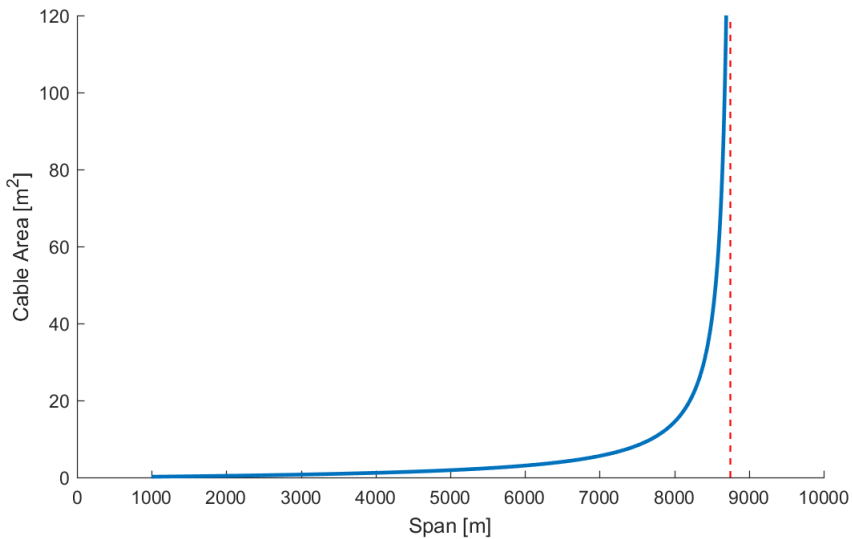


Figure 2.5: Variation in cable size with span for the Sulafjorden bridge.

To reduce the cable area, it is multiple actions which may increase the plausibility of building a super long suspension bridge:

- Designing the deck as lightweight as possible. With high strength materials to reduce the weight.
- Keeping all deck fittings, surfacing and equipment at their lowest weight consistent with suitable performance.
- Careful selection of partial safety factors.
- Designing high towers to get the sag to span ratio as high as possible. This gives smaller cable area.

For example, the Messina Bridge has a structural deck weight of 18 t/m (ton per meter), and an average cable weight of 32 t/m. This means that one extra kilogram of deck weight gives more than one and a half extra kilogram in the main cable. For shorter suspension bridges this ratio is entirely different, and usually, the deck is more massive than the main cable per meter. For the current world record span of the Akashi Bridge, the deck weight about 23 t/m and the cable weight about 12 t/m. This means that one extra kilogram of deck results in only about half an extra kilogram in the main cables [2].

2.2.2 Scale Issue Two: Dynamic Properties and Aeroelastic Stability

It is not only the static behavior which becomes dominated by the mass of the main cables for super long-span suspension bridges. The dynamic response is also highly dependent on the enormous weight of the main cables. Figure 2.6 to 2.10 shows typical dynamic mode shapes for for the Sulafjorden Bridge, which does not necessarily occur in the order listed.

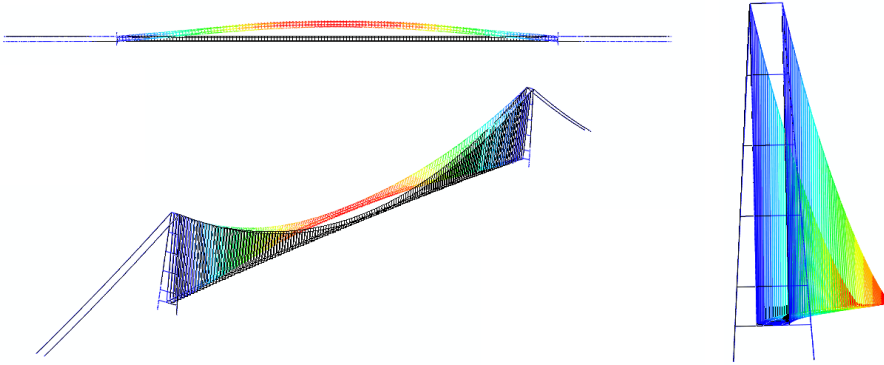


Figure 2.6: Symmetric lateral mode for the Sulafjorden Bridge.

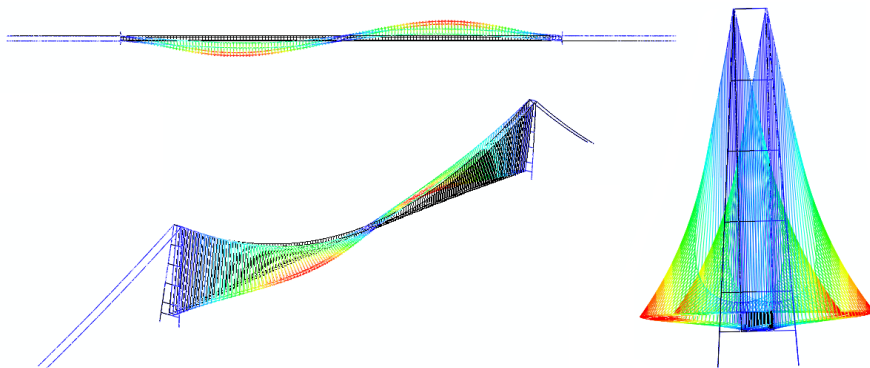


Figure 2.7: Antisymmetric lateral mode for the Sulafjorden Bridge.

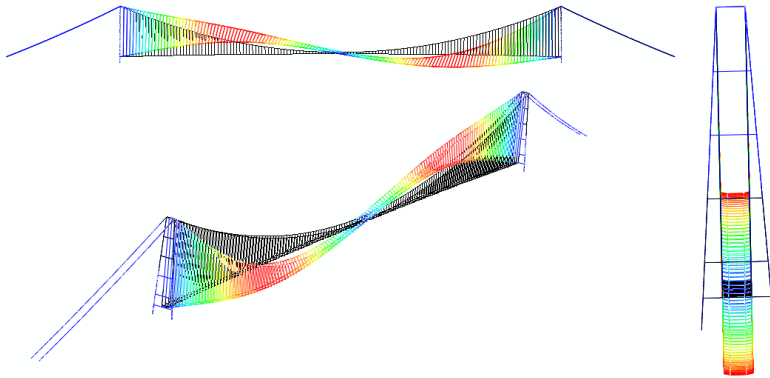


Figure 2.8: Antisymmetric vertical mode for the Sulafjorden Bridge.

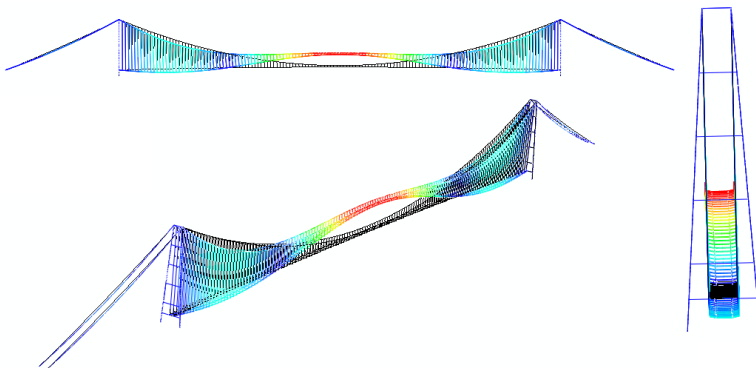


Figure 2.9: Symmetric vertical mode for the Sulafjorden Bridge.

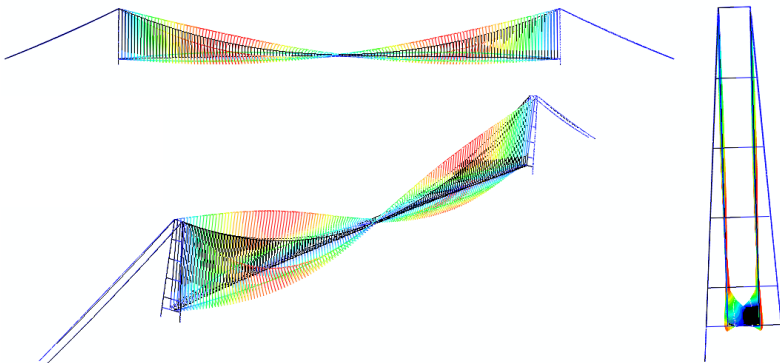


Figure 2.10: Antisymmetric rotational mode for the Sulafjorden Bridge.

The mass of the main cables is so much larger than the mass of the deck that they will dominate the inertia distribution. The frequency modes pictured above will become progressively more similar to those of stand-alone cables, for a super long suspension bridge. This phenomenon is critical to the vertical and rotational modes, as the vertical and rotational modes become closer for increasing spans.

"At the limit, if the two main cables were in a stand-alone, perfectly restrained condition, the two modes (vertical and rotational) would have the same frequency, corresponding to in-phase and out-phase oscillations of the two identical perfect cables[1]."

Similar frequency of vertical and torsional modes are far from ideal because of the most dangerous form of aeroelastic instability, i.e., classic flutter (see Section 3.3.2). There are numerous factors, of different significance, which contribute to maintaining a certain frequency separation between the frequencies, the main one being:

- The ratio between torsional and vertical stiffness of the deck. This can be tuned by modifying the design of the deck, but it is less effective with increasing spans.
- The towers properties, specifically the sag to span ratio and its stiffness for rotation about its vertical axis.
- The connections between the deck and the main cables. At some bridges, the main cables are connected directly to the mid-span via triangulated steel struts and ropes. This helps to modify the relative values of vertical and rotational stiffness in the bridge.
- Use of transversely inclined cross hangers (instead of vertical) or using a mono cable system.
- Cross-section design (aerodynamic properties). This requires testing, but could be the cheapest solution.

The proposed Messina Bridge has a frequency ratio (rotational/vertical) of 1,36. Existing bridges has a frequency ratio typically well over 2, with a minimum of 3,35 for the current world record holder the Akashi Bridge. Existing bridges tend to exhibit critical wind speed for flutter of the order of $60 - 70 \frac{m}{s}$. However, this limit depends on the geographical location of the bridge. Reaching similar values for a bridge with a frequency ratio of 1,36 is extremely difficult. This defines the second main issue with designing super long span bridges, namely achieving a flutter stability.

A major improvement to help solve the problem of aeroelastic instability was the adoption of an orthotropic stiffened plate streamlined closed box deck. Such a deck was light weight and had good torsional stiffness because of the closed box shape. This type of deck has been very successful in the last forty years. However, the closed box deck as its disadvantages. The flat wing shape and large solid lower surface results in

large lift forces and thus creates problems considering the aeroelastic stability. This type of deck is still the best option for bridges up to 1500 meters, but progressively lose its best properties for longer spans.

It was in needed a low-weight, low-lift highly stable deck. A genuine evolution of the concept was proposed in the early seventies by W.C. Brown with the idea of combining low weight Severn type box decks with voids: the so called “vented deck” concept. And it is such a type of deck which is going to be used in this thesis. A twin-box girder type of deck is chosen because of the light-weight and stable properties. Flutter or aeroelastic instability is not optimized in this thesis other than the choice of the twin-box deck. Figure 2.11 shows the twin-deck of Stonecutters Bridge under construction.



Figure 2.11: Building of Stonecutters Bridge (USA 2013) [2].

3 Theory

3.1 Theory Used for Preliminary Design

3.1.1 Cable System

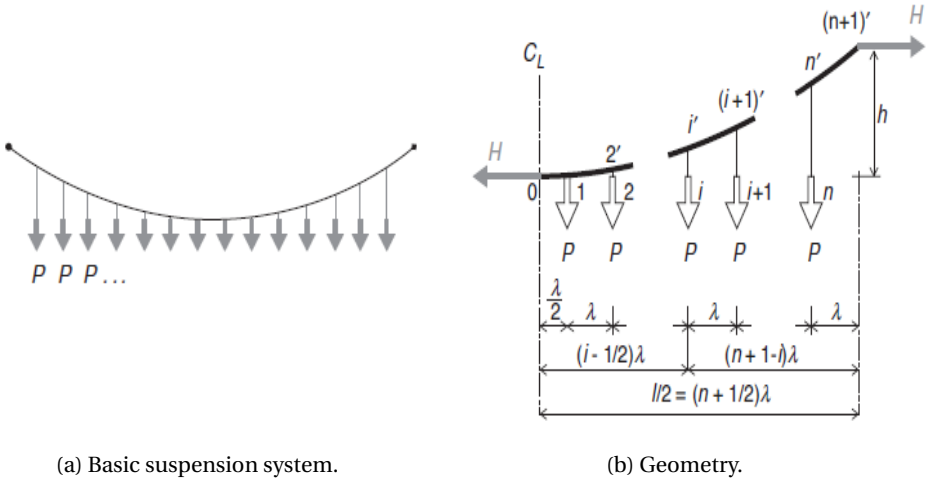
Theory used to determine the theoretical quantity of cable steel are taken from "Cable Suspension Bridges" of Gimsing and Georgakis [6]. For a single cable the theoretical mass of cable steel can be defined by:

$$Q_{cb,1} = \frac{\gamma_{cb}}{f_{cbd}} T_{cb} l_{cb} \quad (3.1)$$

where l_{cb} is the cable length, T_{cb} is the axial force, f_{cbd} is the design cable stress and γ_{cb} is the cable density. By dividing the main cable in n cable elements the total theoretical mass of cable steel is derived as:

$$Q_{cb,tot} = \frac{\gamma_{cb}}{f_{cbd}} \sum_{i=1}^n T_{cb,i} l_{cb,i} \quad (3.2)$$

The cable suspension system considered is shown in Figure 3.1a, where the vertical forces from the hangers are uniformly distributed. Based on a cable system with $2n$ vertical forces P , the theoretical mass of cable steel required can be determined by a summation of the mass in the hanger $i - i'$ and the main cable element $i' - (i + 1)'$, ref. Figure 3.1b. This figure shows the right side of the suspension system, where λ is the internal distance between each hangers, l is the length between the cable supports and h is the cable sag.



(a) Basic suspension system.

(b) Geometry.

Figure 3.1: Suspension bridge concept [6].

From the geometry in Figure 3.1b the theoretical quantity is determined as [6]:

$$Q_{cb,tot} = 2P \frac{\gamma_{cb}}{f_{cbd}} \left[\frac{1}{4} n(n+1) \frac{\lambda^2}{h} + \sum_{i=1}^n \frac{i(i-1)}{n(n+1)} h + \sum_{i=1}^n \frac{n(n+1)}{2h} \left(\lambda^2 + \frac{4h^2}{n^2(n+1)^2} i^2 \right) \right] \quad (3.3)$$

The first and the third term are related to the main cable mass, and the second term is related to the mass of the hangers. Further, the contributions for the hangers are neglected.

When assuming a large number of hangers ($n \rightarrow \infty$), the theoretical mass of main cable steel can be written as:

$$Q_{cb,main} = pl \left(\frac{l^2}{8h} \right) \frac{\gamma_{cb}}{f_{cbd}} \quad (3.4)$$

where p is the load per unit length.

3.2 Dynamic Response

Theory behind the dynamic response computations are presented in this section.

3.2.1 Background Theory

The equation of motion is given by:

$$\mathbf{M}\ddot{\mathbf{r}}(t) + \mathbf{C}\dot{\mathbf{r}}(t) + \mathbf{K}\mathbf{r}(t) = \mathbf{Q}(t) \quad (3.5)$$

where \mathbf{M}, \mathbf{C} and \mathbf{K} are the mass, damping and stiffness matrices related to the structure, and $\mathbf{r}(t)$ and $\mathbf{Q}(t)$ are the response and load vector. The dynamic response get contributions from each modes in the system. These modes are found by solving the following eigenvalue problem:

$$(\mathbf{K} - \omega_i^2 \mathbf{M})\boldsymbol{\phi}_i = \mathbf{0} \quad (i = 1, 2, \dots, n_{modes}) \quad (3.6)$$

where ω_i is the eigenfrequencies and $\boldsymbol{\phi}_i$ is the corresponding shape modes. Now, the modal transformation becomes:

$$\mathbf{r}_i(x, t) = \boldsymbol{\phi}_i(x)\boldsymbol{\eta}_i(t) \quad (3.7)$$

where $\boldsymbol{\eta}_i(t)$ are the time varying unknown values for vibration mode number i . This is used to create a reduced order model. Equation 3.5 can be transformed to generalized form:

$$\tilde{\mathbf{M}}\ddot{\boldsymbol{\eta}}(t) + \tilde{\mathbf{C}}\dot{\boldsymbol{\eta}}(t) + \tilde{\mathbf{K}}\boldsymbol{\eta}(t) = \tilde{\mathbf{Q}}(t) \quad (3.8) \quad \begin{aligned} \tilde{\mathbf{M}} &= \boldsymbol{\phi}^T \mathbf{M} \boldsymbol{\phi}, & \tilde{\mathbf{C}} &= \boldsymbol{\phi}^T \mathbf{C} \boldsymbol{\phi} \\ \tilde{\mathbf{K}} &= \boldsymbol{\phi}^T \mathbf{K} \boldsymbol{\phi}, & \tilde{\mathbf{Q}} &= \boldsymbol{\phi}^T \mathbf{Q} \end{aligned} \quad (3.9)$$

3.2.2 Buffeting Theory

The buffeting theory is used to describe the wind forces acting on the structure. Theory in this section is taken from Strømmen [22]. The underlying assumptions behind buffeting theory are:

- The bridge can be described with a beam-like behaviour (see Figure 3.2).
- Structural displacements and rotations are small.

- Fluctuating wind components are small compared with the mean wind flow.
- Linearization of any fluctuating parts will render results with sufficient accuracy.
- The wind field is stationary and homogeneous.
- Quasi-steady loading. I.e. the aerodynamic forces at any time depend only on the instantaneous position of the girder at that particular moment.

In Strømmen [22] the total wind load is derived as:

$$\mathbf{q}_{tot} = \bar{\mathbf{q}} + \mathbf{B}_q \mathbf{v} + \mathbf{C}_{ae} \dot{\mathbf{r}} + \mathbf{K}_{ae} \mathbf{r} \quad (3.10)$$

where

$$\mathbf{v} = \begin{bmatrix} u & w \end{bmatrix}^T \quad (3.11)$$

$$\mathbf{r} = \begin{bmatrix} r_y & r_z & r_\theta \end{bmatrix}^T \quad (3.12)$$

$$\bar{\mathbf{q}} = \begin{bmatrix} \bar{q}_y \\ \bar{q}_z \\ \bar{q}_\theta \end{bmatrix} = \frac{\rho V^2 B}{2} \begin{bmatrix} (D/B) \bar{C}_D \\ \bar{C}_L \\ B \bar{C}_M \end{bmatrix} \quad (3.13)$$

$$\mathbf{B}_q = \frac{\rho V B}{2} \begin{bmatrix} 2(D/B) \bar{C}_D & (D/B) C'_D - \bar{C}_L \\ 2 \bar{C}_L & C'_L + (D/B) \bar{C}_D \\ 2B \bar{C}_M & B C'_M \end{bmatrix} \quad (3.14)$$

$$\mathbf{C}_{ae} = -\frac{\rho V B}{2} \begin{bmatrix} 2(D/B) \bar{C}_D & (D/B) C'_D - \bar{C}_L & 0 \\ 2 \bar{C}_L & C'_L + (D/B) \bar{C}_D & 0 \\ 2B \bar{C}_M & B C'_M & 0 \end{bmatrix} \quad (3.15)$$

$$\mathbf{K}_{ae} = -\frac{\rho V^2 B}{2} \begin{bmatrix} 0 & 0 & (D/B) C'_D \\ 0 & 0 & C'_L \\ 0 & 0 & B C'_M \end{bmatrix} \quad (3.16)$$

The total wind load includes one static (mean) part, $\bar{\mathbf{q}}$, and one fluctuating (dynamic) part. $\mathbf{B}_q \mathbf{v}$ is the buffeting term, i.e. loading associated with the turbulence, while $\mathbf{C}_{ae} \dot{\mathbf{r}}$ and $\mathbf{K}_{ae} \mathbf{r}$ are the motion induced load term. V is the mean wind velocity, \mathbf{v} is the turbulence wind velocity, ρ is the air density, and B and D are the width and height

of the girder section. The static load coefficients is described by the following linear approximation [22]:

$$C_i = C_i(\bar{\alpha}) + \alpha_f C'_i(\bar{\alpha}), i = D, L, M \quad (3.17)$$

Where $\bar{\alpha}$ and α_f are the mean value and the fluctuating part of the angle of incidence, and where C'_D, C'_L and C'_M are the slopes of the load coefficient curves at $\bar{\alpha}$. D, L and M indicates drag, lift and moment, respectively.

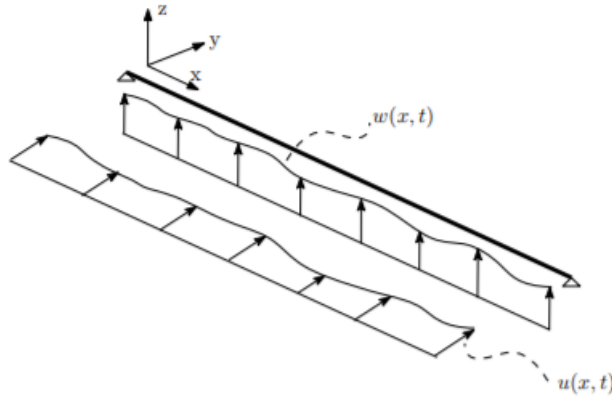


Figure 3.2: Beam representation of the girder including wind fields w and u .

In order to detect the horizontal and vertical response, r_y and r_z , contributions from the vertical wind field to the horizontal response are neglected, and vice versa. This assumption is used to simplify the calculations. However, to get more accurate results, both wind fields should be included in each directions. The system in Equation 3.8 can be reduced to a SDOF system related to both y- and z- direction:

$$\tilde{M}\ddot{\eta}(t) + \tilde{C}\dot{\eta}(t) + \tilde{K}\eta(t) = \tilde{Q}(t) \quad (3.18)$$

$$\begin{aligned} r_y(x, t) &= \phi_y(x)\eta_y(t) \\ r_z(x, t) &= \phi_z(x)\eta_z(t) \end{aligned} \quad (3.19)$$

Extracting the matrix elements from Equation 3.13-3.16 related to the corresponding direction, leads to the following equations (not considering the static part of the loading):

- Y-direction:

$$Q(x, t) = \mathbf{B}_{q[1,1]} u(x, t) + \mathbf{C}_{ae[1,1]} \dot{r}_y(x, t) + \mathbf{K}_{ae[1,1]} r_y(x, t) \quad (3.20)$$

$$\begin{aligned} \tilde{Q}_{Drag}(t) &= \int_0^L \phi_y(x) \rho V D \bar{C}_D u(x, t) dx, \quad \tilde{K}_{ae} = 0 \\ \tilde{C}_{ae} &= -\rho V \int_0^L \phi_y(x)^2 D \bar{C}_D dx \end{aligned} \quad (3.21)$$

- Z-direction:

$$Q(x, t) = \mathbf{B}_{q[2,2]} w(x, t) + \mathbf{C}_{ae[2,2]} \dot{r}_z(x, t) + \mathbf{K}_{ae[2,2]} r_z(x, t) \quad (3.22)$$

$$\begin{aligned} \tilde{Q}_{Lift}(t) &= \int_0^L \phi_z(x) \frac{1}{2} \rho V (B C'_L + D \bar{C}_D) w(x, t) dx, \quad \tilde{K}_{ae} = 0 \\ \tilde{C}_{ae} &= -\frac{1}{2} \rho V \int_0^L \phi_z(x)^2 (B C'_L + D \bar{C}_D) dx \end{aligned} \quad (3.23)$$

By applying the Fourier transform on $r(t)$ and $Q(t)$ it can be shown from Equation 3.8 and 3.10 that the frequency response function (FRF), $\tilde{H}(\omega)$, is written as:

$$\tilde{H}(\omega) = \frac{1}{(-\omega^2 \tilde{\mathbf{M}} + i\omega(\tilde{\mathbf{C}} - \tilde{\mathbf{C}}_{ae}) + \tilde{\mathbf{K}} - \tilde{\mathbf{K}}_{ae})} \quad (3.24)$$

$$\eta(\omega)_{y/z} = \tilde{H}(\omega) \tilde{Q}_{D/L}(\omega) \quad (3.25)$$

The FRF can easily be rewritten to a SDOF (Single Degree of Freedom) system related to each direction.

3.2.3 Fourier Transform

A function $y(t)$ in the time domain can be converted to a function $Y(\omega)$ in the frequency domain by the use of the Fourier transformation. The Fourier transformation splits the function into a sum of harmonic components. For a function $y(t)$ the Fourier transformation is given by Equation 3.26 and 3.27 [14]:

$$Y(\omega) = \int_{-\infty}^{\infty} y(t)e^{-i\omega t} dt \quad (3.26) \quad y(t) = \int_{-\infty}^{\infty} Y(\omega)e^{i\omega t} d\omega \quad (3.27)$$

3.2.4 Power spectral Density

The Power Spectral Density (PSD) gives a representation of how the power of a signal is distributed over its frequencies. For two stochastic signals $x(t)$ and $y(t)$ the cross-correlation function R_{xy} is defined as:

$$R_{xy} = E[x(t)y(t + \tau)] \quad (3.28)$$

Here τ is the time lag. The PSDs can be obtained by computing the correlation functions first and then Fourier transforming them. This approach is known as the Blackman-Tukey procedure [15]:

$$S_{xy}(\omega) = \int_{-\infty}^{\infty} R_{xy}(\tau)e^{-i\omega\tau} d\tau \quad (3.29)$$

Where S_{xy} is the cross-spectral density. If $x = y$ it is called the auto-spectral density. The auto-spectral density functions are real functions, while the cross-spectral density functions are complex.

3.2.5 PSD relations

The auto correlation function for the generalized load related to lift or drag, $\tilde{Q}_{L/D}$, can be obtained from Equation 3.28:

$$R_{\tilde{Q}_{L/D}}(t_1, t_2) = E[\tilde{Q}_{L/D}(t_1)\tilde{Q}_{L/D}(t_2)] \quad (3.30)$$

When assuming a stationary and homogenous wind field, the auto correlation functions can be written as:

$$R_{\tilde{Q}_D}(t_1, t_2) = (\rho V D \bar{C}_D)^2 \int_0^L \int_0^L \phi_y(x_1) \phi_y(x_2) R_u(\delta x, \tau) dx_1 dx_2 \quad (3.31)$$

$$R_{\tilde{Q}_L}(t_1, t_2) = \left(\frac{1}{2} \rho V (B C'_L + D \bar{C}_D)\right)^2 \int_0^L \int_0^L \phi_z(x_1) \phi_z(x_2) R_w(\delta x, \tau) dx_1 dx_2 \quad (3.32)$$

Where $\tau = t_2 - t_1$ and $\delta x = x_2 - x_1$. Inserting the obtained equations for $R_{\tilde{Q}_{D/L}}(\tau)$ in Equation 3.29 gives the following expressions for the auto spectral density:

$$S_{\tilde{Q}_D}(\omega) = (\rho V D \bar{C}_D)^2 \int_0^L \int_0^L \phi_y(x_1) S_{u_1 u_2}(\delta x, \omega) \phi_y(x_2) dx_1 dx_2 \quad (3.33)$$

$$S_{\tilde{Q}_L}(\omega) = \left(\frac{1}{2} \rho V (B C'_L + D \bar{C}_D)\right)^2 \int_0^L \int_0^L \phi_z(x_1) S_{w_1 w_2}(\delta x, \omega) \phi_z(x_2) dx_1 dx_2 \quad (3.34)$$

Where $S_{u_1 u_2}$ and $S_{w_1 w_2}$ is the cross spectral density of the turbulence wind. From Equation 3.25 and an alternative definition of the auto spectral density [15], the relation between the modal FRF and the modal response spectrum can be obtained:

$$S_{\eta_y}(\omega) = \tilde{H}^*(\omega) S_{\tilde{Q}_D}(\omega) \tilde{H}(\omega) \quad (3.35)$$

$$S_{\eta_z}(\omega) = \tilde{H}^*(\omega) S_{\tilde{Q}_L}(\omega) \tilde{H}(\omega) \quad (3.36)$$

And the response spectra becomes:

$$S_{y/z}(\omega) = \phi_{y/z}(\omega) S_{\eta_{y/z}}(\omega) \phi_{y/z} \quad (3.37)$$

From the same alternative definition of the PDS, and the fact that $\dot{r} = i\omega r$, the relation between response-PDS and acceleration-PDS are given as:

$$S_{\dot{r}} = \omega^4 S_r \quad (3.38)$$

Further, the variance of any process, x , can be calculated from [22]:

$$\sigma_x^2 = \int_0^\infty S_x(\omega) d\omega \quad (3.39)$$

3.2.6 Extreme Values

The fluctuating part of the response is assumed to be represented by a narrow banded Gaussian stochastic process with zero as expected value. The maxima of such process are Rayleigh distributed. Consider a time interval with includes N maximum values, then the expected value of the largest maximum can be obtained as [13]:

$$X_{max} = \bar{x} + \sigma_x [\sqrt{2 \ln(N)}] \quad (3.40)$$

where \bar{x} is the static response. The time interval (or reference period), T , is chosen to be 10 minutes in this thesis. Note that this value is uncertain.

In order to find the number of maximum values (N), i.e., the number of oscillations within the time interval, the following relation is used:

$$N = \frac{T}{f_h} \quad (3.41)$$

Where f_h is the first horizontal frequency.

3.3 Motion Induced Instabilities

Long suspension bridges are in general sensitive to wind actions. Both static and dynamic response will increase when the wind velocity increases, and in some cases, the total response develops towards an unstable state. The instability limit is identified as a condition where a small increase of mean wind velocity results in a rapidly increasing response [22]. In this thesis, the instability term is only included in a case study of a bridge where the aerodynamic coefficients are obtained from wind-tunnel tests.

Structural instabilities can be detected by the impedance matrix which is based on the equation of motion [22]:

$$\tilde{\mathbf{E}}_\eta(\omega, V) = \left[\mathbf{I} - \mathbf{K}_{ae} - \left(\omega \cdot \text{diag} \left[\frac{1}{\omega_i} \right] \right)^2 + 2i\omega \cdot \text{diag} \left[\frac{1}{\omega_i} \right] \cdot (\zeta - \zeta_{ae}) \right] \quad (3.42)$$

Where:

$$\tilde{\mathbf{H}}_\eta = \tilde{\mathbf{E}}_\eta^{-1} \quad (3.43)$$

ζ is the damping ratio matrix and ζ_{ae} is the aerodynamic damping ratio matrix. i is the imaginary unit and I is the identity matrix. When the determinant of the impedance matrix is zero, the response goes towards infinity. I.e., the structure reaches the instability limit.

3.3.1 Aerodynamic Derivatives

For strong winds, quasi-static load coefficients are no longer working as an approximation, due to large structural motions. When considering high wind velocities, structural instabilities are in focus. The main use of aerodynamic derivatives (AD) lies in the detection of unstable motions. The theory behind the aerodynamic derivatives and their application on bridges are developed by Scanlan & Tomko [18]. This theory takes into account the fact that the natural frequencies changes due to aerodynamic damping and stiffness. The content of C_{ae} and K_{ae} are now functions of the frequency of motion, in addition to the mean wind velocity and type of cross-section as defined in section 3.2.2:

$$C_{ae} = \frac{\rho B^2}{2} \omega_i(V) \begin{bmatrix} P_1^* & P_5^* & BP_2^* \\ H_5^* & H_1^* & BH_2^* \\ BA_5^* & BA_1^* & B^2 A_2^* \end{bmatrix} \quad (3.44)$$

$$K_{ae} = \frac{\rho B^2}{2} \omega_i(V)^2 \begin{bmatrix} P_4^* & P_6^* & BP_3^* \\ H_6^* & H_4^* & BH_3^* \\ BA_6^* & BA_4^* & B^2 A_3^* \end{bmatrix} \quad (3.45)$$

Here $\omega_i(V)$ is the mean wind velocity dependent resonance frequency associated with mode shape i . P_i^* , H_i^* and A_i^* , $i=1,2..6$, are the dimensionless ADs which are functions of the reduced wind velocity ($V_{red} = \frac{B\omega}{V}$).

3.3.2 Flutter

Flutter is one type of instability issue related to long-span bridges, where the modes couples. The flutter instability limit is identified as when the determinant of the impedance matrix is zero (see Equation 3.42). Since the AD values only can be extracted when the critical frequency and critical wind velocity are known, this is an iterative procedure.

Typically, the coupling is related to the first vertical and first rotational mode, given that these are shape-wise similar. The shape-wise similarity between modes is essential for modal coupling. If two modes are dissimilar shape-wise, the off-diagonal terms in K_{ae} equals zero, which indicates that coupled flutter does not occur [24]. Multiple modes can interact and couple as long as they have some shape-wise similarities.

When induced to high wind speeds the modes changes due to aerodynamic forces (K_{ae} changes). The rotational stiffness tends to decrease with increased wind velocity, while the vertical stiffness is slightly increasing. This coupling effect is shown for two modes in Figure 3.3. Note that flutter instabilities become more and more critical as the bridge span increases, as mentioned in Section 2.2.2.

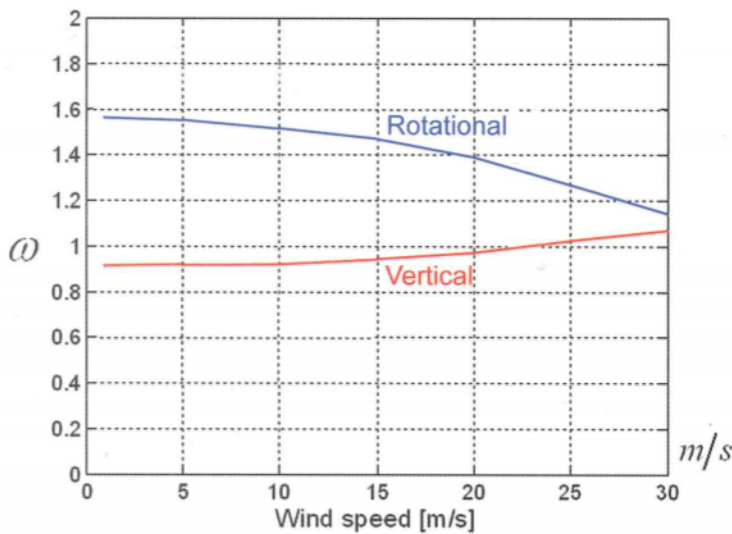


Figure 3.3: Coupling between one rotational and one vertical mode [2].

3.3.3 Multimodal Flutter Computation in MATLAB

The multimodal flutter calculations are in this thesis based on a MATLAB script provided by Ole Øiseth. This script uses an iterative solution method. The flutter computations are based on the eigenvalue which comes from the homogeneous solution of the equation of motion. It is possible to only consider the homogeneous solution because flutter instabilities are based on self-excited forces. The homogeneous solution can be written on the form [4]:

$$r(t) = C e^{St} \quad (3.46)$$

Where C is a constant (not considered any further). This approach gives the following eigenvalue:

$$S = -\zeta_n \omega_n \pm i \omega_n \sqrt{1 - \zeta_n^2} \quad (3.47)$$

Here n indicates the natural mode number, ω_n is the n^{th} natural frequency and ζ_n is the n^{th} damping ratio. The eigenvalues are computed for different wind velocities, and this provides information about changes in frequencies and damping ratios with a wind increase [3]. Eigenvalues have one real and one imaginary part. The imaginary part gives insight into the natural frequencies, whereas the real part is related to the damping. Flutter occurs when the damping (real part) is zero. This is illustrated in Figure 3.4, which is the MATLAB output for an example where two modes couples.

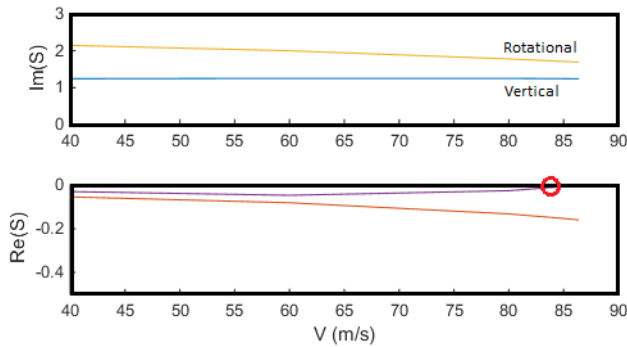


Figure 3.4: Real and imaginary part of the eigenvalue for two modes (torsion and vertical).

4 Loads and Response

In order to compute the static and dynamic response the loads need to be defined, a preliminary design has to be chosen, and the FE-model have to be created. In this section, the loads are defined and response calculation methods are presented, while the preliminary design and the structural model are shown in later chapters.

4.1 Loads

Safety factors used in calculations are listed in Table.4.1.

Table 4.1: Safety factors

Self weight	1.2
Traffic	1.5
Wind	1.6

4.1.1 Permanent Loads

The dead loads are estimated from the weight of the specific load-bearing structure including stiffening plates, asphalt, railings, clamps, and other equipment. The main cable area is computed in MATLAB (see Section 5.3) and to account for non-considered parts this value is increased by five percent. The girder and cross beam area are computed in Cross-X. Due to additional mass, the girder mass is increased with $4262 \frac{kg}{m}$ per girder, which is the value used for added mass in the Hardanger Bridge project [21]. This assumption should be sufficient due to similar geometries. The mass per unit length of each component is adjusted in the optimization process. However, the mass related to the cross-beams are assumed to be constant equal an average value. In Table 4.2 average mass per unit length for different components are tabulated (average values of the design variables are used). This table shows the magnitude of the mass for a bridge in this scale.

Table 4.2: Average component mass added in Abaqus. Values are related to the smallest girder. Steel density: $\rho = 7850 \text{ kg/m}^3$.

Components	Mass [kg/m]
Main cable	4782 (MATLAB) + 5%
Each girder	3474 (Cross-X) + 4262
Cross beam	1970 (Cross-X)

4.1.2 Traffic loads

Traffic loads are computed according to NS-EN 1991-2, Traffic loads on bridges. It is assumed two driving lanes for each girder section, in total 9 meters carriageway, see Figure 5.3. The computationally driving lane width is 3 meters. Thus, it is required to include three driving lanes for the carriageway, but only two are loaded at the same time. Each girder section also has a 1.5 meters wide pedestrian rail.

The traffic load models are divided into two parts: Long influence lengths and short influence lengths. Long influence lengths are used for the global calculations in the initial design. Horizontal traffic loads are neglected. According to the standard, the girder is loaded as shown in Figure 4.1.

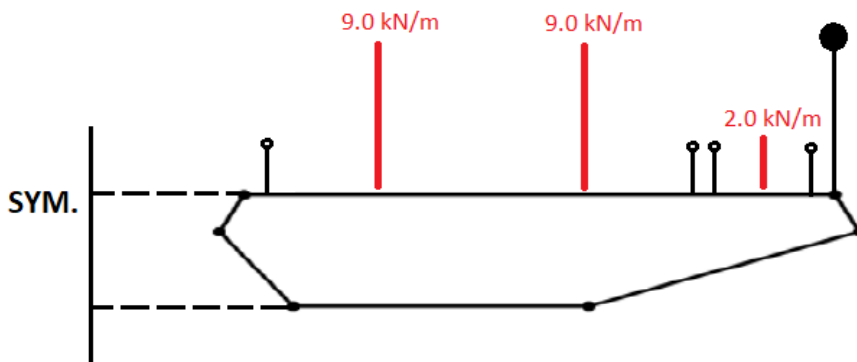


Figure 4.1: Traffic load model for long influence lines. 9 kN/m on the driving lanes and 2 kN/m on the pedestrian rail.

Short influence length load models are related to the girder, cross-beams and hangers. In this study, the cross-beams are controlled according to traffic loads from the short influence length model. In this load-model it is possible to load all three driving lanes at the same time.

Table 4.3: Uniformly distributed loads for short influence lengths.

Location	Square load $Q[kN/m^2]$	Corr-factor α	Width $b[m]$	Length load $q=Qb\alpha[kN/m]$
Lane 1	9	0.6	3	16.2
Lane 2	2.5	1.0	3	7.5
Lane 3	2.5	1.0	3	7.5
Pedestrian road	-	-	1.5	2 (Assumed)

The most critical load combination for the cross-beams is shown in Figure 4.2. This load situation induces max moment along the cross-beams. The calculations are completed in preliminary design, see Section 5.5. Note that concentrated loads due to traffic not are considered in this thesis.

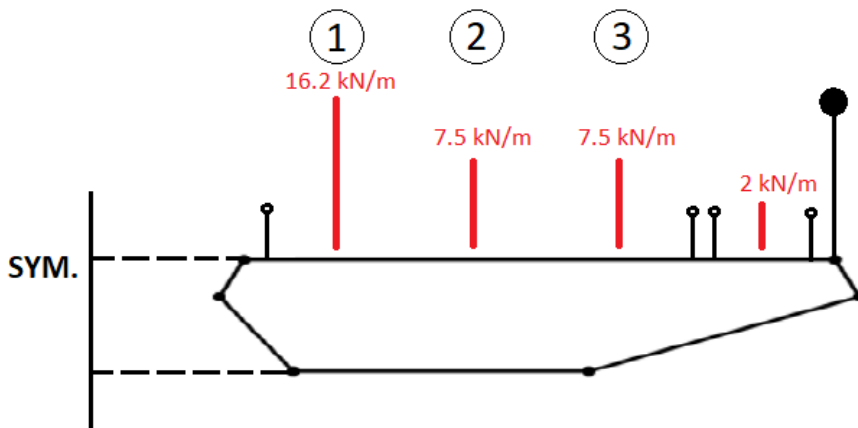


Figure 4.2: Short influence length load model: Critical load combination for the cross-beams.

4.1.3 Wind Loads

Static wind induces forces in the entire structure. The girder is subjected to drag, lift and rotational forces, while the main cable is induced to drag effects, only. Static wind loads on the pylons and the hangers are neglected.

Wind velocities:

The 10 minutes mean wind velocity are computed according to NS EN 1991-1-4:2005+NA:2009, and depend on terrain roughness, terrain shape and basic wind velocity. The mean wind velocity are defined as:

$$v_m(z) = c_r(z) c_0(z) v_b \quad (4.1)$$

Where c_r is the roughness factor and c_0 is the terrain factor. v_b is the basic wind velocity which is defined as:

$$v_b = c_{dir} c_{season} v_{b,0} v_{prob} \quad (4.2)$$

The direction and season factor are conservatively set equal 1. The reference wind velocity, $v_{b,0}$, varies geographically according to Table NA.4(901.1). These values are valid for a 50 years return period. The probability factor, v_{prob} , is used to adjust reference wind velocities for other return periods, and is defined as:

$$v_{prob} = \left(\frac{1 - K \ln(-\ln(1-p))}{1 - K \ln(-\ln(0.98))} \right)^n, K = 0.2, n = 0.5, p = \frac{1}{R} \quad (4.3)$$

Where R is the return period in years. Note that $v_{prob} = 1$ when $R = 50$. As recommended in the Eurocode, the roughness factor calculations are based on a logarithmic function:

$$c_r(z) = k_r \ln\left(\frac{z}{z_0}\right) \quad (4.4)$$

The listed values in Table 4.4 are used in the calculations of the mean wind velocities. V_{mean} is plotted in Figure 4.3. The return period is set to 50 years.

Table 4.4: Mean wind parameters (NS-EN 1991-1-4:2005)

Terrain category	k_r	$z_0[m]$	$z_{min}[m]$	$V_{b,0}[\frac{m}{s}]$
1	0.17	0.01	2	30

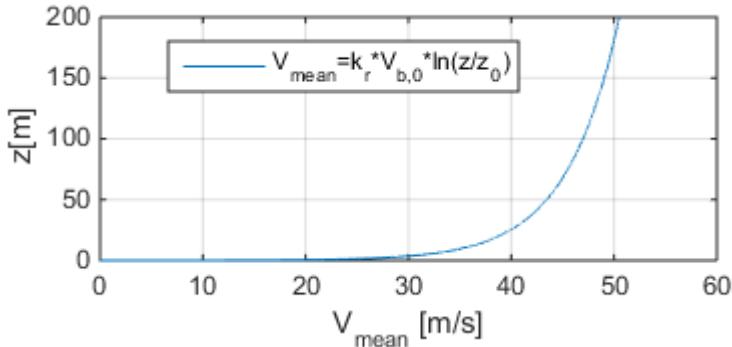


Figure 4.3: Mean wind velocity.

Girder loads:

The static wind loads are based on the buffeting theory explained in Section 3.2.2. The mean wind velocity used in computations are related to the mean deck height. The deck is set to vary from 57.5 m to 77.5 m above medium sea level, which results in a mean height equal 70.8 m. From Figure 4.3 the mean wind velocity is:

$$v_{m,Girder}(70.8) = 45.2 \frac{m}{s} \quad (4.5)$$

Wind force coefficients for the chosen design should be determined by wind tunnel testing. In this study the coefficients are based on the report from Rambøll [16], due to a similar girder design. Note that these coefficients are based on the Eurocode, and may be inaccurate for such complex twin-deck design. Equation 3.13 is used to compute the static wind forces.

Table 4.5: Wind force coefficients.

Structure	C_D	C_L	C_M	C'_L	C'_M
Girder	1.20	-0.15	0.30	6.30	1.00

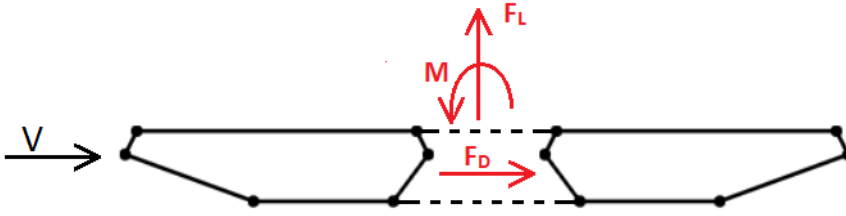


Figure 4.4: Static wind forces on girder.

Cable Loads:

The resulting cable drag varies for different bridge geometries due to varying cable diameter and sag values. As a simplification the mean wind velocity is based on the cable geometry with the lowest sag value. The mean height for 260 meter sag is approximately 117 meter above medium sea level.

$$v_{m,Cable(117)} = 47.8 m/s \quad (4.6)$$

The drag coefficient on the main cable are computed according to NS-EN 1991-1-4 chapter 7.9: Circular Cylinders. Calculations are carried out in Mathcad, see Appendix B. The cable diameter calculated in the preliminary design is increased with about 15% to include the cable protection layers.

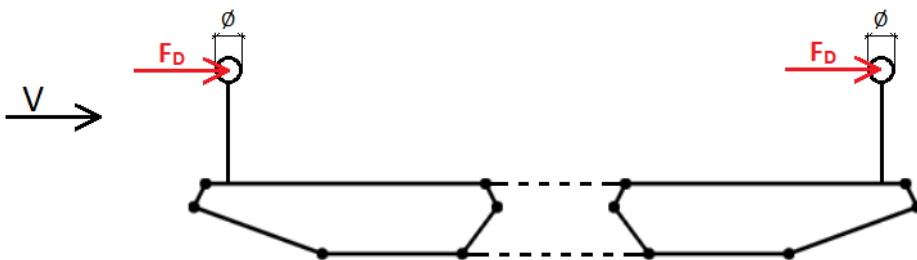


Figure 4.5: Cable drag forces.

4.2 Static Response

To compute the static displacement due to mean wind, the forces are applied in Abaqus as shown in Figure 4.4 and 4.5. Drag, lift and moment loads are applied as concentrated forces in the middle of each cross-beam, i.e., 20 meters loading intervals. Drag load on the main cables are applied to each node, i.e., for every second meter.

Displacement values from Abaqus are extracted through a MATLAB-script. In Abaqus keyword, a node set is selected, and the displacement of these nodes can be printed as output in the data file from Abaqus. The script reads this data file, and gather the information. Similar methods are used to extract other information from Abaqus, such as sectional forces.

4.3 Dynamic Response

The dynamic response is based on buffeting load theory with aerodynamic derivatives and still-air natural frequencies. A simplified response calculation is applied to the system: Single mode single component response calculations [22]. The underlying assumption related to this method is that each mode shape contains only one component, i.e., any mode shape is purely horizontal, vertical or torsional. Calculations will be included in the optimization process. The dynamic response is computed in order to introduce a dynamic term to the optimization. Due to limited time, only this simplified calculation method is applied.

The variance of the fluctuating part of the response is carried in the MATLAB script "*calc_resp_spectra_u.m.*" Information about the chosen mode is gathered from Abaqus. The modal frequency, mode shape and modal mass are extracted and used as input in the script. Damping is set equal 0.002 for all geometries.

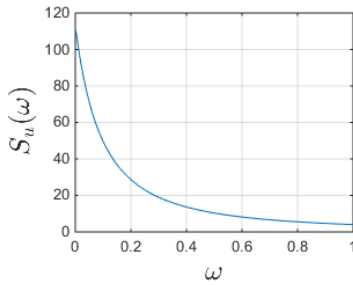


Figure 4.6: Horizontal wind spectra.

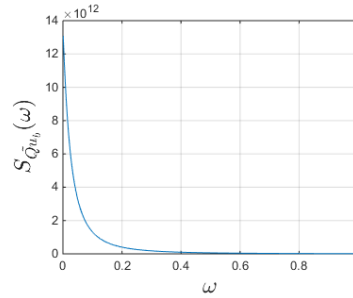


Figure 4.7: Generalized drag load spectra.

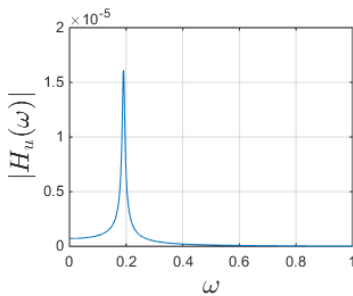


Figure 4.8: Frequency response function.

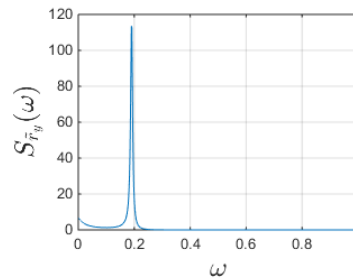


Figure 4.9: Response spectra mid span.

To compute the standard deviation of the wind, the chapter about wind turbulence in NS-EN 1991-1-4 is used. Further, manual N400 for bridge design is used to compute the wind spectra. Typically low frequent wind induces the largest amount of energy to the system. This is shown in Figure 4.6. The generalized load spectra is computed from Equation 3.34 or 3.33, depending on which load that is of interest. The load spectra is shown in Figure 4.7.

The FRF gives information about the relationship between load and response, related to each mode. $Abs(\tilde{H}(\omega))$ is plotted in Figure 4.8 for the first horizontal mode. To compute the response spectra, the FRF is used in following Equations: 3.35, 3.36 and 3.37. In Figure 4.9 the horizontal response spectra are plotted for the mid-bridge span. Note that the figures used for visualization in this section are based on one specific geometry: Tower height of 340m and gap between girders of 10m.

Numerical integration of the response spectrum obtains the variance of the response. When calculating the final dynamic response, extreme values are of interest. The maximum response is found by using Equation 3.40.

5 Preliminary Design of the Bridge

When designing a bridge, an estimate of forces and dimensions of main structural parts are of interest. The preliminary design is based on simplified calculations using basic structural mechanics. These calculations are often conservative and give room for improvements. The initial estimate is used in the design of the FE model, which is further used to make a more accurate design of the structure.

Preliminary designs for different construction parts are presented in this section. The design is inspired by conceptual suggestions provided by Rambøll and Multiconsult, in addition to the Hardanger bridge project. When calculating the initial design, a worst case scenario for each structural part (girder, hangers, cables) is considered.

Due to a parametrized bridge model, the preliminary design needs to adapt for different geometries. How the design of each structural part is varied will be emphasized.

5.1 Geometry

The main span of the bridge is set to 2800 meters, based on Multiconsults suggestion (see Figure 5.1) [12]. Another report created by Rambøll [16] suggest a two-span solution where each span is around 2000 meters. However, a one-span system is chosen in this thesis. Figure 5.1 shows the dimensions of the bridge. Dimensions related to the girder cross-section is presented later in Section 5.4.

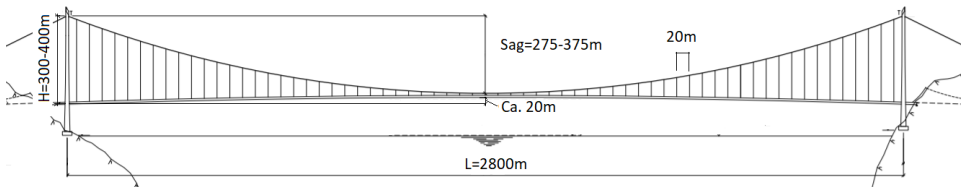


Figure 5.1: Sketch with dimensions

5.2 Materials

The material properties for the bridge components are given in Table 5.1. Values are taken from the Hardanger bridge project [21], except for the main cable tensile strength which is increased to the highest available quality [12].

Table 5.1: Material properties.

	[Mpa]	[Gpa]
Girder	$f_y = 355$	$E = 210$
Cross beam	$f_y = 355$	$E = 210$
Main cable	$f_u = 1860$	$E = 200$
Hangers	$f_u = 1570$	$E = 200$
Pylon	$f_{ck} = 45$	$E = 40$

5.3 Cables and Hangers

5.3.1 General Design

Preliminary design of the main cables is based on a suspension system with vertical loads working on the main cable from the hangers ($P + G2$) in addition to the cable self-weight ($G1$), as shown in Figure 5.2. Load from the hangers includes both girder self-weight and dead load ($G2$), and traffic load (P), while the hanger self-weight is neglected. The cable self-weight is calculated based on the assumption of a parabolic cable shape and adjusted to work as a load per unit length of the bridge. Calculations are carried out through the MATLAB script "cablepreliminarydesign.m".

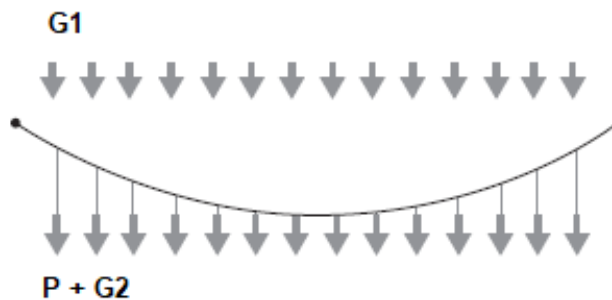


Figure 5.2: Cable loads.

From Equation 3.4 the cable cross section area is derived:

$$p = G1 + (P + G2) \quad (5.1) \quad G1 = A_{main}\hat{\gamma}_{cd}g \quad (5.2)$$

$$\hat{\gamma}_{cd} = \gamma_{cd} \frac{l_{cable}}{l} \quad (5.3) \quad A_{main} = \frac{Q_{cb,main}}{(l\gamma_{cb})} \quad (5.4)$$

$$\Rightarrow A_{main} = \frac{(P + G2)l^2}{(8hf_{cbd} - \hat{\gamma}_{cd}gl^2)} \quad (5.5)$$

Where g is the gravity and $\hat{\gamma}_{cd}$ is the cable density related to the length l between the supports. The design stress (f_{cbd}) is set equal the ultimate tensile strength divided by the material coefficient ($\gamma_m = 2$). I.e., the cables are set to 50% utilization when subjected to traffic- and dead load.

5.3.2 Cable Variations in Parametrization

The "Cablepreliminarydesign" script is implemented in the geometry parametrization and is used to adjust the cable area with different sag heights. As a simplification the side cables are assumed to be equal the main cables. For the hangers, area values from Hardanger Bridge are used. It is also created a script, "sag_calc.m", that calculates the initial cable geometry used as Abaqus input, related to the final cable geometry after elongation. This is necessary because the elongation of the cable varies.

5.4 Cross Section of the Girder

5.4.1 General Design

The girder design is mainly taken from Rambølls conceptual report of the Sula Bridge Crossing [16] and the Hardanger Bridge Project [20]. The chosen design is shown in Figure 5.3. The girder plate thicknesses, which are one of the design variables in the optimization (see 5.4.2), is defined in Figure 5.5. The dimensions of the road rail and pedestrian rail are assumptions, which affects the applied traffic load.

To prevent buckling, longitudinal stiffeners are added to the section. These stiffeners are taken from the cross section of the Hardanger Bridge [21], with approximately the same spacing. The stiffeners are assumed to be unchanged for all cross sections. Transverse bulkheads are added to the girder with four meters intervals. These stiffeners are also based on the Hardanger project, see Figure 5.4.

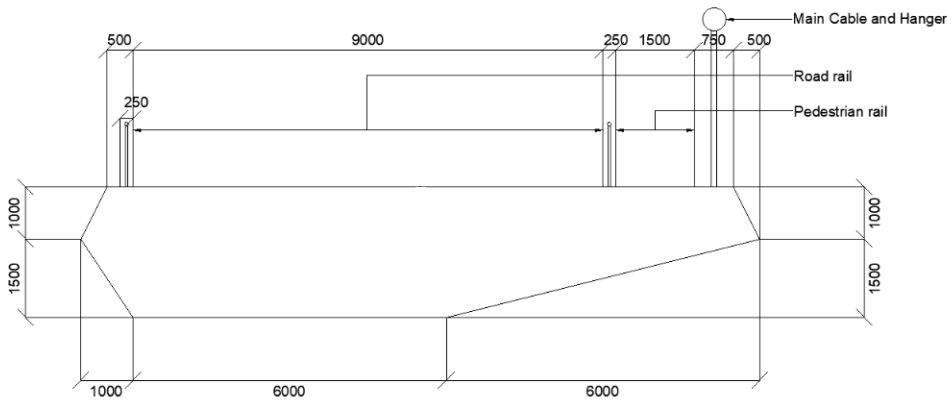


Figure 5.3: Suggested cross section .

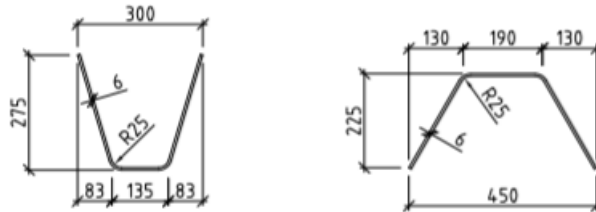


Figure 5.4: Stiffeners. Left: Used for the top plate. Right: Used for the remaining section plates [21].

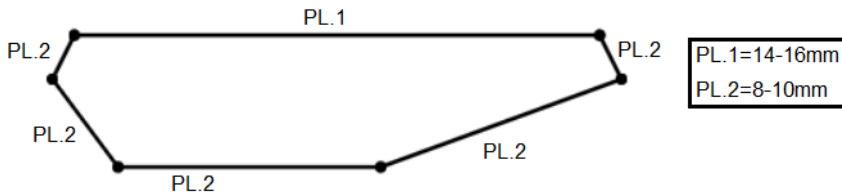


Figure 5.5: Girder plate thickness.

The cross section is modelled in Cross-X, see Figure 5.6. This program is used to compute sectional parameters, but the mass of inertia has to be estimated manually. These calculations are shown in Appendix B. It is assumed that the only contributions are the box girder itself, in addition to the railings and slab.



Figure 5.6: Right box girder modelled in Cross-X.

5.4.2 Girder Variations in Parametrization

The girder plate thickness is chosen to be the varying parameter related to the cross-section. By varying the plate thickness only, it is possible to change the girder parameters without changing the bridge geometry in Abaqus. This is mainly because the center of mass location (where the beam is placed in Abaqus) is close to unchanged when the thickness is increased uniformly. Due to limited time, this approach is beneficial.

Advantages to alter the cross section parameters by varying the plate thickness:

- The aerodynamic coefficients are constant due to unchanged outer geometry
- The additional weight (asphalt, railings, etc.) are constant
- The cross section geometry implemented in Abaqus remains unchanged
- The optimization becomes less complex when the varying parameters does not introduce other changes in the model

5.4.3 Ultimate Limit State (ULS)

Complete stress analysis of the girder could be a complicated and time-consuming task. Optimally, a comprehensive stress analysis should have been included in each geometrical combination. In this study, buckling and yield capacity are only controlled for the smallest cross-section of the ones included. This reduces the complexity of the optimization. However, this gives an indication of the girder utilization.

The main forces acting on the deck are bending moment about the horizontal and vertical axis, and axial forces. Note that pretension forces are not included in calculations. The design bending moment about the horizontal axis, $M_{Ed,y}$, are based on both traffic and wind loads. Sectional forces due to traffic loads are carried out using influence lines (explained in Section 5.6.2). Here, the long influence length model is

used as traffic load, ref. 4.1.2. Actions due to wind are extracted directly from Abaqus. The sectional forces used in design caused by wind are reduced to N_x , M_y and M_z . See Figure 5.7 for directions. Load combinations with corresponding factors are listed in Table 5.2:

Table 5.2: Load combinations. NS-EN 1990:2002, Eq.6.10b.

Load comb.(LC)	Leading live load	Load factors		
		Self weight	Traffic	Wind
1	Traffic	1.2	1.5	$1.6*0.7=1.12$
2	Wind	1.2	$1.5*0.7=1.05$	1.6

The design forces are computed for both maximum and minimum gap width, and compared. Resulting forces are shown in Table 5.3.

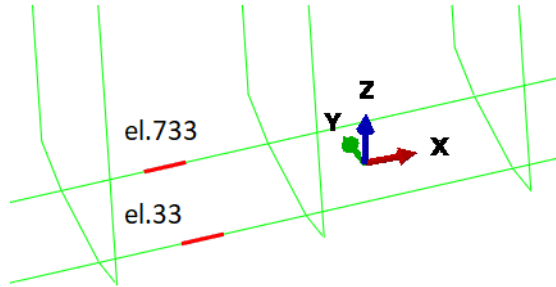


Figure 5.7: Visualization of elements.

Table 5.3: Design forces in critical point($0.05*L$), ref. Figure 5.18. Values extracted from a model with tower height of 350m, and the smallest girder (w=wind, t=traffic, sw=self weight).

LC	Gap[m]	El.	$N_{x,w}$ [kN]	$M_{z,w}$ [kNm]	$M_{y,w}$ [kNm]	$M_{y,(t+sw)}$ [kNm]
1	7	33	-17220	13600	4347	46327
		733	17290	13600	-4551	46327
	14	33	-15220	6217	3379	46327
		733	15290	6200	-3402	46327
2	7	33	-23980	19390	6032	42870
		733	24106	19390	-6538	42870
	14	33	-21280	8850	4735	42870
		733	21430	8817	-4889	42870

Design forces are applied as sectional forces in Cross-X. All force combinations are controlled. Figure 5.8 and 5.9 shows the resulting critical stress state for the top and bottom plate. Note that a smaller gap between girders results in higher forces, since the drag forces are taken up in the structure as a force pair working as axial forces. I.e., when the gap increases, the forces are lowered. Since the drag is added in positive y-direction, the inner girder (el. 33) is in compression whereas the outer girder (el. 733) is in tension.

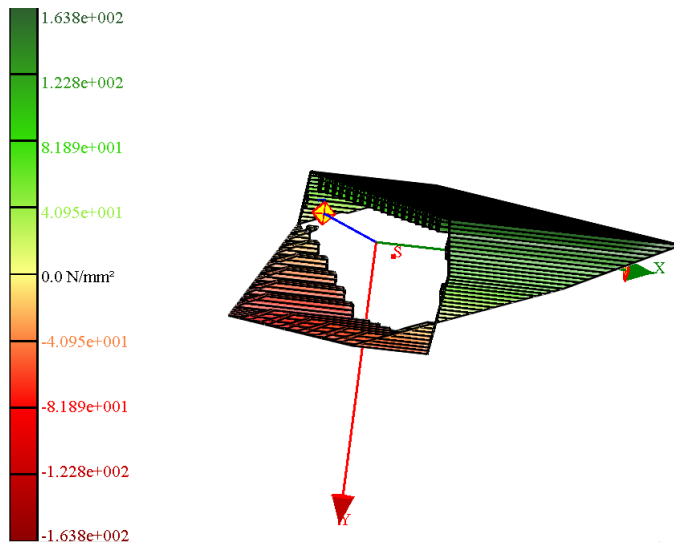


Figure 5.8: CrossX: Stress distribution. Critical for top-plate.

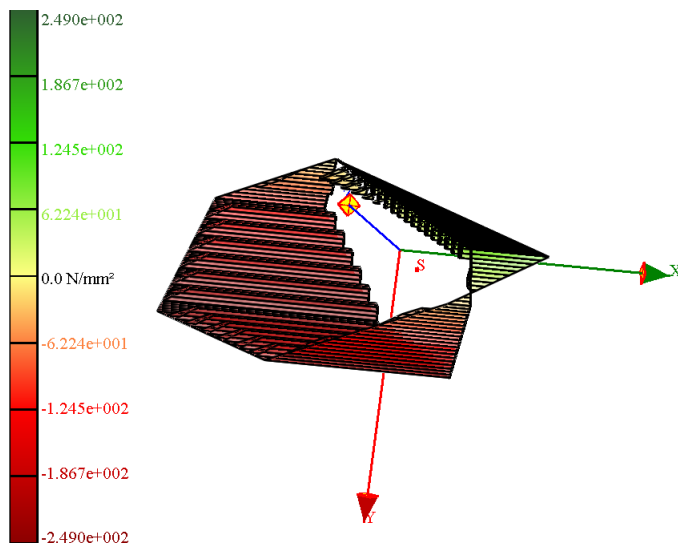


Figure 5.9: CrossX: Stress distribution. Critical for bottom-plate.

Buckling:

Buckling capacity are computed for the top and bottom plate in Appendix B, according to NS-EN 1993-1-1(General rules) and NS-EN 1993-1-5(Plates). Short distance between the transverse stiffeners make the girder plates stiff against buckling. Due to local buckling the section will have a reduced active area, and the critical axial forces found can be computationally equivalent to a reduced critical stress:

$$\sigma_{cr}^{top} = 261\text{Mpa}, \quad \sigma_{cr}^{bottom} = 260\text{Mpa} \quad (5.6)$$

Based on the stress-distribution shown in Figure 5.8, the top plate is within the design limits, with only 63 percent utilization. Note that point loads from local traffic not are considered in the calculations. These loads will affect the degree of utilization significantly for the top plate. However, due to a low utilization percent, it is assumed that the cross-section has enough capacity.

The bottom plate is also within the limitations, and have an utilization degree of 96 percent (see Figure 5.9). Note that these simplified calculations not are sufficient, and more detailed calculations should be carried out, e.g. in a design program. However, these calculations provides a useful estimate of the capacity.

5.5 Cross Beams

5.5.1 General design

The design of the cross beams are also taken from Rambølls conceptual report [16]. The stiffeners are similar the ones used for the girder top plate, see Figure 5.10. It is assumed that each cross-beam carries load from 20 meters, since they are situated with the same spacing as the hangers. The most critical traffic load combination are shown in Section 4.1.2, based on the short influence length load model.

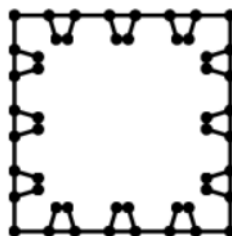


Figure 5.10: Cross beam modelled in CrossX.

The cross-sectional properties are computed in Cross-X. A simply supported beam model is created in Robot, which is used to find the design bending moment. Figure 5.11 shows how the loads are applied, and the moment along the beam. The load input are computed according to Figure 4.2. The span is equal to the distance between the main cables, and it is assumed a constant stiffness along the entire beam. The cross-beam length (gap width) does not rise any changes in moment since contributions from self-weight are relatively small. In reality the cross-beams have limited stiffness compared with the main girders. However, the resulting mid-span moment is almost unaffected by a stiffness change along the loading zone of the beam (where the girders are located).

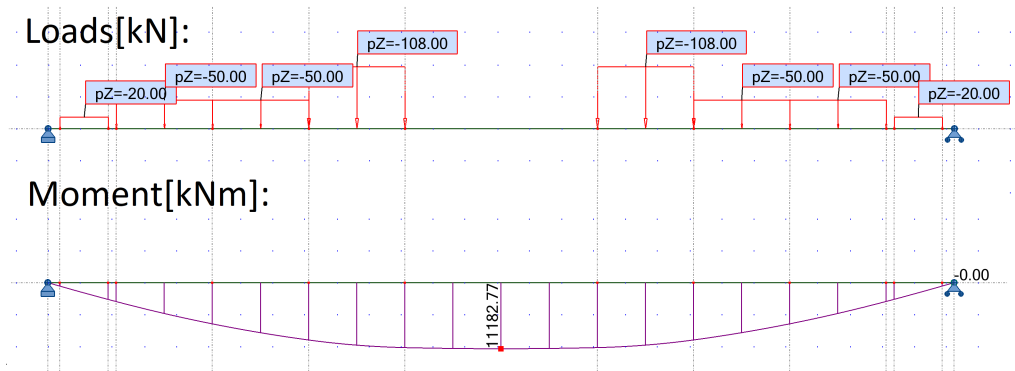


Figure 5.11: Robot: Applied load and resulting bending moment.

The moment mid-span is applied as a section force in Cross-X. The resulting stress-distribution is shown in Figure 5.12, and is within the design limits. Buckling is not taken into consideration.

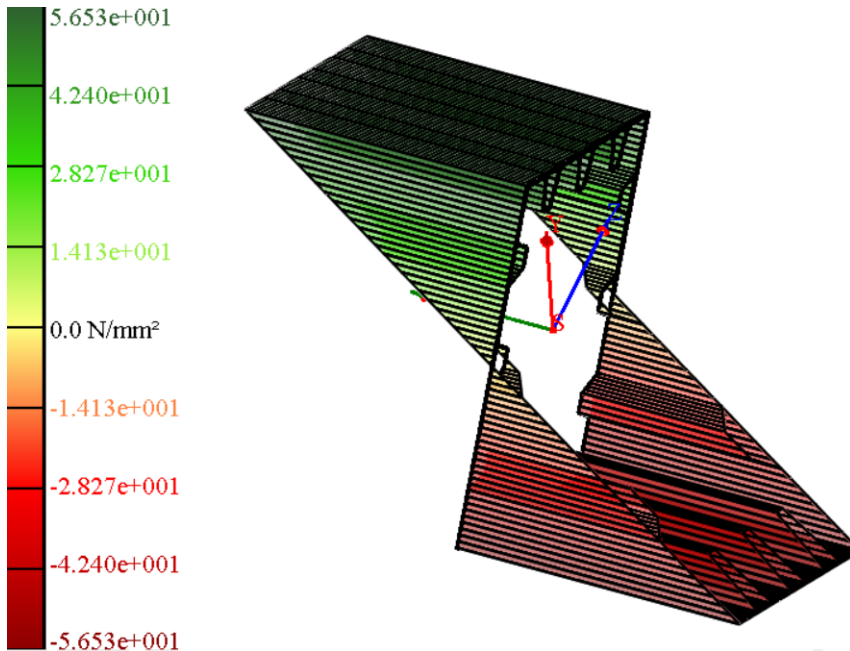


Figure 5.12: CrossX: Stress distribution.

5.5.2 Girder Variations in Parametrization

The cross beam design is unchanged in the parametrization procedure, only the span length varies. This is due to the fact that the beam forces are unaffected by the span length. Note that buckling is more critical as the span length increases. However, this is not in focus.

5.6 Pylons

The pylon design is taken from Multiconsults conceptual report [12] because they have also have a one-span system. Compared with Rambølls design, with two spans, a one-span system requires higher towers. Due to limited time, calculations related to the pylons are not considered in this thesis. When the towers are at its highest (400m) buckling becomes an important consideration. Computations done by Multiconsult for a 343 meter high pylon (similar design) shows a large degree of security towards buckling [12].

5.6.1 Pylon Variations in Parametrization

The tower height is one of the parameterized terms in the optimization process. The placement of the tower foundations is kept unchanged, which results in a varying tower inclination. This is visualized in Figure 5.13. The number of transverse pylon-beams is held constant to simplify the parametric model. Also, the cross-sections are kept unchanged. Hence, the stiffness will be reduced as the tower height is magnified. It is possible to make this parametrization with more accurate approaches, but it will not affect the model significantly. Note that the distance between the tower legs is adjusted when the box-girder gap width alters.

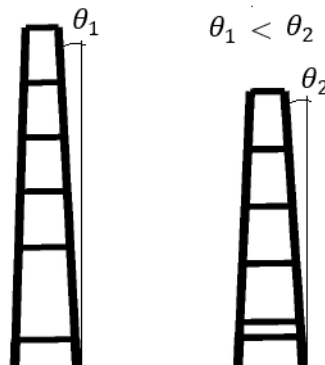


Figure 5.13: Visualization of varying tower inclination (height: 400-300m).

5.6.2 Influence Lines

Influence lines are an essential tool in designing beams and trusses used in bridges. The influence lines show where a load will create the maximum stress for a chosen part of the bridge. Influence lines are found by loading the girder with a unit load, and noting the force in a selected node as the unit load moves across the bridge. Influence lines are both scalar and additive. This means that the principle of superposition is valid, and it is possible to find the forces even if the applied load is not a unit load or if there are multiple loads applied.

In the Abaqus model a unit load will be placed on both girders every 10th meter, i.e. at every hanger, and once between every hanger, see Figure 5.14. Figure 5.15 shows the process of creating influence lines in Abaqus.

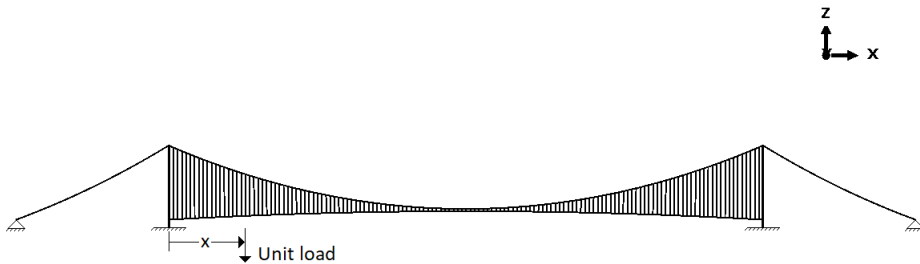


Figure 5.14: The Sulafjorden bridge is shown with a unit load placed a distance x from the left end. The influence lines is created by plotting the force in a node for each distance x .

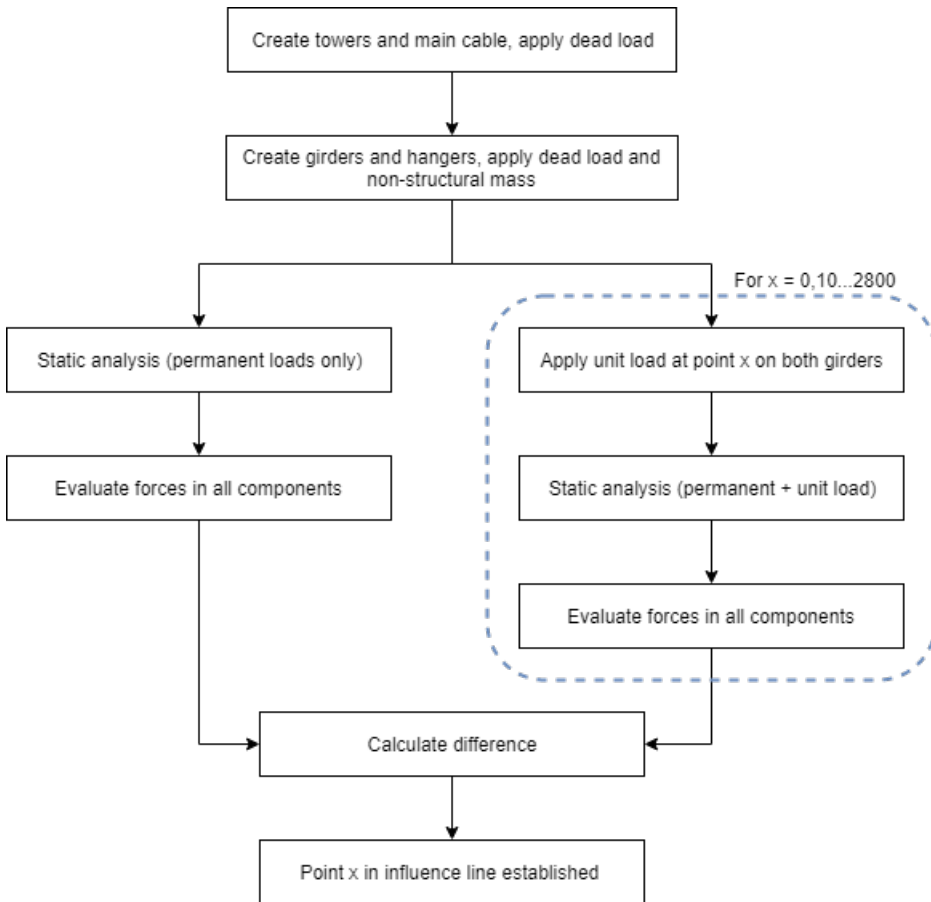
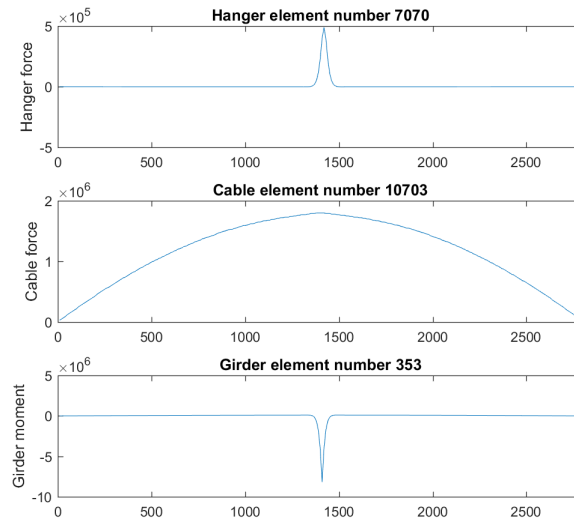
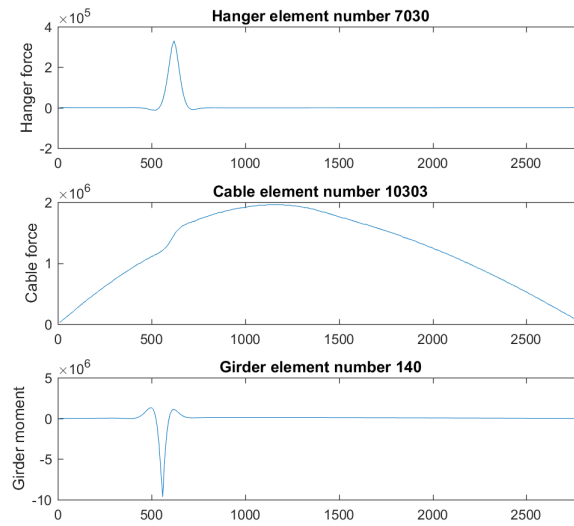


Figure 5.15: Structure of ABAQUS analysis for generating influence lines.

Influence lines for the main cable, hanger and girder are pictured in Figure 5.16, 5.17 and 5.18. Note that the maximum girder moment appears at $x = 0.05 \cdot L$ and maximum hanger stress at $x = 0.5 \cdot L$.

Figure 5.16: Influence lines for $x = 0.5 \cdot L$.Figure 5.17: Influence lines for $x = 0.2 \cdot L$.

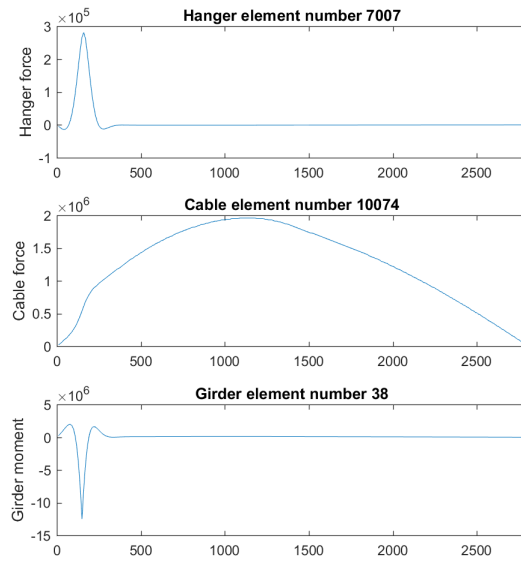


Figure 5.18: Influence lines for $x = 0.05 \cdot L$.

6 Parametric Modelling of the Sulafjorden Bridge

Abaqus is the chosen finite element (FE) software used to model the Sulafjorden bridge. Instead of using Abaqus CAE (Complete Abaqus Environment), Abaqus analysis is used (also called Keywords Edition). When using Abaqus (keywords edition), the bridge is going to be modeled by writing the input file (.inp) directly. MATLAB is used to define node coordinates and element properties. It is vital that the MATLAB function that generates the nodes can tolerate changes to the geometry. See Figure 6.1 for an illustration of one of the bridge geometries.

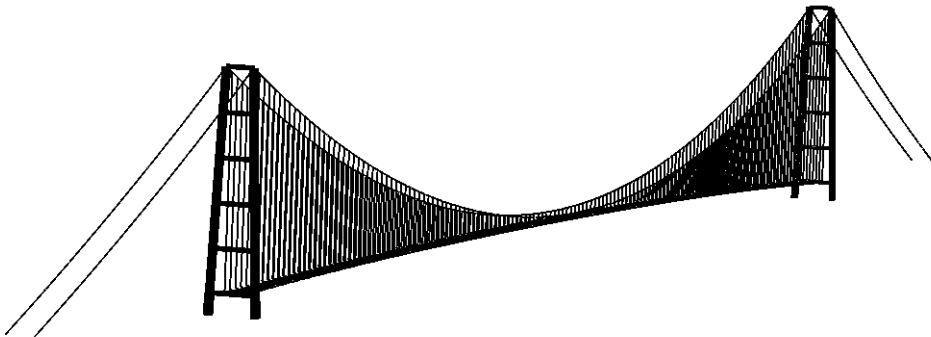


Figure 6.1: The sulafjorden bridge modelled in Abaqus.

6.1 Simplification of the Model

Modeling an exact copy of the original structure will obviously give the most accurate results. However, a complex model also has its drawbacks. A large and complex model will be very time consuming for the engineer to make. A detailed model with many sharp edges requires a very fine mesh in order to obtain a precise solution. This again will cause a long run time for the finite element analysis. Making decisions about what to be simplified, without losing vital information is an important task. If the wrong simplifications are made, the model will become inaccurate, and lose its validity compared to the actual structure.

6.1.1 Towers

A suspension bridge with such a span as the Sulafjorden bridge the towers is going to be very tall. Even with an enormous cross-section, the towers will be able to bend. Therefore it is essential to include the towers into the FE-model. The pylons are modeled with a constant distance between the "tower legs". As mentioned in Section 5.6.1, the tower height is parameterized, and both the incline and the width at the top of the tower are dependent on the width between the two girder boxes. See Figure 6.2 for a illustration of the towers and the coordinate direction. Note that the main cable thickness is correlated with the tower height, and will change area as the tower alter height.

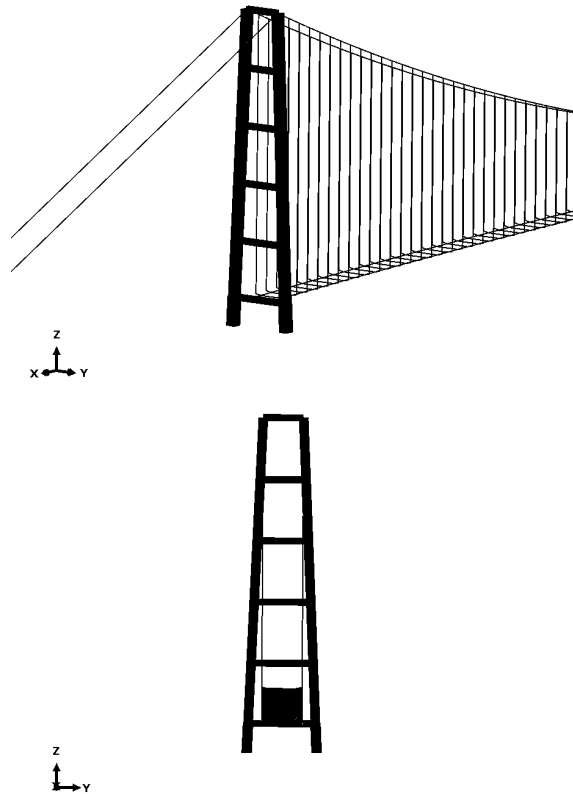


Figure 6.2: One of the towers modelled in Abaqus.

6.1.2 Twin-Box Girder

The twin-box girder will be modeled as two separate continuous beams, with cross-beam connections situated for each 20th meter. All the mass, stiffness and other properties will be assigned to each of the beam elements separately. The mass attached to the beams is the mass of the steel box including the non-structural mass. In the Abaqus model, it is assumed that the center of mass can be taken as the center of the girder beam.

The hangers are connected to the lateral edge of the box girder. To simulate the correct placement of the hangers, it is necessary to include some connection elements. These elements are supposed to connect the hangers at the exact place of the girder. The connection elements are incredibly stiff which creates the assumption that the girder is unable to bend in z-direction, see Figure 6.3. The two girders are also connected by an extremely rigid connection element, trying to represent the cross beam. A cross beam is placed once for every hanger. The connection elements have zero mass, as the mass of the connection elements is included in the girder elements.

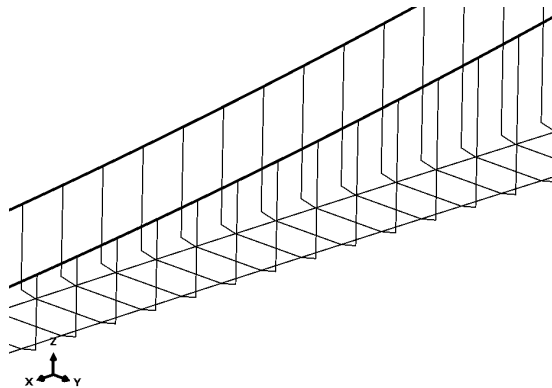


Figure 6.3: Close up illustration of the girders with connection elements, hangers and cables.

6.1.3 Boundary Condition

The boundary conditions (BC) at the bottom of the two towers and the end of each side cable are fixed. Which is a good representation of the BCs in reality. In the actual structure, the main cable can glide at the top of the towers. In the model, the cable is just connected to the top of the tower without being able to slide.

The connection between the twin-box girder and the towers are modeled with a more

complex BC. The box girders are fixed in y- and z-direction and for rotation about the x-direction. The structure can move in x-direction to avoid constraining forces in the girder. See Figure 6.3 for coordinate directions.

6.2 Prestressing / Model Tensioning

The tensioning is created by the dead weight and some procedures of forced tensioning. An illustration of how this is done for the Hardanger Bridge is shown in Figure 6.4. The FE model needs to replicate this effect before running a modal analysis. By using the same deck curvature as used at the Hardanger bridge, the Sulafjorden bridge will curve 20m upwards when exposed to gravity load. One simplified approach to obtain an equivalent stiffness is to apply a load to induce the axial forces. The method consists of three steps in Abaqus.

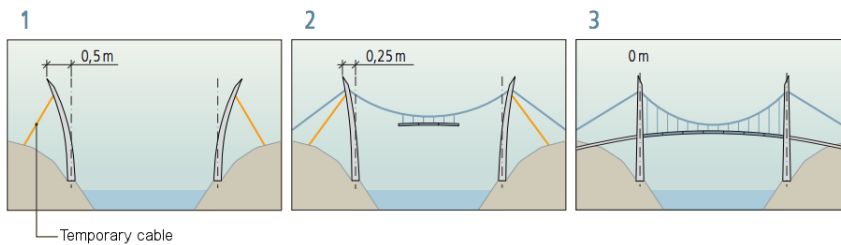


Figure 6.4: Before the cables are built, the top of the towers are pulled ca 50 cm backwards. When the steel boxes are installed the temporary cable is slackened and the towers go back to their original positions (modified, [21]).

Step 1:

In the first step, the hangers and girders are removed, and the cables are affected by gravity load. The cables will be stretched to get increased geometrical stiffness. See Figure 6.5 for an illustration of the BCs and the load.

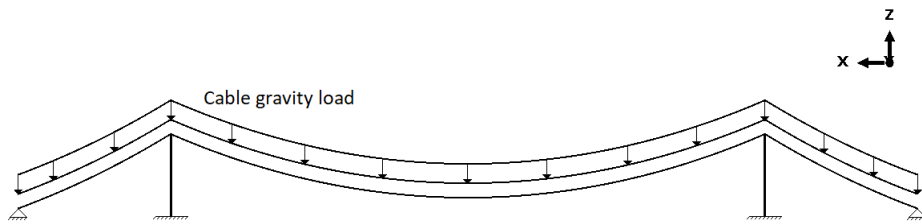


Figure 6.5: Step 1 in the tensioning process.

Step 2:

In this step, the girders and hangers are added. The gravity load on the cables is still active. Gravity load on the girders are also added. The girders is created with a 30 meters initial curve upwards. After this step is completed, the bridge will curve upwards by approximately 20 meters. See Figure 6.6 for the final state of the model before the frequency analysis is done, note the curve of the bridge deck.

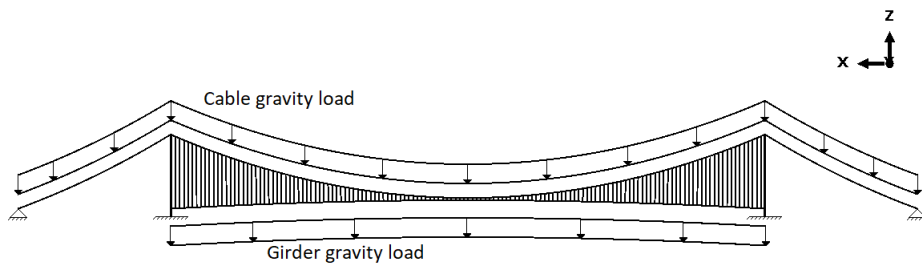


Figure 6.6: Step 2 in the tensioning process.

Step 3:

After step 2 the prestressing process is finished. In step 3 the modal analysis is carried out, and the live loads can be applied. Information related to the modal analysis, displacements and section-forces are printed. This way the data is gathered.

6.3 Possible Improvements

The cross-section of the towers does not change as the towers alter height. The bridge deck may also be more detailed modeled. This will cause a more accurate model, but increase the complexity of the parameterization and the computational cost of the analysis.

As the prestressing is done by applying dead weight to the main cables before adding the bridge deck with an initial curvature, it is difficult to ensure the correct geometry when changing parameters. As the tower height increases, the main cables gets smaller which gives a different displacement when exposed to gravity. The complexity of the prestressing makes the model challenging to parameterize. An alternative prestressing method should be investigated to simplify the modeling.

The MATLAB script which generates the nodes to the parametric model does not cope with large changes to the geometry because of the node numbering. If the bridge length is expanded over a certain distance, the node numbering of the girders will collide with the nodes of the main cables. The length of each girder element is 2 meters, which will cause problems if an odd number of meters between each hanger is desired. This problem should be solved when improving the model.

7 Optimizing the Bridge Geometry

Design optimization in engineering has been used from around 1960. As the computational capacity has developed, optimization tools have been more commonly used. Today, several types of optimization procedures are in use in structural design, also for bridges. Optimization methods provide a final design of better quality, in less time, which is very cost efficient [8].

In order to optimize a model, it needs to be parameterized. "To parameterize" by itself means "to express in terms of parameters". In practice, this means that the model can change geometry depending on a parameter, such as tower height or cable thickness.

7.1 Objective Function and Design Variables

Optimization includes finding best available values of some objective function given a defined domain. The objective function, sometimes called cost function, links different parameters together in order to compare them to each other. It is the objective function which is going to be minimized or maximized. The different variables in the objective function are called design variable. The chosen design variables are shown in Figure 7.1.

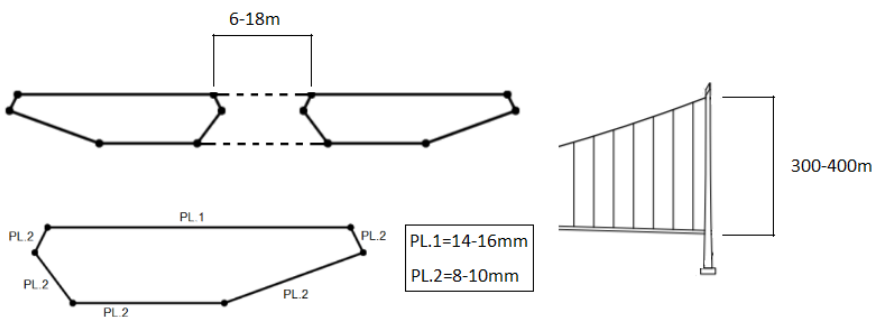


Figure 7.1: The design variables.

In this thesis, the different parameters will be prioritized in term of cost. The solution of the objective function results in an estimation of the total material cost of the bridge, who is going to be minimized. The price per kg of the different types of steel used in the main cables, hangers, and box girders is based on the cost estimates from Multiconsults

report of the Sula crossing. As well as the price per m^3 concrete used in the towers. These cost estimates create the basis of the objective function.

7.2 Types of Optimization Methods

There are two main types of methods used for solving optimization problems: Gradient based method and derivative-free method. Both methods will be explained in this section, but only a derivative-free method is used to solve the optimization problem in this thesis.

7.2.1 Gradient Based Method

The gradient based method's approach is to run an analysis with an initial geometry and have an optimizing algorithm calculate the next geometry to be analyzed. This will lead to fewer analyzes and a lot of time saved. A design optimization research of a long-span suspension bridge is performed by Ibuki Kusano [10], where gradient based solutions are used. The chosen design variables in this research are main cable and girder plate thickness, where flutter constraints are included. The study tested multiple optimization algorithms, all gradient based. A flowchart explaining this process is shown in Figure 7.2.

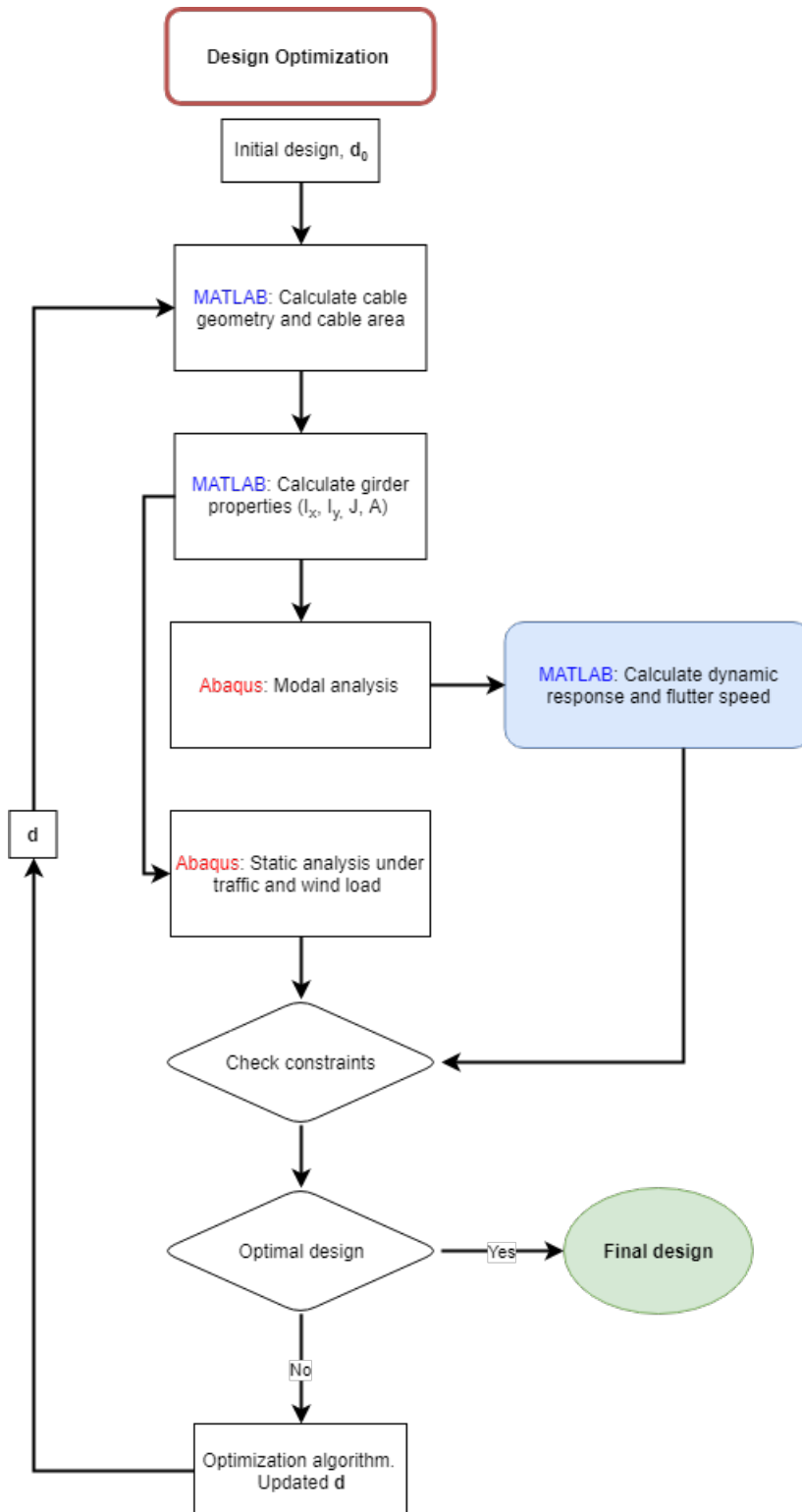


Figure 7.2: Flowchart of optimization process using gradient based optimization.

7.2.2 Derivative-Free

In this thesis, derivative-free optimization is going to be used. When the model can change geometry, one parameter at a time, an FE-analysis can be run on every combination of parameters. This type of optimization process is called derivative-free optimization [5]. The results of every parameter combination can create a response surface. The response surface gives a great overview of how the structure reacts to changes in parameters. The parameters may then be optimized by maximizing or minimizing the surface. A flowchart explaining the process which is going to be used in this thesis is shown in Figure 7.3.

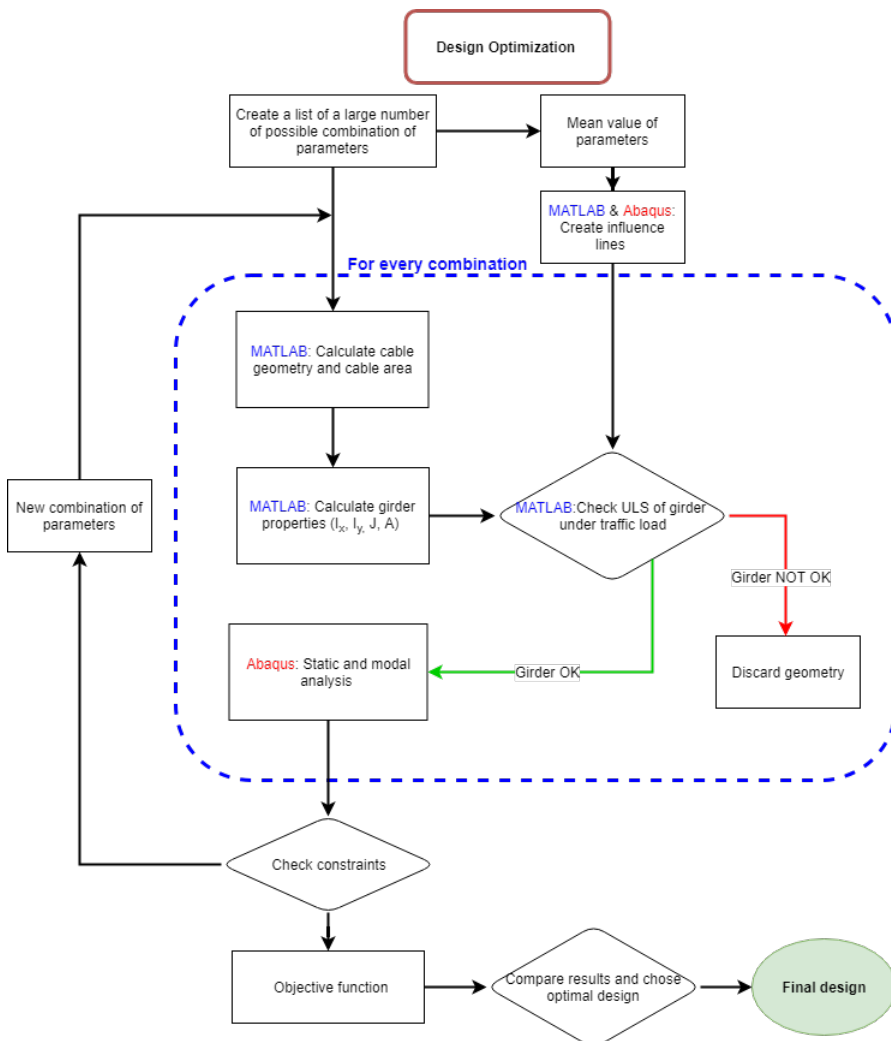


Figure 7.3: Flowchart of derivative-free optimization.

Optimally, an infinitely number of different geometries is tested and analyzed, but that is clearly not possible. After analyzed an adequate amount of geometries, the objective function is used to compare the parameters. An approximation is made by interpolating the results. This creates a plot of every possible solution for the objective function in as many dimensions as varying parameters.

Every time the optimization algorithm modifies the design variables, the MATLAB main code carries out the following main tasks:

1. Calculate the new dimensions of the main cables area according to the tower height and girder self-weight.
2. Perform Newton-Raphson iterations to determine the initial geometry of the main cable. Figure 7.4 shows the initial (C') and final (C_f) position of the cable. This step is necessary because any variation in tower height and cable thickness affects the initial length and stress of the main cables, and consequently the stiffness of the bridge.

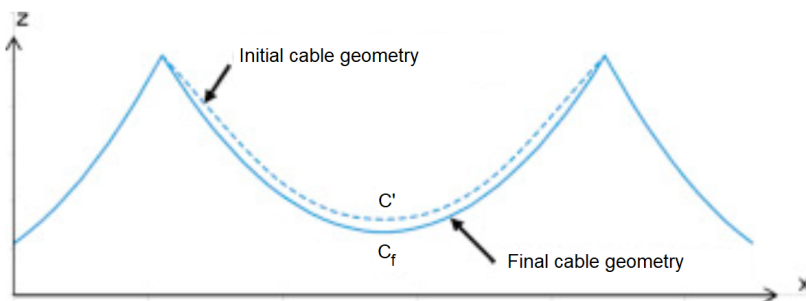


Figure 7.4: Initial and final cable geometry (modified [10]).

3. Write the Abaqus input file. This includes the initial geometry of the structure and element properties. The properties of the three box girders are all computed in advantage of the optimization process.
4. MATLAB launches Abaqus nonlinear static analysis to compute stress in the entire bridge, natural frequencies and vibration modes. This information is saved for every parameter combination.

The derivative-free optimization process is going to be used in this thesis partly because of its simplicity. Sometimes information about the derivative of the objective function is unavailable, unreliable or impractical to obtain. Gradient based methods require less computational costs, compared with the gradient-free optimization [5]. However, since a gradient-free solution receives the results from all design combinations, this

method provides more information about how the model responds to design variations. Because computational cost is not considered a problem in this thesis and the great overview of how the model responds to design variations, a derivative-free algorithm is used.

7.3 Constraints

It is essential to have some constraints when designing structures. Constraints, in this case, are boundaries or limits of the structure. The constraints may be physical limits as the maximal tower height or total girder width. Serviceability constraints such as maximal displacement and acceleration may also be a deciding limit for the design.

In this thesis the following constraints are used:

- **Maximal displacement:**

There are not found any specific standard value for max displacements for bridges, but for different construction materials (wood, steel and concrete) the value varies between $L/100 - L/300$. In this thesis $\delta = \frac{L}{120} = 23m$ is used.

- **Maximal acceleration:**

According to ISO 6897 [7], two curves of maximum acceleration for a given frequency are considered the comfort-limit for humans. Curve one is for general purpose buildings, curve two is for fixed offshore structures. Bridges can be considered as a type two structure. This gives a conservatively acceleration limit of $0.156 \frac{m}{s^2}$.

- **Maximum and minimum tower height:**

There are no standardized limits for the height of towers in a suspension bridge. The constraint set to prevent the optimizing process ending in infinitely tall or no towers at all. The height of the towers must also be practical to build, outside the boundary where the objective function is valid. In this thesis, the towers must be between 200 and 450 meters tall (from the bridge deck to top of the tower).

- **Flutter speed**

The critical flutter speed is an essential constraint for long-span bridges and works as a total cut-off criterion. Reaching a sufficient value for the critical flutter speed can be very challenging for super long span bridges. According to N400-Bridge Design, the critical wind velocity related to flutter, V_{cr} , is based on a return period of 500 years and defined as in Equation 7.1. Note that the return period for the wind velocity in previous computations was set to 50 years.

$$V_{cr} \geq \gamma_{cr} V_s \quad (7.1)$$

Here, $\gamma_{cr} = 1.6$ and V_s is the wind velocity. The mean height above sea level is 70.8 meters, as used for the mean wind velocity computations. Equation 4.3 with a 500 years return period gives a basic wind velocity $v_b = 1.1223$, which leads to $V_s = 50.74 \text{ m/s}$. See section 4.1.3 for the underlying equations used in this calculation. Further, Equation 7.1 results in $V_{cr} = 81.18 \text{ m/s}$. However, in this thesis, the flutter speed is included in the case study, only. To include flutter constraints in the optimization, it is essential to have experimentally obtained flutter derivatives for each girder design.

7.4 Challenges

7.4.1 Objective Function

The objective function creates the foundation of the optimizing process. The solution is highly dependent on the objective function. To define a good objective function is extremely difficult.

The objective function used in this thesis is a rough estimate only based on the price of the physical material needed, for one specific design. Planning and execution is a significant part of the total expenses in a large structural project. Those types of costs may increase or decrease with changes in the geometry, but are not included in the objective function.

7.4.2 FE-Analysis

The FE-analysis is a time-consuming job. Even with a simplified model, finding stresses, displacements, and natural frequencies take some time. This analysis has to be repeated for all possible combination of parameters. The range and interval each parameter may operate in can be limited, but to get a good result, the process will still take some time. In this thesis, it is used three different girder sizes, six different tower heights and four gap sizes, i.e., 72 Abaqus analyses are required.

7.4.3 Aeroelastic Coefficients

A challenge with changing the size of the deck or changing the gap between the box girders is the aeroelastic coefficients. It has been researched how the pressure on the box girders changes with different gap sizes, see Figure 7.5. Since the pressure distribution along the girder surfaces varies for different gap sizes, the aerodynamic properties also vary. I.e., for more realistic results, the aerodynamic coefficients should depend on the gap width. In this thesis, the aerodynamic properties are kept constant [11].

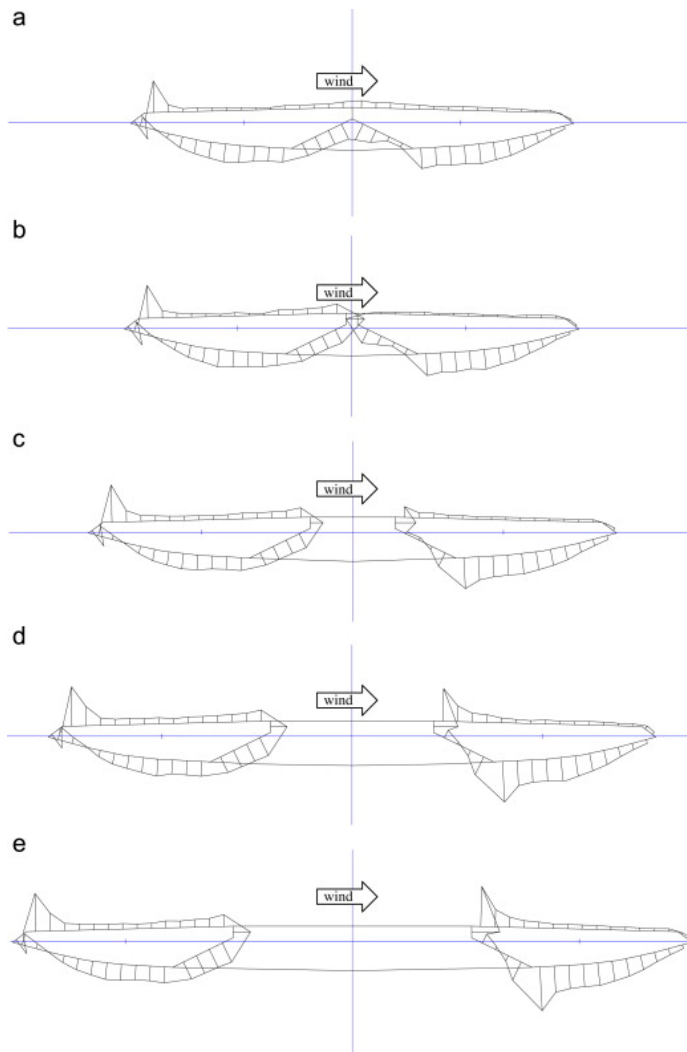


Figure 7.5: Mean pressure distribution for gap widths equivalent to 0m(a), 1m(b), 7.5(c), 14.3(d) and 21.1 m(e). Negative pressures are away from the surface[11].

7.4.4 Comparing Frequencies

The FE-analysis returns the results of the natural frequencies sorted from lowest to highest frequency. When reviewing this result, it is wanted to compare the same type of modal frequency, e.g., vertical and torsional frequency modes with similar shape. The modal assurance criterion (MAC), which is also known as mode shape correlation coefficient (MCC), between mode i and mode j is defined as[23]:

$$MAC(\Phi_i, \Phi_j) = \frac{|\Phi_i^T \Phi_j|^2}{\Phi_i^T \Phi_i \Phi_j^T \Phi_j} \quad (7.2)$$

Where Φ_i and Φ_j are the mode shapes for mode i and j . A MAC value close to 1 suggests that the two modes are well correlated and a value close to 0 indicates uncorrelated modes. Figure 7.6 illustrates the MAC number to frame 2 of different geometries. One geometry (top left in the figure) is chosen as a reference mode and is compared to all other geometries.

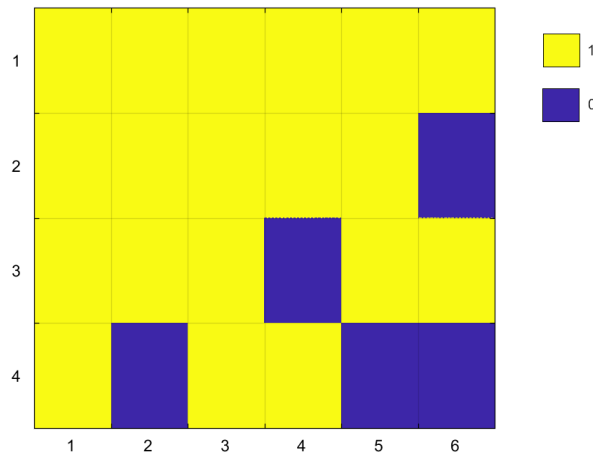


Figure 7.6: MAC number of frame 2. One geometry is chosen as a reference mode and is compared to all other geometries.

Figure 7.6 is one of several examples that shows the order of the frequencies change frames when the geometry change. This makes it hard to compare every frequency. The frequencies which are going to be analyzed may be reduced to the first frequency of each type (vertical, horizontal and torsion). In the case study, the 30 first frames/frequencies are considered.

8 Case Study

This case study shows how the parameterized model can be modified to represent a specific suspension bridge design. The objective of this case study is to examine the adaptability of the parameterized model and to include aerodynamic stability computations for a wind tunnel tested cross-section.

A flutter computation is carried out based on the bridge design presented by Multiconsult in their feasibility study of the Sulafjord crossing [12], see Figure 8.1 and 8.2.

Aerodynamic data related to this design are obtained from wind tunnel tests completed by Johannes Grongstad and Oddbjørn Kildal in their master thesis[9], where the static force coefficients and the aerodynamic derivatives are found, for the wind directions shown in Figure 8.2. Results from these tests are added in Appendix A. Note, only flutter computations related to wind direction 1 will be included in the results and discussion. The access of accurate aerodynamic coefficients makes it possible to include aerodynamic stability issues in the design. Since these coefficients vary as the gap width changes, they are only valid for one particular gap width. It is possible to include the gap width as an altering parameter if each geometry has one coinciding set of aerodynamic coefficients.

8.1 Bridge Design

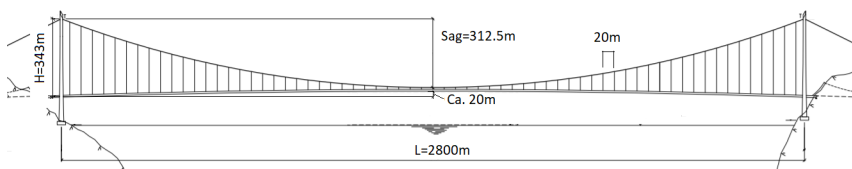


Figure 8.1: Sketch with dimensions.

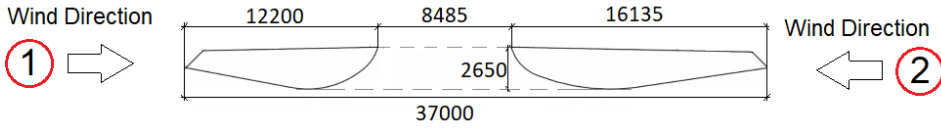


Figure 8.2: Wind direction and deck dimensions [mm] [12].

The cross-sectional parameters for the main components are listed in Table 8.1. The mass of inertia, I^m , for the biggest and smallest girder (see Figure 8.2) are estimated with the same assumptions as for the original section. Computations are shown in Appendix B.

Table 8.1: Cross-sectional parameters of cross-section in Figure 8.2 provided by Multiconsult[12].

Param./Part	Big Girder	Small Girder	Hanger	Big Cable	Small Cable
Area [m ²]	6.076e-1	4.599e-1	6.333e-3	6.311e-1	6.206e-1
I_{33} [m ⁴]	4.768e-1	3.600e-1	3.192e-6	3.170e-2	3.065e-2
I_{22} [m ⁴]	1.335e+1	5.581e+0	3.192e-6	3.170e-2	3.065e-2
I_{23} [m ⁴]	0.0	0.0	0.0	0.0	0.0
I_t [m ⁴]	1.141e+0	1.052e+0	6.284e-6	6.34e-2	6.129e-2
I_z^m [kg $\frac{m^2}{m}$]	1.050e+5	2.426e+5	-	-	-
I_y^m [kg $\frac{m^2}{m}$]	6.000e+3	7.000e+3	-	-	-

The static wind coefficients related to this section are presented in Table 8.2, and the measurements obtained for a wind speed of $6 \frac{m}{s}$ are shown in Figure 8.3. Compared with the static coefficients for the cross-section presented in Section 5, these values are significantly lower.

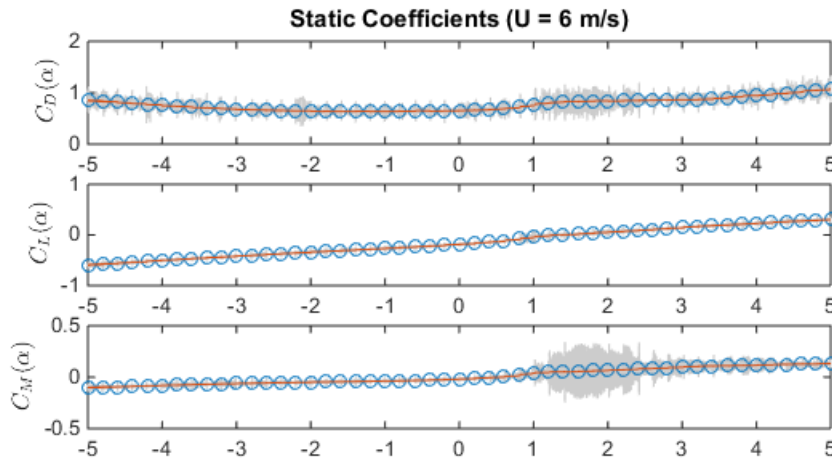


Figure 8.3: Wind force coefficients versus wind angle (wind direction 1).

Table 8.2: Wind force coefficients obtained from static wind tests (wind direction 1).

Structure	$C_D(\alpha=0)$	$C_L(\alpha=0)$	$C_M(\alpha=0)$	C'_L	C'_M
Girder	0.70	-0.17	-0.01	0.11	0.04

8.2 Flutter Computations

Aerodynamic derivative measurements related to vertical movements are graphically shown in Figure 8.4 (see Appendix A for all measurements). A fitted 2nd degree function will be added to each data set in the results, both for horizontal, vertical and rotational motions. A MATLAB program created by Ole Øiseth is used to compute the critical multimode flutter velocity. Required inputs are the fitted AD-functions from measurements, in addition to the vibration modes, modal mass and natural frequencies from the Abaqus model. Background for the MATLAB-script is more closely described in Section 3.3.3.

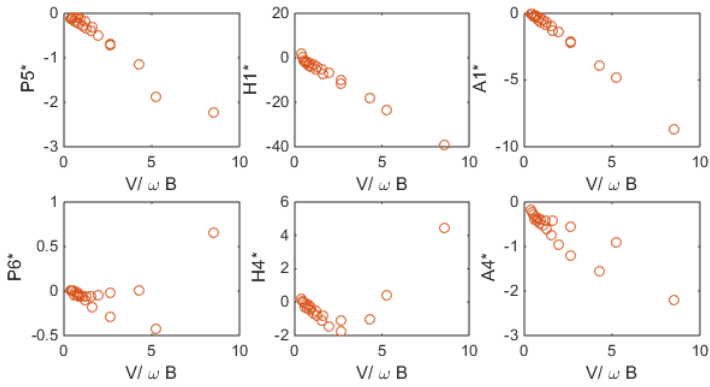


Figure 8.4: Aerodynamic derivatives from vertical motion (wind direction 1).

The MATLAB-script provides information about used values along the approximated AD-functions. This is shown graphically in Figure 8.5. The blue line shows the fitted AD-functions and the red dots indicates values extracted in calculations.

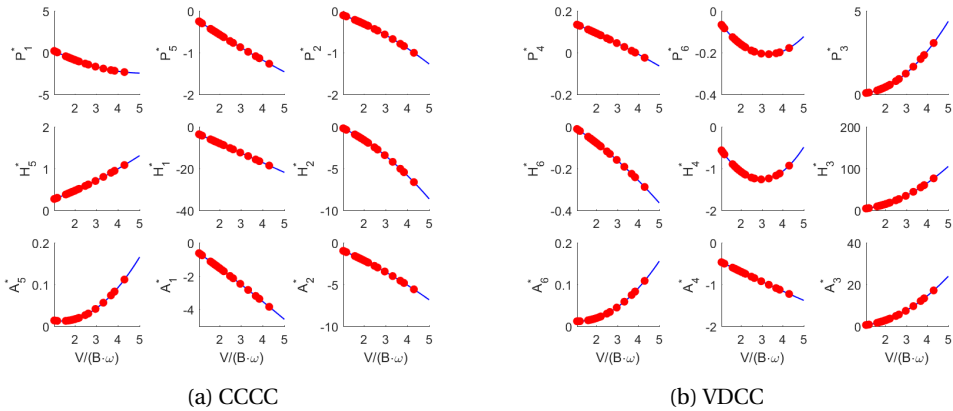


Figure 8.5: Visualization of extracted AD-values used in flutter iterations (wind direction 1).

8.2.1 Uncertainties in Computations

The flutter result is highly dependent on the experimental results. Flutter sensitivity research related to the degree of details in the model used in the wind tunnel testing shows that small geometrical changes have a significant impact on the resulting flutter speed. The results from this research done by Siedziako [19] on the Hardanger bridge, and are shown graphically in Figure 8.6.

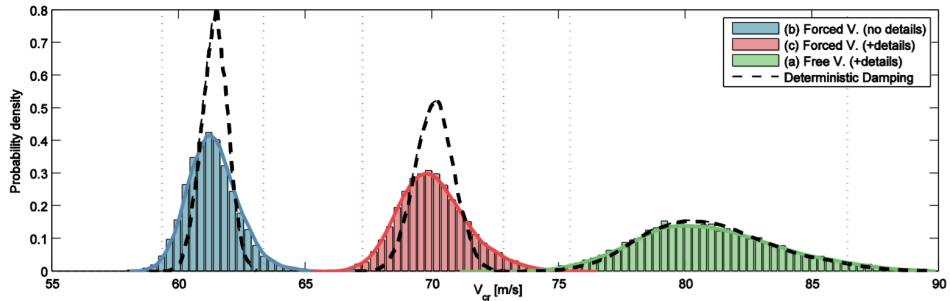


Figure 8.6: Distributions of critical flutter speed for section (a), (b) and (c) for the Hardanger bridge. [19].

The research presented above shows that when bridge deck details are added to the section model, the critical flutter velocity will be postponed by 9.1 m/s, but that the ADs becomes more scattered. The experimental data used in this case study is based on forced vibrations, with no details. I.e., it could be that the resulting flutter speed will be underestimated.

9 Results

9.1 The Optimizing Process

The optimization are performed on the basis of the following design variables (see Figure 7.1 for a graphical illustration):

- Tower height: 300-400m, interval: 20m.
- Gap width: 6-18m, interval: 4m.
- Box girder thickness: uniform increase with an interval of 1mm.

Multiple analysis has been completed for all design combinations. Tables 9.1-9.4 shows how the natural frequencies change with the tower height and the gap between the girders. Note that these results are related to the smallest girder. The corresponding frequency ratio presented in Table 9.5. This is the ratio between the first torsional and first vertical mode.

Table 9.1: Frequencies of the first horizontal mode [rad/s].

Tower Height / Gap [m]	6	10	14	18
300	0.2023	0.2039	0.2055	0.2072
320	0.1954	0.1970	0.1987	0.2004
340	0.1892	0.1908	0.1926	0.1944
360	0.1835	0.1852	0.1870	0.1889
380	0.1783	0.1801	0.1819	0.1839
400	0.1736	0.1754	0.1772	0.1793

Table 9.2: Frequencies of the first vertical mode [rad/s].

Tower Height / Gap [m]	6	10	14	18
300	0.3897	0.3897	0.3897	0.3897
320	0.3714	0.3714	0.3714	0.3714
340	0.3564	0.3564	0.3564	0.3564
360	0.3419	0.3419	0.3419	0.3418
380	0.3277	0.3277	0.3277	0.3276
400	0.3158	0.3158	0.3158	0.3158

Table 9.3: Frequencies of the asymmetric torsional mode (double sine wave) [rad/s].

Tower Height / Gap [m]	6	10	14	18
300	0.9877	0.9689	0.9601	0.9519
320	1.0034	0.9821	0.9714	0.9638
340	1.0179	0.9953	0.9827	0.9745
360	1.0204	1.0072	0.9946	0.9827
380	1.0411	1.0154	1.0022	0.9865
400	1.0512	1.0248	1.0103	0.9858

Table 9.4: Frequencies of the symmetric torsional mode (single sine wave) [rad/s].

Tower Height / Gap [m]	6	10	14	18
300	0.1656	0.1587	0.1532	0.1488
320	0.1720	0.1642	0.1583	0.1535
340	0.1723	0.1657	0.1598	0.1546
360	0.1830	0.1750	0.1681	0.1627
380	0.1857	0.1784	0.1714	0.1658
400	0.1881	0.1811	0.1743	0.1685

Table 9.5: Frequency Ratio (*Torsional/Vertical*).

Tower Height / Gap [m]	6	10	14	18
300	2.53	2.49	2.46	2.44
320	2.70	2.64	2.62	2.60
340	2.86	2.79	2.76	2.73
360	2.98	2.95	2.91	2.88
380	3.18	3.10	3.06	3.01
400	3.33	3.25	3.20	3.12

In the objective function, the cost per unit of cables, hangers, towers, and the deck is based on the cost estimates from Multiconsults conceptual report of the Sula crossing. The unit price for concrete in the towers is adjusted relative to the height with a cubic polynomial, whereas the other unit prices are constant. This is to compensate for the for the cost of building very tall towers. See Table 9.6 for unit prices.

Table 9.6: Material Cost.

Component	price	unit
Main Cable Steel	125	kr/kg
Girder Steel	45	kr/kg
Concrete in Tower	12,5	kr/m^3
Hanger Steel	150	kr/kg

Curve fitting is used to estimate the resulting cost surfaces. Figure 9.1 shows a surface plot of the estimated total cost of the smallest girder type, whereas Figure 9.2 includes all girder types tested. In Figure 9.4 the design variations where lateral deflections exceeds the limitations are removed. The acceleration constraint is never violated. The optimal geometry is shown in Figure 9.1, which is for the smallest girder type, and lies on the displacement limit.

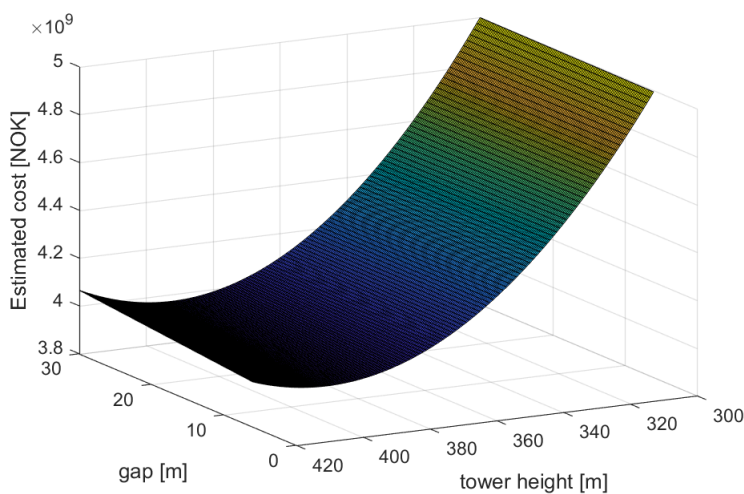


Figure 9.1: Estimated total cost for one type of box girder dependent on tower height and gap between girders.

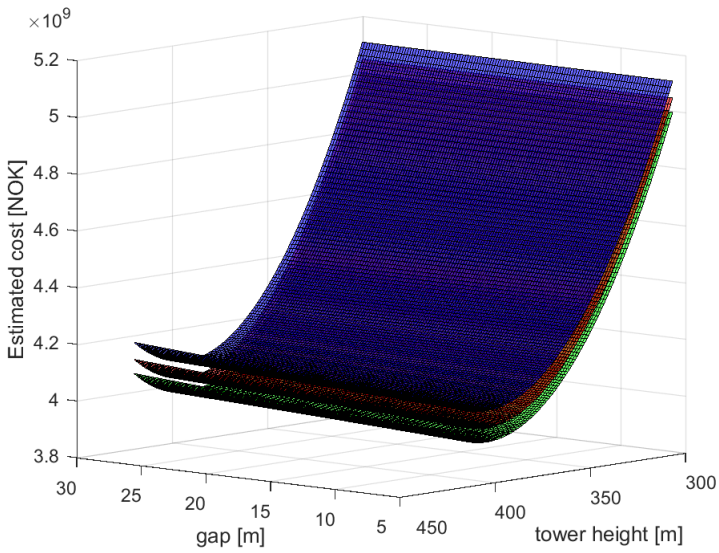


Figure 9.2: Estimated total cost for three types of box girders dependent on tower height and gap between girders. Girder 1=green, Girder 2=red, Girder 3=blue.

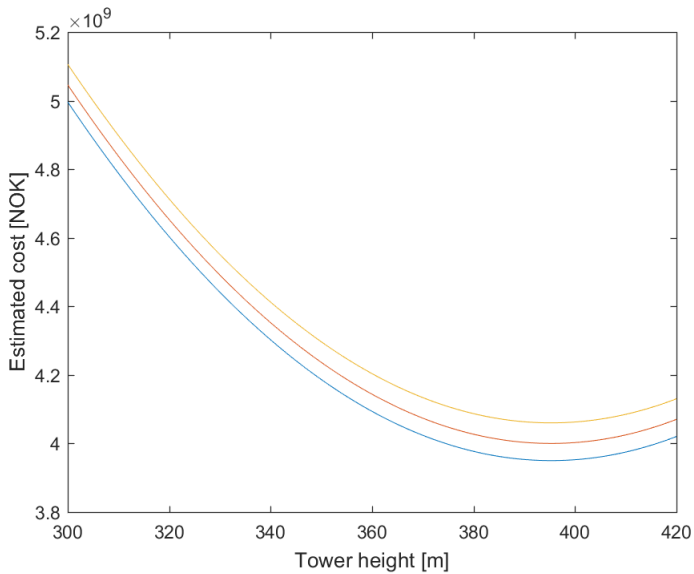


Figure 9.3: Estimated total cost for three sizes of box girders dependent on tower height when the gap is 16m.

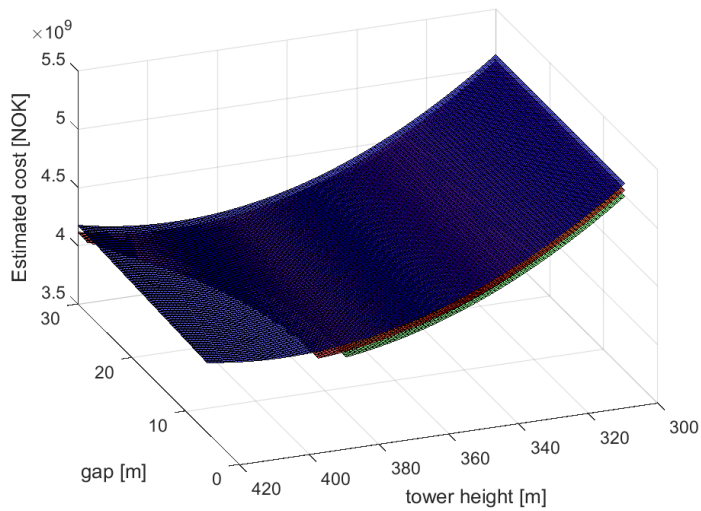


Figure 9.4: Estimated total cost for three types of box girders dependent on tower height and gap between girders. Combinations of parameters where lateral deflection exceeds limitations are removed.

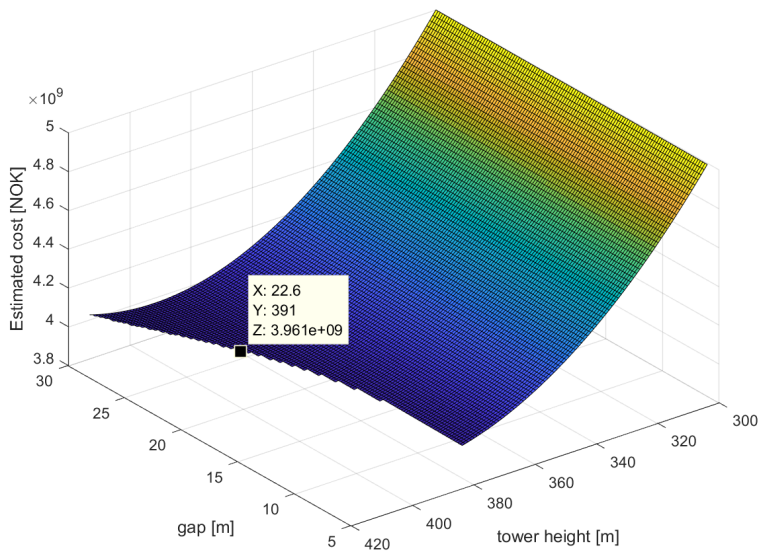


Figure 9.5: Estimated total cost for the smallest box girder. Design variations where the lateral deflection exceeds limitations are removed. The optimal (smallest) value is marked at gap=22.6 and tower height=391 is 3.961e+09 NOK.

Since the optimal design lies in the interpolated area, one additional FE-analysis is created for this design in order to obtain the modal frequencies. Results are shown in Table 9.7.

Table 9.7: First frequency of each type for bridge with optimal geometry [rad/s]
Tower height=391 m and Gap=22.6 m.

Horizontal	Vertical	Torsional
0.1838	0.3200	1.003

9.2 Case Study

9.2.1 Flutter

The bridge dimensions for the case study is introduced in Section 8.1. The results from the flutter computations are presented in this section, and are related to wind direction 1 (see Figure 8.2). Flutter analysis is carried out for various combinations of the natural modes. This way it is possible to investigate the modal flutter participation. The calculated flutter conditions for the investigated mode-sets are shown in Table 9.4. See Appendix A.1.1 for an illustration of the modes used in the flutter analysis. The estimated frequency and damping for the modes in mode set 8 are visualized in Figure 9.6.

Note, a flutter computation related to wind direction 2 is also completed. See Appendix A.2 for the flutter results and corresponding AD-measurements.

Table 9.8: Flutter conditions (wind direction 1).

Mode set	Mode no.	Velocity [m/s]	Frequency [Hz]	Reduced velocity
1	5,13	151.60	0.7847	5.22
2	2,13	140.35	0.8191	4.63
3	4,15	92.92	0.7297	3.44
4	2,14	76.83	0.6097	3.41
5	5,14	75.59	0.6398	3.19
6	2,5,14	71.05	0.7096	2.71
7	2,5,13,14	68.55	0.6953	2.66
8	2,5,13,14,15,18	67.69	0.6934	2.34
9	1-20	67.23	0.7701	2.36

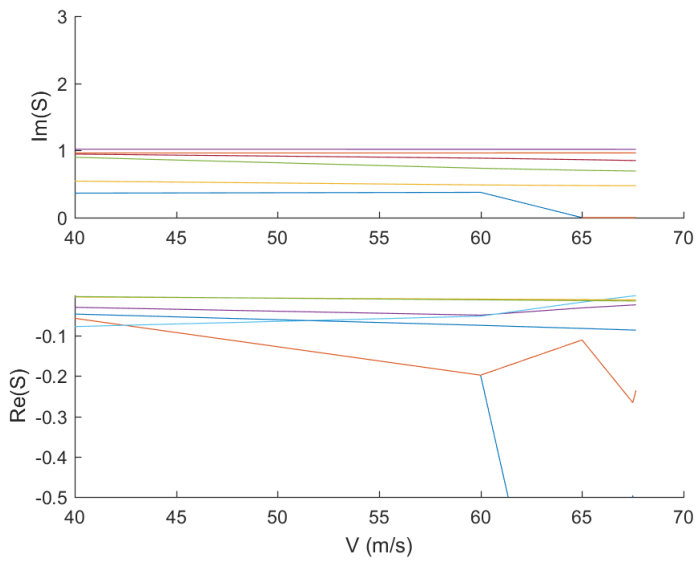


Figure 9.6: Real and imaginary part of the eigenvalue related to mode set number 8. (Re=damping, Im=freq) (wind direction 1).

In Figure 9.7-9.9 the reduced velocity for mode set 8 is highlighted with a vertical dotted line in the same plot as the real measurements are shown. Graphically, the aerodynamic derivative used in the last flutter iteration (the one resulting in the instability state) can be compared with the measured value (circle).

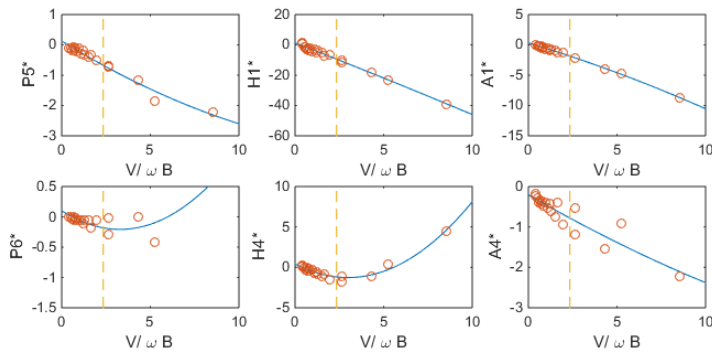


Figure 9.7: Plotted ADs related to vertical motion where the reduced velocity for mode set 8 is shown with the vertical dotted line (wind direction 1).

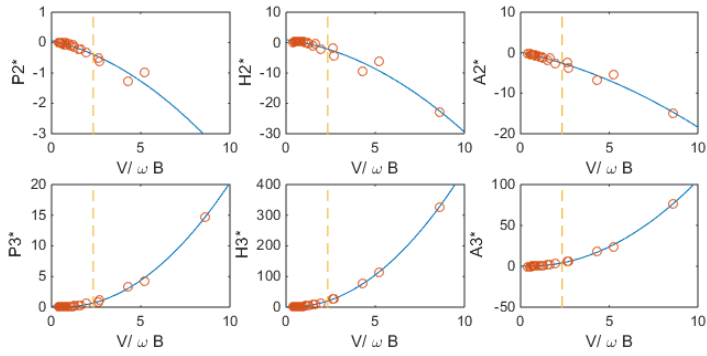


Figure 9.8: Plotted ADs related to rotational motion where the reduced velocity for mode set 8 is shown with the vertical dotted line (wind direction 1).

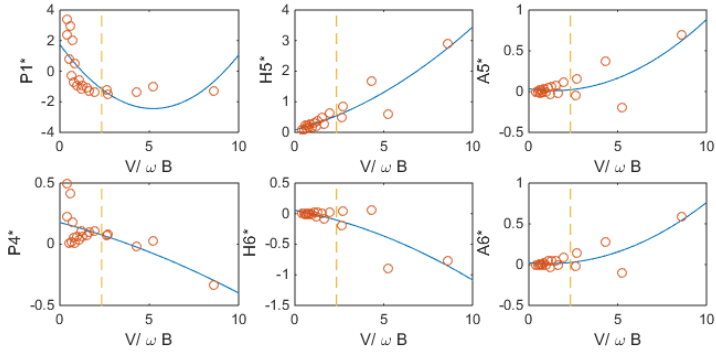


Figure 9.9: Plotted ADs related to horizontal motion where the reduced velocity for mode set 8 is shown with the vertical dotted line (wind direction 1).

10 Discussion

10.1 Optimization Results

The estimated cost of the materials needed for the Sulefjorden Bridge presented in Figure 9.1 to 9.3 indicates that the optimal geometry is a tower height of 391 meters and a gap of 22.6 meters, when choosing the smallest girder.

Figure 9.3 shows how the girder size affects the cost of the bridge. As expected, the girder with the smallest plate thickness is the cheapest, and therefore the optimal choice. However, it is needed to perform more detailed calculations on the girder to make sure it is within the design limits. The smallest girder within the design limits tends to be the optimal choice since the geometrical stiffness from the cables dominates the bridge stiffness. Note that the only varying parameter related to the cross-section is the thickness. A change in section height may be the ideal choice, but this is challenging to implement in the parametric model.

Figure 9.3 also shows how the estimated cost of the bridge depends on the tower height, for a given gap size. Taller towers tend to give lower estimated costs. By increasing the tower height, the sag increases which reduces the forces in the main cables. Less stress in the main cables gives the opportunity to design thinner cables, which affect the total cost. It is also a material cost related to building taller towers, but compared to the amount saved by getting smaller cables, it is profitable. In this thesis, it is assumed that the cost of building towers are nonlinear. E.g., it is more expensive to increase the tower height from 380-400m than from 300-320m.

From Figure 9.1 to 9.5 it can be seen that the total estimated cost is almost constant when the girder gap change. The material cost of increasing the gap is negligible compared to the price reduction of decreasing the main cable area. In the model, a large gap is favored due to large horizontal stiffness and low cost.

The reason for having a gap between the girders is due to structural advantages related to buffeting loads and aerodynamic stability. In the Abaqus model, the aeroelastic characteristics (static coeff. and ADs) are kept unchanged as the gap gets more substantial. The gap between the girders directly affects the aerodynamic properties, as mentioned in Section 7.4.3. Obtaining the aeroelastic properties for different cross-sections requires multiple wind tunnel experiments. Wind tunnel testing is both expensive and time-consuming. However, since flutter computations are not included

in this optimization process, only the buffeting loads are affected by this simplification.

The calculated optimal gap of 22.6 m may be considered too large. There have never been built a twin-box girder with such a large gap. According to the results presented in Section 9.1, a maximal gap constraint would give shorter towers and a more expensive structure. Despite a theoretical more expensive material cost, a smaller gap could be more realistic to build.

As mentioned, a gradient-free optimization method can provide structural information about the bridge. Table 9.1-9.4 shows how the natural frequencies varies. Both the horizontal and vertical modes is reduced by lowering the towers, which is as expected. However, relative to the magnitude of the design variation, the frequencies do not change in large extent. By carrying out optimization analysis related to a different set of design variables, it could be possible to observe potential parameters with greater influence on the natural frequencies.

Flutter calculations are not included in the optimization process, due to lack of experimental data. However, the frequency ratio works as an indicator of the bridge's exposure to flutter instabilities and is desired to be as high as possible. But note that the frequency ratio is unfit as a design criterion. The frequency ratios for different geometries (see Table 9.5) indicates that it is most convenient to shorten the gap and increase the tower height. By shortening the gap, the rotational mass of inertia is reduced, which increases the torsional frequency. As the towers are enlarged the generalized mass in the vertical direction are increased, which can explain the reduced vertical frequency. Hence, this combination leads to the highest frequency ratio. It is reasonable to assume that the natural frequency would have the same tendency for similar bridges.

10.2 The Optimization Process

The objective function is based on the material prices in Table 9.6. Note that these prices are an estimate, and are related to one specific design. The prices are based on previous projects. The cost of the construction of the bridge is not included in the objective function. This is not covered because of lack of information found, and it is tough to estimate the construction cost without years of experience.

A disadvantage of the derivative-free method is the computational costs. The complete analysis with 72 different parameter combination takes two hours (with a 2.40GHz processor and 8GB RAM). If two parameters with five combinations each were added, the number of analysis would be 1800. 1800 analysis would take approximately 50 hours to complete with identical hardware. However, the time-demanding analysis is not

considered a large problem. The analysis is only needed to be completed once, and with current technology, a cloud-based computing service could reduce the computing time drastically. An important advantage related to the derivative-free method is that multiple potential solutions will be found, unlike a gradient based method where a local minimum may be found instead of the actual solution.

10.3 Case Study

The case study shows the advantages of a parametric model and how it can be modified to resemble a specific bridge design. Even when the new construction has different sizes for each main cable and unsymmetrical box girders, the modification does not require much work.

The computation of the critical flutter speed gives a critical wind speed of $67.23 \frac{m}{s}$ when including the first 20 modes. Based on Figure 9.7 - 9.9 the estimated AD coincides well with the measured data, which is important for the flutter computation accuracy.

The resulting flutter velocity is less than the design limit computed in Equation 7.1, where the critical wind speed is calculated to $81.18 \frac{m}{s}$. The design limit for flutter speed is based on the N400-Bridge Design manual. This manual is established in 2009, and could be intended for smaller-scaled bridges. Thus, the design limit may be too conservative. In addition, the research presented in Section 8.2.1, indicate that the estimated flutter speed may increase if the experimental data was obtained using a more detailed section model. However, these results are based on a single-deck system, and, thus, may not be valid for a twin-deck design.

To reach the required flutter speed, the shape of the girders and the gap width would be the most expedient factors to change. These terms will directly affect the ADs, and thus, the instability limit. Cost related to changing these parameters is mainly related to research and not the amount of used materials.

It must be noted that for the type of cross-section used in the case study, it is challenging to get exact results from wind tunnel testing. This is due to its smooth surface and unsymmetrical shape. To assess the quality of the measurements and the aerodynamic derivatives, it is essential to have an idea of what might have affected the results. Testing at low Reynolds number, imperfections in foil application and the limited amount of tests are believed to be the most significant sources of error in the wind tunnel testing[9].

11 Conclusion

This research demonstrated the feasibility of the application of using an optimizing process when designing super long span suspension bridges. A derivative-free optimization method is used to optimize the tower height and girder gap, considering the total material cost. Three girders with different plate thicknesses is analyzed. A parameterized finite element model is created in Abaqus. The optimizing process gives a proposed tower height of 391 meters and a gap of 22.6 meters, when the smallest girder is used. However, this proposal is highly dependent on the objective function, which has several uncertainties.

The objective function is based on the material costs of the structure. It is simplified and has significant shortcomings, but it shows how an objective function may be used to optimize the structure. A more advanced objective function will give a different result, but the approach will be the same as is this thesis.

The parametric model can be used to provide essential information when designing complex structures, and to investigate effects of structural changes. It is shown how the natural frequencies change with tower height and girder gap. The first vertical mode is reduced from 0.3897 to 0.3158 $\frac{rad}{s}$ (19,0%) when the towers are increased with 100 meters (gap width do not affect this mode). The first asymmetric torsional mode is increased from 0.9519 to 1.0512 $\frac{rad}{s}$ (10,4%) as the gap width is reduced with 12 meters and the tower height are increased with 100 meters. Relative to the magnitude of the design variations, the modal frequencies do not change in large extent. An optimization related to a different set of parameters could be completed in order to investigate how these influence the results.

Despite the fact that the optimization process is tested on a suspension bridge in this thesis, it is reasonable to assume that the field of application could be related to other types of civil engineering structures. The principle and the approach would be identical as is this thesis. As parametric modeling software improves and computational costs not being a problem in the future, designing civil engineering structures as optimization problems may be highly beneficial.

11.1 Case Study

The case study evaluates the modifiability of the parametric model by creating a specific bridge design. Further, flutter computations are completed, where aerodynamic derivatives obtained from wind tunnel tests are used.

The critical flutter speed is calculated to $67.23 \frac{m}{s}$, which is less than the calculated criteria for flutter speed. However, the flutter criteria for such large-scale bridges should be based on local wind measurements, and the safety factors included should be carefully chosen. The flutter speed could be included in the optimization process as a cut off constraint, but it requires a lot of experimental results.

11.2 Recommendations for Further Work

The parametric model should be investigated further and improved. Additional variable parameters and more detailed modeling of towers and box girders should be implemented. More research to improve the objective function may be conducted to get more precise results. A gradient based optimization method should be considered when the number of parameters increases.

To include other aeroelastic phenomena such as vortex shedding or flutter in the optimization, it would be necessary to perform wind tunnel testing on each individual cross-sectional design, which is very time-consuming. Otherwise, one solution is to employ a Computational Fluid Dynamic (CFD) model whenever the bridge design changes. The implementation of a CFD model is quite challenging for its high computational cost. However, with the development of more powerful computers in the future, there will be more realistic to introduce more parameters to the model and using CFD.

Regarding the case study: Experimental data from wind tunnel tests should be obtained for a section-model with details, in order to investigate how this will affect the critical flutter velocity.

Bibliography

- [1] Brancaleoni, F. (2016). Concepts and new perspectives for long span bridges. *Romanian journal of transport infrastructure*.
- [2] Brancaleoni, F., Diana, G., Faccioli, E., Fiammenghi, G., Firth, I. P., Gimsing, N. J., Jamiolkowski, M., Sluszkza, P., Solari, G., Valensise, G., et al. (2009). *The Messina Strait Bridge: a challenge and a dream*. CRC Press.
- [3] Chen, X., Kareem, A., and Matsumoto, M. (2001). Multimode coupled flutter and buffeting analysis of long span bridges. *Journal of Wind Engineering and Industrial Aerodynamics*, 89(7-8):649–664.
- [4] Chopra, A. K. (2014). *Dynamics of structures*. Pearson, 4th edition.
- [5] Conn, A. R., Scheinberg, K., and Vicente, L. N. (2009). *Introduction to derivative-free optimization*, volume 8. Siam.
- [6] Gimsing, N. J. and Georgakis, C. T. (2012). *Cable Supported Bridges. Concept and design, Third Edition*. John Wiley Sons, Hoboken, NJ.
- [7] International Organization for Standardization (1984). Iso 6897. *Guidelines for the evaluation of the response of occupants of fixed structures, especially buildings and off-shore structures, to low frequency horizontal motion(0.063 to 1Hz)*.
- [8] Jurado, J. and Albarracín, J. Á. J. (2011). *Bridge aeroelasticity: sensitivity analysis and optimal design*, volume 10. WIT press.
- [9] Kildal, O. and Grongstad, J. (2018). *Master thesis: Wind tunnel testing of bridge decks*.
- [10] Kusano, I., Baldomir, A., Jurado, J. Á., and Hernández, S. (2015). Probabilistic optimization of the main cable and bridge deck of long-span suspension bridges under flutter constraint. *Journal of Wind Engineering and Industrial Aerodynamics*, 146:59–70.
- [11] Kwok, K. C., Qin, X. R., Fok, C., and Hitchcock, P. A. (2012). Wind-induced pressures around a sectional twin-deck bridge model: Effects of gap-width on the aerodynamic forces and vortex shedding mechanisms. *Journal of wind engineering and industrial aerodynamics*, 110:50–61.
- [12] Multiconsult (2015). Concept Study.
- [13] Myrhaug, D. (2005). *TMR4235, Stochastic Theory of Sealoads*. Department of marine technology.

- [14] Newland, D. (2014). *An Introduction to Random Vibrations, Spectral Wavelet Analysis*. Dover publication, 3rd edition.
- [15] Rainieri, C. and Fabbrocino, G. (2014). *Operational Modal Analysis of Civil Engineering Structures, An Introduction and Guide for Applications*. Springer, 1st edition.
- [16] Rambøll (2015). Concept Study.
- [17] Rothwell, A. (2017). *Optimization Methods in Structural Design*, volume 242. Springer.
- [18] Scanlan, Robert H and Tomo, J (2001). Airfoil and bridge deck flutter derivatives. *Engineering Mechanics Structures*.
- [19] Siedziako, B. and Øiseth, O. (2017). On the importance of cross-sectional details in the wind tunnel testing of bridge deck section models. *Procedia Engineering*, 199:3145–3151.
- [20] Statens vegvesen (2013a). Beregninger, grunnlag: Hardangerbura.
- [21] Statens vegvesen (2013b). Teknisk brosjyre: Hardangerbura.
- [22] Strømmen, E. (2010). *Theory of Bridge Aerodynamics*. Springer, 2nd edition.
- [23] Wilhehnina Josefine Visser (1992). Updating Structural Dynamics Models Using Frequency Response Data. *Department of Mechanical Engineering, Imperial College of Science, Technology and Medicine London*.
- [24] Øiseth, Ole and Sigbjørnsson, Ragnar (2010). An alternative analytical approach to prediction of flutter stability limits of cable supported bridges. *Department of Structural Engineering, Norwegian University of Science and Technology*.

Appendix

A Case Study

A.1 Wind Direction 1

A.1.1 Mode Illustrations

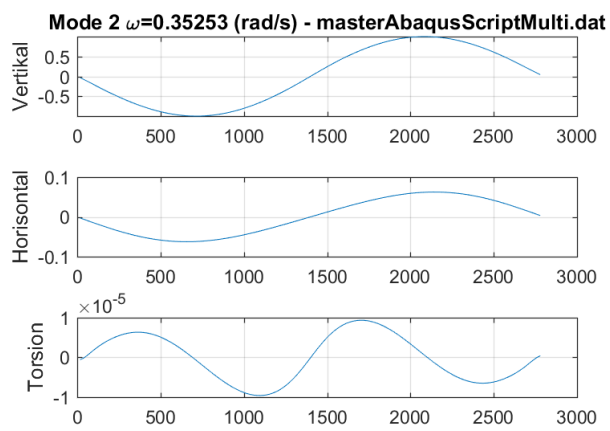


Figure A.1: Mode 2.

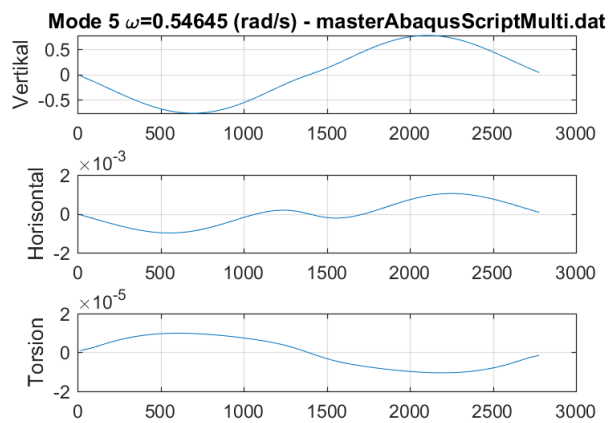


Figure A.2: Mode 5.

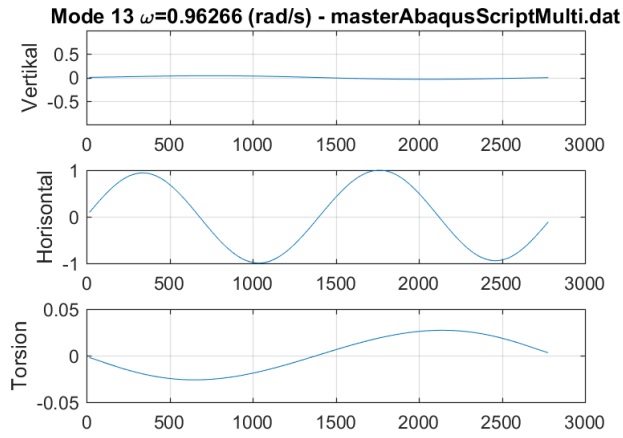


Figure A.3: Mode 13.

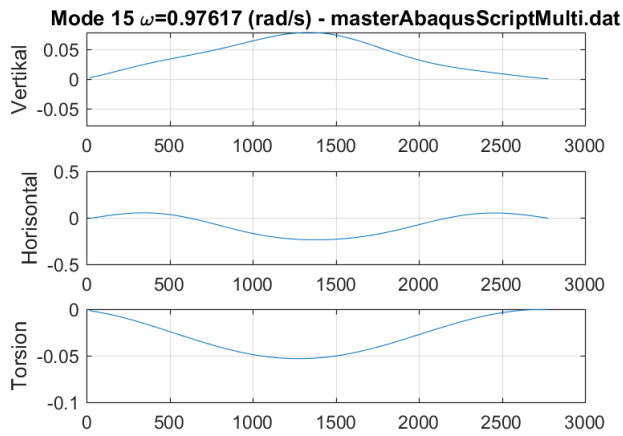


Figure A.4: Mode 15.

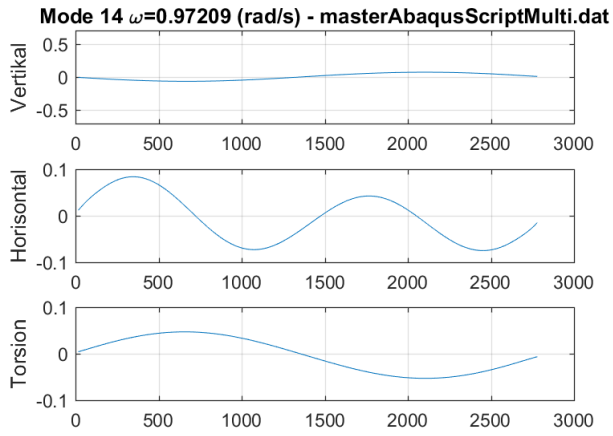


Figure A.5: Mode14.

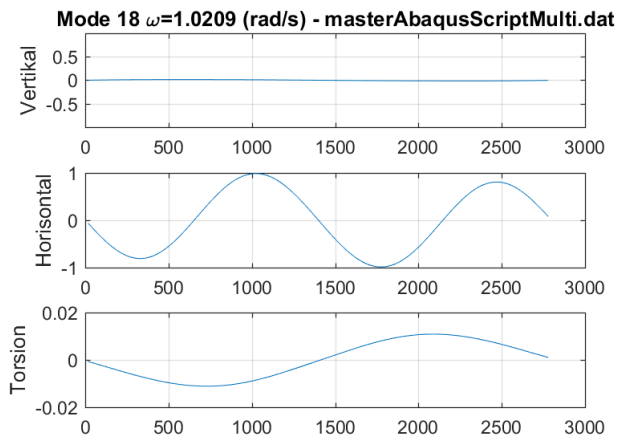
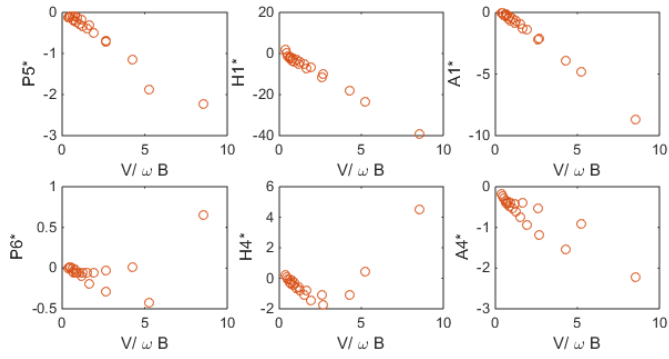
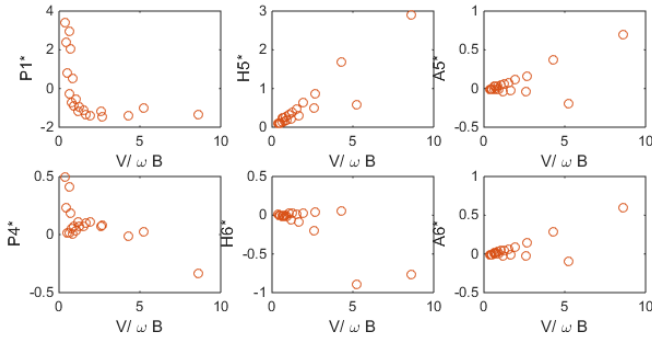


Figure A.6: Mode 18.

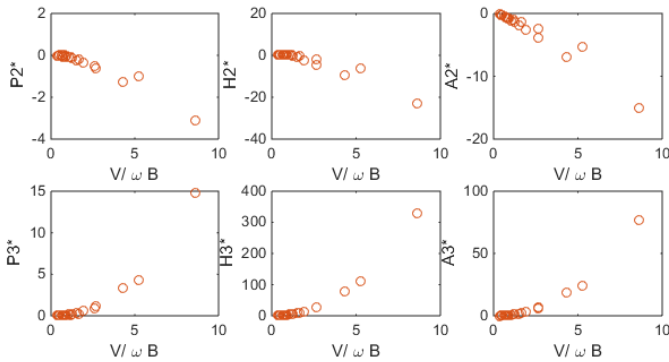
A.1.2 Aerodynamic Derivatives



(a)



(b)



(c)

Figure A.7: Aerodynamic derivatives for vertical (a), horizontal (b) and rotational (c) motions (wind direction 1).

A.2 Wind Direction 2

A.2.1 Flutter Results

Table A.1: Flutter conditions (wind direction 2).

Mode set	Mode no.	Velocity [m/s]	Frequency [Hz]	Reduced velocity
1	5,13	139.10	0.8508	4.42
2	2,13	122.38	0.8777	3.77
3	4,15	83.79	0.7940	2.85
4	2,14	76.21	0.6888	2.99
5	5,14	76.83	0.6841	3.04
6	2,5,14	67.46	0.7643	2.39
7	2,5,13,14	65.27	0.7496	2.35
8	2,5,13,14,15,18	64.57	0.7475	2.33
9	1-20	59.10	0.8081	1.97

A.2.2 Aerodynamic Derivatives

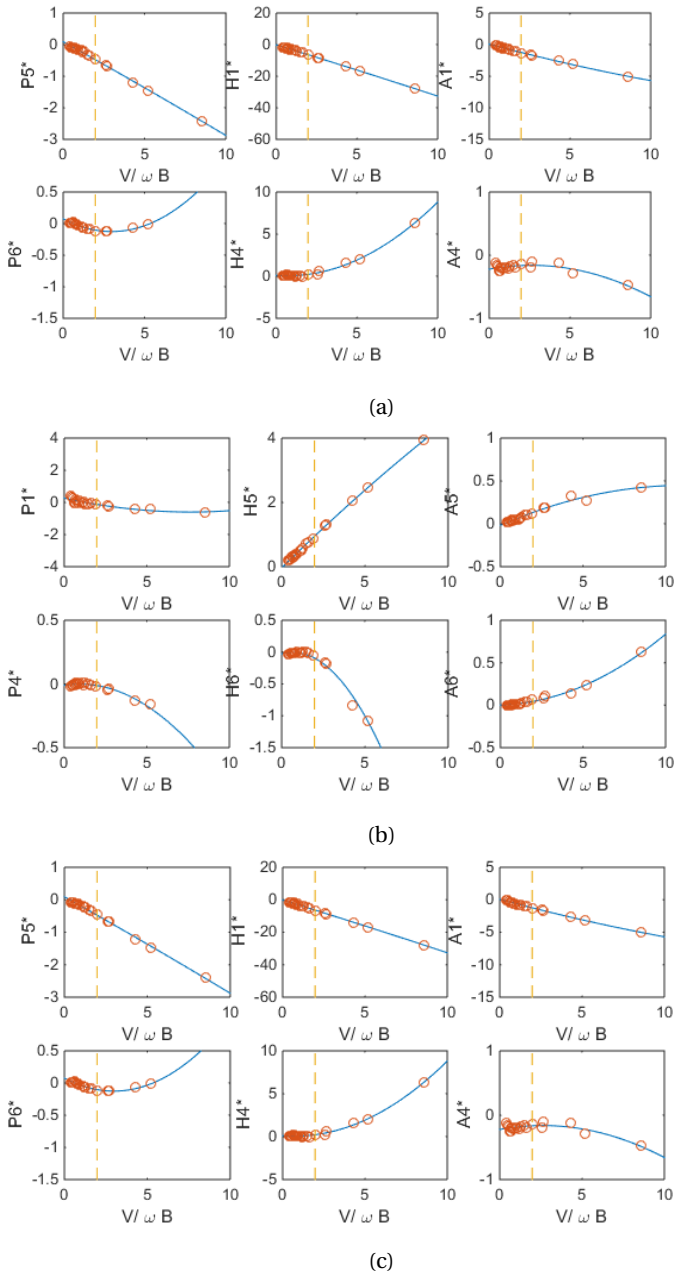


Figure A.8: Aerodynamic derivatives, including fitted line(blue) and reduced velocity value(dotted vertical line) for vertical (a), horizontal (b) and rotational (c) motions (wind direction 2).

B Preliminary Design

Load combinations taken from NS-EN 1990-2002 +N.A.

Eq. 6.10b, tab. N.A. A1.2 (B)

Load comb 1 (Traffic loading):

Vertical load: $Q_{\text{vert.girder.1}} := 1.2 \cdot q_{\text{selfweight}} + 1.5 \cdot q_{\text{traffic}} = 120.644 \cdot \frac{\text{kN}}{\text{m}}$

Using influence lines, the design moment due to vertical loading is:

$$M_{\text{ed.1}} := 384\text{m}^2 \cdot Q_{\text{vert.girder.1}} = 4.633 \times 10^4 \cdot \text{kN} \cdot \text{m}$$

Horizontal load: $Q_{\text{hor.girder.1}} := 1.6 \cdot 0.7 \cdot q_{\text{wind.y}} = 4.386 \cdot \frac{\text{kN}}{\text{m}}$

$$Q_{\text{hor.cable.1}} := 1.6 \cdot 0.7 \cdot q_{\text{wind.cable.y}} = 1.38 \cdot \frac{\text{kN}}{\text{m}}$$

Rotational load: $Q_{\text{rot.girder.1}} := 1.6 \cdot 0.7 \cdot q_{\text{wind.rot}} = 394.722 \cdot \frac{\text{kN}}{\text{m}}$

$$Q_{\text{vert.girder.wind.1}} := 1.6 \cdot 0.7 \cdot q_{\text{wind.z}} = -6.579 \cdot \frac{\text{kN}}{\text{m}}$$

Load comb 2 (Wind loading):

Vertical load: $Q_{\text{vert.girder.2}} := 1.2 \cdot q_{\text{selfweight}} + 1.5 \cdot 0 \cdot q_{\text{traffic}} = 90.644 \cdot \frac{\text{kN}}{\text{m}}$

Using influence lines, the design moment due to vertical loading is:

$$M_{\text{ed.2}} := 384\text{m}^2 \cdot Q_{\text{vert.girder.2}} = 3.481 \times 10^4 \cdot \text{kN} \cdot \text{m}$$

Horizontal load: $Q_{\text{hor.girder.2}} := 1.6 \cdot q_{\text{wind.y}} = 6.265 \cdot \frac{\text{kN}}{\text{m}}$

$$Q_{\text{hor.cable.2}} := 1.6 \cdot q_{\text{wind.cable.y}} = 1.972 \cdot \frac{\text{kN}}{\text{m}}$$

Rotational load: $Q_{\text{rot.girder.2}} := 1.6 \cdot q_{\text{wind.rot}} = 563.888 \cdot \frac{\text{kN}}{\text{m}}$

$$Q_{\text{vert.girder.wind.2}} := 1.6 \cdot q_{\text{wind.z}} = -9.398 \cdot \frac{\text{kN}}{\text{m}}$$

Load combinations taken from NS-EN 1990-2002 +N.A.

Eq. 6.10b, tab. N.A. A1.2 (B)

Load comb 1 (Traffic loading):

Vertical load: $Q_{\text{vert.girder.1}} := 1.2 \cdot q_{\text{selfweight}} + 1.5 \cdot q_{\text{traffic}} = 120.644 \cdot \frac{\text{kN}}{\text{m}}$

Using influence lines, the design moment due to vertical loading is:

$$M_{\text{ed.1}} := 384\text{m}^2 \cdot Q_{\text{vert.girder.1}} = 4.633 \times 10^4 \cdot \text{kN} \cdot \text{m}$$

Horizontal load: $Q_{\text{hor.girder.1}} := 1.6 \cdot 0.7 \cdot q_{\text{wind.y}} = 4.386 \cdot \frac{\text{kN}}{\text{m}}$

$$Q_{\text{hor.cable.1}} := 1.6 \cdot 0.7 \cdot q_{\text{wind.cable.y}} = 1.38 \cdot \frac{\text{kN}}{\text{m}}$$

Rotational load: $Q_{\text{rot.girder.1}} := 1.6 \cdot 0.7 \cdot q_{\text{wind.rot}} = 394.722 \cdot \frac{\text{kN}}{\text{m}}$

$$Q_{\text{vert.girder.wind.1}} := 1.6 \cdot 0.7 \cdot q_{\text{wind.z}} = -6.579 \cdot \frac{\text{kN}}{\text{m}}$$

Load comb 2 (Wind loading):

Vertical load: $Q_{\text{vert.girder.2}} := 1.2 \cdot q_{\text{selfweight}} + 1.5 \cdot 0 \cdot q_{\text{traffic}} = 90.644 \cdot \frac{\text{kN}}{\text{m}}$

Using influence lines, the design moment due to vertical loading is:

$$M_{\text{ed.2}} := 384\text{m}^2 \cdot Q_{\text{vert.girder.2}} = 3.481 \times 10^4 \cdot \text{kN} \cdot \text{m}$$

Horizontal load: $Q_{\text{hor.girder.2}} := 1.6 \cdot q_{\text{wind.y}} = 6.265 \cdot \frac{\text{kN}}{\text{m}}$

$$Q_{\text{hor.cable.2}} := 1.6 \cdot q_{\text{wind.cable.y}} = 1.972 \cdot \frac{\text{kN}}{\text{m}}$$

Rotational load: $Q_{\text{rot.girder.2}} := 1.6 \cdot q_{\text{wind.rot}} = 563.888 \cdot \frac{\text{kN}}{\text{m}}$

$$Q_{\text{vert.girder.wind.2}} := 1.6 \cdot q_{\text{wind.z}} = -9.398 \cdot \frac{\text{kN}}{\text{m}}$$

Mass of inertia estimation:

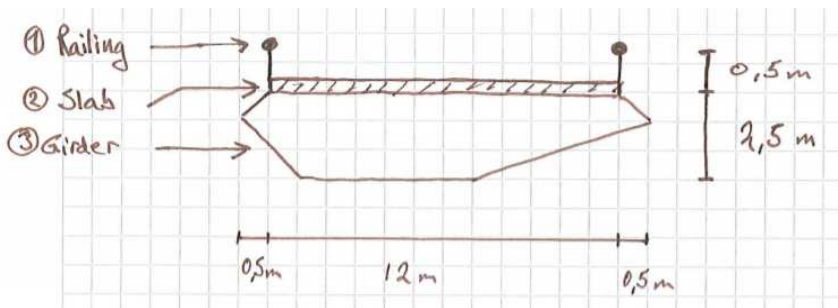
Original design

From Cross-X:

$$I_z := 6.3188 \text{m}^4 \quad I_y := 0.4398 \text{m}^4$$

$$\rho := 7850 \frac{\text{kg}}{\text{m}^3}$$

Assumption: Here z-direction is vertical, and y-direction is horizontal.



$$m_{\text{railing}} := 150 \frac{\text{kg}}{\text{m}} \quad (\text{for each railing})$$

$$m_{\text{slab}} := \frac{12}{12} 3000 \frac{\text{kg}}{\text{m}} = 3 \times 10^3 \frac{\text{kg}}{\text{m}}$$

Scaled value from the Hardanger bridge
Here: same width of the slab*y-direction:*

$$1: \quad I_{m,y.1} := 2 \cdot 1.75^2 \text{m}^2 \cdot m_{\text{railing}} = 918.75 \cdot \text{kg} \cdot \frac{\text{m}^2}{\text{m}}$$

$$2: \quad I_{m,y.2} := 1.25^2 \text{m}^2 \cdot m_{\text{slab}} = 4.688 \times 10^3 \cdot \text{kg} \cdot \frac{\text{m}^2}{\text{m}}$$

$$3: \quad I_{m,y.3} := I_y \cdot \rho = 3.452 \times 10^3 \cdot \text{kg} \cdot \frac{\text{m}^2}{\text{m}}$$

$$I_{m,y.\text{tot}} := I_{m,y.1} + I_{m,y.2} + I_{m,y.3} = 9.059 \times 10^3 \cdot \text{kg} \cdot \frac{\text{m}^2}{\text{m}}$$

z-direction:

$$1: \quad I_{m.z.1} := 2 \cdot 12^2 \text{ m}^2 \cdot m_{\text{railing}} = 4.32 \times 10^4 \cdot \text{kg} \cdot \frac{\text{m}^2}{\text{m}}$$

$$2: \quad I_{m.z.2} := \frac{1}{12} 12^2 \text{ m}^2 \cdot m_{\text{slab}} = 3.6 \times 10^4 \cdot \text{kg} \cdot \frac{\text{m}^2}{\text{m}}$$

$$3: \quad I_{m.z.3} := I_z \cdot \rho = 4.96 \times 10^4 \cdot \text{kg} \cdot \frac{\text{m}^2}{\text{m}}$$

$$I_{m.z.\text{tot}} := I_{m.z.1} + I_{m.z.2} + I_{m.z.3} = 1.288 \times 10^5 \cdot \text{kg} \cdot \frac{\text{m}^2}{\text{m}}$$

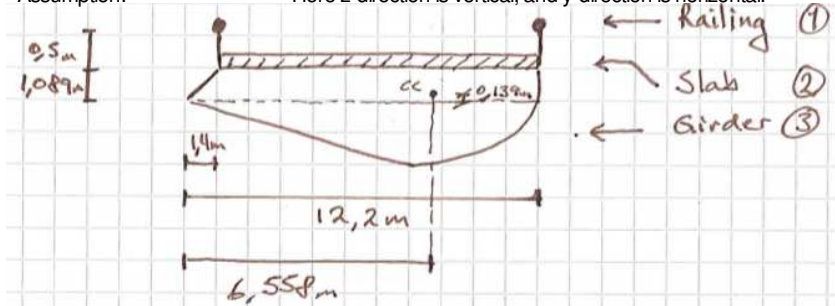
The example study - multiconsult design

From multiconsult:

$$I_z := 5.581 \text{ m}^4 \quad I_y := 0.36 \text{ m}^4$$

Assumption:

Here z-direction is vertical, and y-direction is horizontal.



$$m_{\text{slab}} := \frac{10.8}{12} 3000 \frac{\text{kg}}{\text{m}} = 2.7 \times 10^3 \frac{\text{kg}}{\text{m}}$$

Scaled value from the Hardanger bridge

y-direction:

$$1: \quad I_{m,y.1} := 2 \cdot 1.458^2 \text{ m}^2 \cdot m_{\text{railing}} = 637.729 \cdot \text{kg} \cdot \frac{\text{m}^2}{\text{m}}$$

$$2: \quad I_{m,y.2} := 0.958^2 \text{ m}^2 \cdot m_{\text{slab}} = 2.478 \times 10^3 \cdot \text{kg} \cdot \frac{\text{m}^2}{\text{m}}$$

$$3: \quad I_{m,y.3} := I_y \cdot \rho = 2.826 \times 10^3 \cdot \text{kg} \cdot \frac{\text{m}^2}{\text{m}}$$

$$I_{m,y.\text{tot}} := I_{m,y.1} + I_{m,y.2} + I_{m,y.3} = 5.942 \times 10^3 \cdot \text{kg} \cdot \frac{\text{m}^2}{\text{m}}$$

z-direction:

$$1: \quad I_{m.z.1} := 2 \cdot 10.8^2 \text{ m}^2 \cdot m_{\text{railing}} = 3.499 \times 10^4 \cdot \text{kg} \cdot \frac{\text{m}^2}{\text{m}}$$

$$2: \quad I_{m.z.2} := \frac{1}{12} 10.8^2 \text{ m}^2 \cdot m_{\text{slab}} = 2.624 \times 10^4 \cdot \text{kg} \cdot \frac{\text{m}^2}{\text{m}}$$

$$3: \quad I_{m.z.3} := I_z \cdot \rho = 4.381 \times 10^4 \cdot \text{kg} \cdot \frac{\text{m}^2}{\text{m}}$$

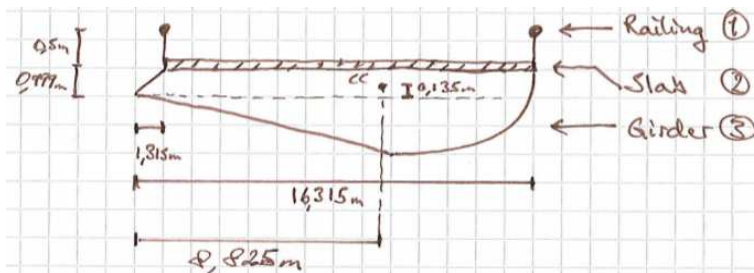
$$I_{m.z.\text{tot}} := I_{m.z.1} + I_{m.z.2} + I_{m.z.3} = 1.05 \times 10^5 \cdot \text{kg} \cdot \frac{\text{m}^2}{\text{m}}$$

The example study - multiconsult design

From multiconsult:

$$I_z := 13.35\text{m}^4 \quad I_y := 0.4768\text{m}^4$$

Assumption: Here z-direction is vertical, and y-direction is horizontal.



$$m_{\text{slab}} := \frac{15}{12} 3000 \frac{\text{kg}}{\text{m}} = 3.75 \times 10^3 \frac{\text{kg}}{\text{m}}$$

Scaled value from the Hardanger bridge

y-direction:

$$1: \quad I_{m,y.1} := 2 \cdot 1.364^2 \text{m}^2 \cdot m_{\text{railing}} = 558.149 \cdot \text{kg} \cdot \frac{\text{m}^2}{\text{m}}$$

$$2: \quad I_{m,y.2} := 0.864^2 \text{m}^2 \cdot m_{\text{slab}} = 2.799 \times 10^3 \cdot \text{kg} \cdot \frac{\text{m}^2}{\text{m}}$$

$$3: \quad I_{m,y.3} := I_y \cdot \rho = 3.743 \times 10^3 \cdot \text{kg} \cdot \frac{\text{m}^2}{\text{m}}$$

$$I_{m,y.\text{tot}} := I_{m,y.1} + I_{m,y.2} + I_{m,y.3} = 7.1 \times 10^3 \cdot \text{kg} \cdot \frac{\text{m}^2}{\text{m}}$$

z-direction:

$$1: \quad I_{m.z.1} := 2 \cdot 15^2 \text{ m}^2 \cdot m_{\text{railing}} = 6.75 \times 10^4 \cdot \text{kg} \cdot \frac{\text{m}^2}{\text{m}}$$

$$2: \quad I_{m.z.2} := \frac{1}{12} 15^2 \text{ m}^2 \cdot m_{\text{slab}} = 7.031 \times 10^4 \cdot \text{kg} \cdot \frac{\text{m}^2}{\text{m}}$$

$$3: \quad I_{m.z.3} := I_z \cdot \rho = 1.048 \times 10^5 \cdot \text{kg} \cdot \frac{\text{m}^2}{\text{m}}$$

$$I_{m.z.\text{tot}} := I_{m.z.1} + I_{m.z.2} + I_{m.z.3} = 2.426 \times 10^5 \cdot \text{kg} \cdot \frac{\text{m}^2}{\text{m}}$$

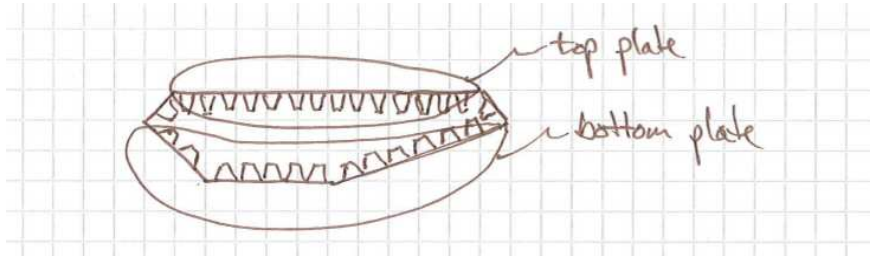
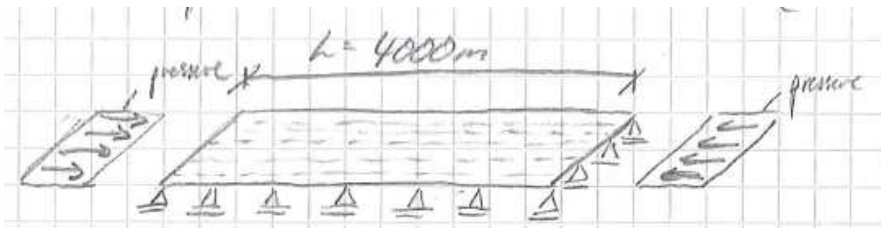
Buckling load for plates with longitudinal stiffeners:

Figure above shows the parts which are included for top and bottom plate.

The assumed boundary conditions are shown below, and is the same for both top and bottom plate.



$L := 4000\text{mm}$ (This is the distance between the transverse stiffening plates along the girder)

Bottom plate:

Cross-X gives:

$$I_{y,b} := 4.09 \cdot 10^{10} \text{ mm}^4$$

$$A_b := 1.7152 \cdot 10^5 \text{ mm}^2$$

$$f_y := 355 \text{ MPa} \quad E := 210000 \text{ MPa}$$

$$f_d := \frac{f_y}{1.05}$$

Cross section class: $\epsilon := 0.81$

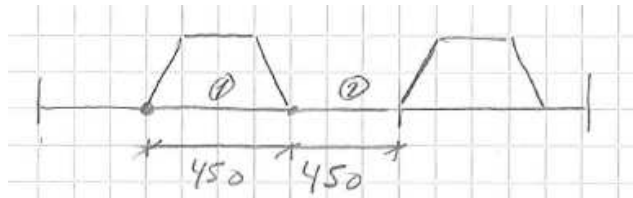
NS-EN 1993-1-1, Tab.5.2

Plate: $t_p := 8 \text{ mm}$ $c_p := 450 \text{ mm}$

(See the preliminary design section for dimensions)

$$\frac{c_p}{t_p \cdot \epsilon} = 69.444 \rightarrow \text{Class 4}$$

Plate 1 and 2 is identical,
i.e., the reduction is the
same



Stiffeners:

Number 1: $t_{s1} := 6 \text{ mm}$ $c_{s1} := 260 \text{ mm}$

$$\frac{c_{s1}}{t_{s1} \cdot \epsilon} = 53.498 \rightarrow \text{Class 4}$$

Number 2: $t_{s2} := 6 \text{ mm}$ $c_{s2} := 190 \text{ mm}$

$$\frac{c_{s2}}{t_{s2} \cdot \epsilon} = 39.095 \rightarrow \text{Not class 4}$$

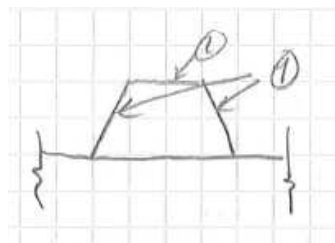


Plate reductions:

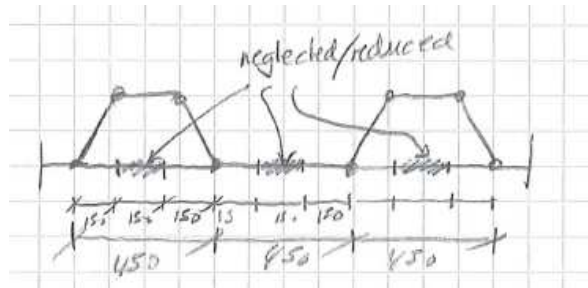
NS-EN 1993-1-5, 4.4 (Assumed pure pressure)

$$\text{Slenderness factor: } \lambda_p := \frac{c_p}{t_p} = 1.223$$

$$\text{Eq.(4.2) } \rho := \frac{\lambda_p - 0.055 \cdot (3 + 1)}{\lambda_p^2} = 0.671$$

$$\text{Tab 4.1 } b_{\text{eff}} := \rho \cdot c_p = 0.302 \text{ m}$$

$$\text{Sets it to: } b_{\text{eff}} := 0.3 \text{ m}$$



$$A_{c,\text{eff},\text{loc},\text{plate}} := 1.1190 \cdot 10^5 \text{ mm}^2 - 33600 \text{ mm}^2 = 7.83 \times 10^4 \cdot \text{mm}^2 \text{ (Cross X)}$$

Stiffeners reduction:

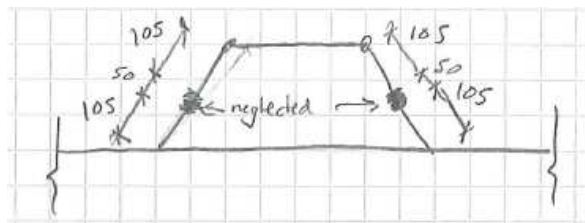
NS-EN 1993-1-5, 4.4

$$\text{Slenderness factor: } \lambda_p := \frac{c_{s1}}{28.4 \cdot \varepsilon \cdot 2} = 0.942$$

$$\text{Eq.(4.2) } \rho := \frac{\lambda_p - 0.055 \cdot (3 + 1)}{\lambda_p^2} = 0.814$$

$$\text{Tab 4.1 } b_{\text{eff}} := \rho \cdot c_{s1} = 0.212 \text{ m}$$

$$\text{Sets it to: } b_{\text{eff}} := 0.2 \text{ m}$$



$$A_{c,\text{eff},\text{loc},\text{tot}} := A_b - 33600\text{mm}^2 - 5600\text{mm}^2 = 1.323 \times 10^5 \cdot \text{mm}^2 \quad (14 \text{ stiffeners})$$

Annex A: Calculations related to the bottom plate:

$$b := 12000\text{mm} \quad (\text{The width of the bottom plate})$$

$$\nu := 0.3$$

$$A_p := 1.119 \cdot 10^5 \text{mm}^2$$

$$A_{sl} := A_b - A_p = 5.962 \times 10^4 \cdot \text{mm}^2 \quad (\text{The gross area of the longitudinal stiffeners})$$

$$I_p := 2.74 \cdot 10^{10} \text{mm}^4$$

$$I_{sl} := 4.0921 \cdot 10^{10} \text{mm}^4 \quad (\text{Value from Cross-X})$$

$$\gamma := \frac{I_{sl}}{I_p} = 1.493$$

$$\delta := \frac{A_{sl}}{A_p} = 0.533$$

$$\alpha := \frac{L}{b} = 0.333$$

$$\psi := 1 \quad \alpha \leq \sqrt[4]{\gamma} \quad \rightarrow \quad k_{\sigma,p} := \frac{\left[2 \cdot \left[(1 - \alpha^2)^2 + \gamma - 1 \right] \right]}{\alpha^2 \cdot (\psi + 1) \cdot (1 + \delta)} = 7.537 \quad (\text{Buckling factor})$$

$$\sigma_E := 190000 \text{MPa} \cdot \left(\frac{t_p}{b} \right)^2 = 0.084 \cdot \text{MPa}$$

$$\sigma_{cr,p} := k_{\sigma,p} \cdot \sigma_E = 0.636 \cdot \text{MPa}$$

NS-EN 1993 1-5,4.5.3

$$(3) \quad \sigma_{\text{cr.sl}} := \frac{(\pi^2 \cdot E \cdot I_{\text{sl}})}{A_{\text{b}} \cdot L^2} = 3.091 \times 10^4 \cdot \text{MPa}$$

NS-EN 1993 1-3,4.5.4

Interaction between column and plate buckling:

$$\xi := \frac{\sigma_{\text{cr.p}}}{\sigma_{\text{cr.sl}}} - 1 = -1$$

$$\rightarrow \quad \rho_{\text{c}} := 1$$

$$N_{\text{x.Rd}} := f_{\text{d}} \cdot A_{\text{c.eff.loc.tot}} \cdot \rho_{\text{c}} = 4.474 \times 10^4 \cdot \text{kN}$$

This force is computational equivalent to a reduced critical design stress:

$$\sigma_{\text{cr.red}} := \frac{N_{\text{x.Rd}}}{A_{\text{b}}} = 260.825 \cdot \text{MPa}$$

Top plate:

$$I_y := 2020 \cdot 10^6 \text{ mm}^4$$

$$A_t := 24.28 \times 10^4 \cdot \text{mm}^2$$

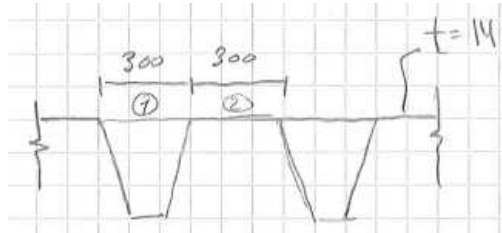
Cross section class: $\epsilon := 0.81$

NS-EN 1993-1-1, Tab.5.2

Plate: $t_p := 14 \text{ mm}$ $c_p := 300 \text{ mm}$

(See the preliminary design section for dimensions)

$$\frac{c_p}{t_p \cdot \epsilon} = 26.455 \rightarrow \text{Not Class 4}$$



Here plate 1 and 2 are in equal class

Stiffener 1 (See Fig.):

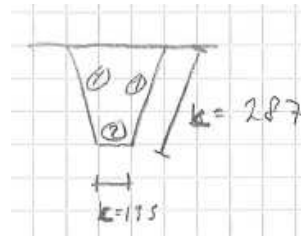
$$c_{s1} := 287 \text{ mm} \quad t_{s1} := 6 \text{ mm}$$

$$\frac{c_{s1}}{t_{s1} \cdot \epsilon} = 59.053 \rightarrow \text{Class 4}$$

Stiffener 2 (See Fig.):

$$c_{s2} := 135 \text{ mm} \quad t_{s2} := 6 \text{ mm}$$

$$\frac{c_{s2}}{t_{s2} \cdot \epsilon} = 27.778 \rightarrow \text{Not Class 4}$$



Reduction of stiffener 1:

NS-EN 1993-1-5, 4-4 (Assumed pure pressure)

$$\text{Slenderness factor: } \lambda_p := \frac{\frac{c_{s1}}{t_{s1}}}{28.4 \cdot \varepsilon \cdot 2} = 1.04$$

$$\text{Eq.(4.2) } \rho := \frac{\lambda_p - 0.055 \cdot (3 + 1)}{\lambda_p^2} = 0.758$$

$$\text{Tab 4.1 } b_{\text{eff}} := \rho \cdot c_{s1} = 0.218 \text{ m}$$

$$\text{Sets it to: } b_{\text{eff}} := 0.22 \text{ m} \quad b_{\text{red}} := 67 \text{ mm}$$

$$A_{c,\text{eff},\text{loc},\text{tot}} := A_t - 18 \cdot 2 \cdot t_{s1} \cdot b_{\text{red}} = 2.283 \times 10^5 \cdot \text{mm}^2 \quad (\text{Tot. 18 stiffeners})$$

Annex A: Calculations related to the top plate:

$$b := 12000\text{mm} \quad (\text{The width of the bottom plate})$$

$$\nu := 0.3$$

$$A_p := b \cdot t_p = 1.68 \times 10^5 \cdot \text{mm}^2$$

$$A_{sl} := 244600\text{mm}^2 - A_p = 7.66 \times 10^4 \cdot \text{mm}^2 \quad (\text{The gross area of the longitudinal stiffeners})$$

$$I_p := \frac{b t_p^3}{12 \cdot (1 - \nu^2)} = 3.015 \times 10^6 \cdot \text{mm}^4$$

$$I_{sl} := 2026.2 \cdot 10^6 \text{mm}^4 \quad (\text{Value from Cross-X})$$

$$\gamma := \frac{I_{sl}}{I_p} = 671.954$$

$$\delta := \frac{A_{sl}}{A_p} = 0.456$$

$$\alpha := \frac{L}{b} = 0.333$$

$$\psi := 1$$

$$\alpha \leq \sqrt[4]{\gamma} \quad \rightarrow \quad k_{\sigma,p} := \frac{\left[2 \cdot \left[(1 - \alpha^2)^2 + \gamma - 1 \right] \right]}{\alpha^2 \cdot (\psi + 1) \cdot (1 + \delta)} = 4.152 \times 10^3 \quad (\text{Buckling factor})$$

$$\sigma_E := 190000\text{MPa} \cdot \left(\frac{t_p}{h} \right)^2 = 0.259 \cdot \text{MPa}$$

$$\sigma_{cr,p} := k_{\sigma,p} \cdot \sigma_E = 1.074 \times 10^3 \cdot \text{MPa}$$

NS-EN 1993 1-5,4.5.3

$$A_{sl,1} := 244600\text{mm}^2$$

$$E := 210000\text{MPa}$$

$$(3) \quad \sigma_{cr,sl} := \frac{\left(\pi^2 \cdot E \cdot I_{sl} \right)}{A_{sl,1} \cdot L^2} = 1.073 \times 10^3 \cdot \text{MPa}$$

Reduction factor, χ :

$$i := \sqrt{\frac{I_{sl}}{A_{sl.1}}} = 91.015 \cdot \text{mm} \quad e := 112.4 \text{mm} \quad (\text{Cross X})$$

$$\alpha_e := 0.34 + \frac{0.09}{\frac{i}{e}} = 0.451$$

NS-EN 1993 1-1, 6.3.1.2

$$N_{cr} := \frac{\pi^2 \cdot E \cdot I_{sl}}{L^2} = 2.625 \times 10^5 \cdot \text{kN}$$

$$\lambda := \sqrt{\frac{A_{c,eff,loc,tot} \cdot f_y}{N_{cr}}} = 0.556$$

$$\phi := 0.5 \cdot \left[1 + \alpha_e \cdot (\lambda - 0.2) + \lambda^2 \right] = 0.735$$

$$\chi_c := \frac{1}{\phi + \sqrt{\phi^2 - \lambda^2}} = 0.823$$

NS-EN 1993 1-3, 4.5.4

Interaction between column and plate buckling:

$$\xi := \frac{\sigma_{cr,p}}{\sigma_{cr,sl}} - 1 = 7.406 \times 10^{-4}$$

4.4 (2)

$$\lambda_p := \frac{\frac{b}{t_p}}{28.4 \cdot 0.81 \cdot 2} = 18.63 \quad \rightarrow \quad \rho := \frac{\lambda_p - 0.055 \cdot 4}{\lambda_p^2} = 0.053$$

4.5.4:

$$\rho_c := (\rho - \chi_c) \xi \cdot (2 - \xi) + \chi_c = 0.822$$

$$N_{x,Rd} := f_d \cdot A_{c,eff,loc,tot} \cdot \rho_c = 6.344 \times 10^4 \cdot \text{kN}$$

This force is computational equivalent to a reduced critical design stress:

$$\sigma_{cr,red} := \frac{N_{x,Rd}}{A_t} = 261.285 \cdot \text{MPa}$$

Static load: Cables

$$A := 0.53375 \text{ m}^2 \quad (\text{The average main cable area})$$

$$\varnothing := \left(\sqrt{A \cdot \frac{4}{\pi}} \right) = 0.824 \text{ m}$$

$$v := 15 \cdot (10)^{-6} \frac{\text{m}^2}{\text{s}}$$

$$v := 45.7 \frac{\text{m}}{\text{s}} \quad (\text{See wind load section})$$

$$\rho := 1.25 \frac{\text{kg}}{\text{m}^3}$$

NS-EN 1991-1-4(7.9):

The Raynolds number becomes:

$$\text{Re} := \frac{\varnothing \cdot v}{\nu} = 2.512 \times 10^6$$

Surface roughness is set equal as for the Hardanger bridge

$$k := 0.2 \text{ mm}$$

$$\frac{k}{\varnothing} = 2.426 \times 10^{-4}$$

Based on Figure 7.28:

$$C_1 := 0.7$$

The value is increased due to additional materials on the cables

$$C_1 := 1.0$$

The drag force becomes:

$$q := 0.5 \cdot \rho \cdot v^2 \quad (\text{Velocity pressure})$$

$$F_{\text{drag}} := C_1 \cdot q \cdot \varnothing = 1.076 \times 10^3 \cdot \frac{\text{N}}{\text{m}}$$

C MATLAB Code

Listing C.1: generateNodes1.m

```
1 function [A_chosen, sag]=generateNodes1(dist, towerHeight, sag)
2 %Genererer noder og element til Abaqus
3 % Nullpunkt satt til senteret av brobanen i en ende av banen (under tarn)
4
5 girderLength = 2800; %lengde av girder
6
7 %dist = 25; %avstand fra senter brobane til senter box girder
8 connDist = 7; %avstand fra senter box girder feste henger (halve bredden av en box girder)
9 connHeight = 1.5; %hoyde pa feste mellom henger of box girder (ift. senter til girder)
10 distHanger = 10; %antall elmenter mellom hengere
11 SClength = 720; %lengde (x-retning) sidekabler
12 %towerHeight = 350; %hoyde pa tarn (fra senter av brobane til topp tarn)
13 %sag = 320; %sag pa kabel (avstand fra topp kabel til labeste punkt pa kabel)
14 breddebunn = 80; %Avstand mellom benene pa tarn
15 ben = 35; %Avstand fra veibane til bakke/lengde pa ben
16
17 [sag, A_chosen] = sag_calc(sag); %korrigerer sa faktisk sag blir riktig etter prestressing
18
19 dx=2; %Spacing between nodes at girder/lengden pa element
20 N = girderLength/dx; %Number of nodes along girder
21
22 % x=[0,N, girderLength];
23 x=[0, girderLength/dx, girderLength];
24 y=[towerHeight, towerHeight-sag, towerHeight];
25 p=polyfit(x,y,2);
26 y=[0,40,0];
27 q=polyfit(x,y,2);
28
29 %lage noder til girderen, connection, kabler og elementene til connection
30 fid=fopen('geoGirders.txt','w');
31 fid2=fopen('geoConnection.txt','w');
32 j=1000;
33 k=N/2+1000;
34 fid4=fopen('geoCable.txt','w');
35 for i=1:N+1
36     b=dx*i-dx;
37     x=(i-1)*dx;
38
39     z=q(1)*x^2+q(2)*x+q(3);
40     fprintf(fid, '%i, %f, %f, %f\r\n', i, b, -dist, z);
41     fprintf(fid, '%i, %f, %f, %f\r\n', i+N+1, b, dist, z);
42     fprintf(fid, '%i, %f, %f, %f\r\n', i+30000, b, 0, z);
```

```

43     fprintf(fid2, '%i, %f, %f, %f\r\n', i+4000,b,-dist-connDist,z+connHeight);
44     fprintf(fid2, '%i, %f, %f, %f\r\n', i+N+1+4000,b,dist+connDist,z+connHeight);
45
46     j=j+1;
47     k=k+1;
48     z=p(1)*x^2+p(2)*x+p(3);
49     fprintf(fid4, '%i, %f, %f, %f\r\n', i+10000,b,-dist-connDist,z);
50     fprintf(fid4, '%i, %f, %f, %f\r\n', i+N+1+10000,b,dist+connDist,z);
51 end
52 fprintf(fid, '%i, %f, %f, %f\r\n', 2*N+4,0,-dist,0);
53 fprintf(fid, '%i, %f, %f, %f\r\n', 2*N+5,0,dist,0);
54 fprintf(fid, '%i, %f, %f, %f\r\n', 2*N+6,b,-dist,0);
55 fprintf(fid, '%i, %f, %f, %f\r\n', 2*N+7,b,dist,0);
56
57 fclose(fid);true;
58 fclose(fid2);true;
59 fclose(fid4);true;
60 fid=fopen('topTowerNodes.txt','w');
61 a=10001;
62 fprintf(fid, '%i, %i, %i, %i\r\n', a,a+N,a+N+1,a+2*N+1);
63 fclose(fid);true;
64 fid=fopen('girderEndNodes.txt','w');
65 fprintf(fid, '%i, %i, %i, %i\r\n', 1,N+1,N+2,2*N+1);
66 fclose(fid);true;
67
68 %lage element til girder
69 fid=fopen('elGirders1.txt','w');
70 fid3=fopen('elGirders2.txt','w');
71 fid2=fopen('elCable.txt','w');
72 j=1;
73 k=N/2+1;
74 for i=2:2:N
75     a=i-1;
76     b=i;
77     c=i+1;
78     fprintf(fid, '%i, %i, %i, %i\r\n', j,a,b,c);
79     fprintf(fid3, '%i, %i, %i, %i\r\n', k,a+N+1,b+N+1,c+N+1);
80     j=j+1;
81     k=k+1;
82 end
83 fclose(fid);true;
84 fclose(fid2);true;
85 fclose(fid3);true;
86
87 fid=fopen('elHangers.txt','w');
88 fid2=fopen('elConnection.txt','w');
89 fid3=fopen('elGirderConnection.txt','w');
90 fid4=fopen('midtNoder.txt','w');
91 j=2000;
92 k=3000;

```

```

93 for i=(distHanger:distHanger:N-distHanger)+1
94     a=4000;
95     fprintf(fid, '%i, %i, %i\r\n', j+5000,a+i,i+10000);
96     fprintf(fid, '%i, %i, %i\r\n', k+5000,a+i+N+1,i+10000+N+1);
97     fprintf(fid2, '%i, %i, %i\r\n', j,i,i+a);
98     fprintf(fid2, '%i, %i, %i\r\n', j+1000,i+N+1,i+a+N+1);
99
100     p=30000;
101     fprintf(fid3, '%i, %i, %i\r\n', j+200,i,i+p);
102     fprintf(fid3, '%i, %i, %i\r\n', j+500,i+p,i+N+1);
103     fprintf(fid4, '%i\r\n', i+p);
104
105     j=j+1;
106     k=k+1;
107 end
108 fclose(fid); true;
109 fclose(fid2); true;
110 fclose(fid3); true;
111 fclose(fid4); true;
112
113 fid=fopen('elCable.txt','w');
114 j=10000;
115 k=12000;
116 for i=1:N
117     a=i+10000;
118     %     b=i+11501;
119     b=i+10001+N;
120     fprintf(fid, '%i, %i, %i\r\n', j,a,a+1);
121     fprintf(fid, '%i, %i, %i\r\n', k,b,b+1);
122     j=j+1;
123     k=k+1;
124 end
125 fclose(fid); true;
126
127 %Lage noder til sidekabler
128 fid=fopen('geoSideCable.txt','w');
129 fid2=fopen('elSideCable.txt','w');
130 fprintf(fid2, '%i, %i, %i\r\n', 14999,15000,10000+2*N+2);
131 fprintf(fid2, '%i, %i, %i\r\n', 15999,16000,10000+N+1);
132 fprintf(fid2, '%i, %i, %i\r\n', 16999,17000,10000+N+2);
133 fprintf(fid2, '%i, %i, %i\r\n', 17999,18000,10001);
134 j=15000;
135 k=16000;
136 for i=0:(SLength/dx)-1
137     a= (i+1)*dx;
138     b= towerHeight-dx*(towerHeight/SLength)*(i+1);
139
140     fprintf(fid, '%i, %f, %f, %f\r\n', i+15000,girderLength+a,dist+connDist,b);
141     fprintf(fid, '%i, %f, %f, %f\r\n', i+16000,girderLength+a,-dist-connDist,b);
142     fprintf(fid, '%i, %f, %f, %f\r\n', i+17000,-a,dist+connDist,b);

```

```

143     fprintf(fid, '%i, %f, %f, %f\r\n', i+18000,-a,-dist-connDist,b);
144
145     if j==15000+(Sclength/dx)-1
146         break
147     end
148     fprintf(fid2, '%i, %i, %i\r\n', j,i+15000,i+15000+1);
149     fprintf(fid2, '%i, %i, %i\r\n', k,i+16000,i+16000+1);
150     fprintf(fid2, '%i, %i, %i\r\n', j+2000,i+17000,i+17000+1);
151     fprintf(fid2, '%i, %i, %i\r\n', k+2000,i+18000,i+18000+1);
152     j=j+1;
153     k=k+1;
154 end
155 fclose(fid); true;
156 fclose(fid2); true;
157 fid=fopen('supportNodes.txt','w');
158 a=1000;
159 fprintf(fid, '%i, %i, %i, %i\r\n', j,j+a,j+2*a,j+3*a);
160 fclose(fid); true;
161
162 %Tarn
163 breddetopp = 2*(dist+connDist);
164 d=(breddebunn-breddetopp)/2;
165 totthoyde = towerHeight+ben;
166 s=d/totthoyde;
167 fid=fopen('geotarn.txt','w');
168 fid2=fopen('eltarn.txt','w');
169 j=20000;
170 for i = 1:totthoyde
171     if i==towerHeight
172         fprintf(fid2, '%s\r\n','*ELEMENT, TYPE=B31, ELSET=tarnBenElements');
173     end
174     h = towerHeight-i;
175     y = (breddetopp/2)+i*s;
176     fprintf(fid, '%i, %f, %f, %f\r\n', j,0,y,h);
177     fprintf(fid, '%i, %f, %f, %f\r\n', j+1000,0,-y,h);
178     fprintf(fid, '%i, %f, %f, %f\r\n', j+2000,girderLength,y,h);
179     fprintf(fid, '%i, %f, %f, %f\r\n', j+3000,girderLength,-y,h);
180     if i==totthoyde
181         break
182     end
183     fprintf(fid2, '%i, %i, %i\r\n', j,j,j+1);
184     fprintf(fid2, '%i, %i, %i\r\n', j+1000,j+1000,j+1001);
185     fprintf(fid2, '%i, %i, %i\r\n', j+2000,j+2000,j+2001);
186     fprintf(fid2, '%i, %i, %i\r\n', j+3000,j+3000,j+3001);
187
188     j=j+1;
189 end
190 fid3=fopen('botTowerNodes.txt','w');
191 fprintf(fid3, '%i, %i, %i, %i\r\n', j,j+1000,j+2000,j+3000);
192 fclose(fid3); true;

```

```

193
194 k=10001;
195 fprintf(fid2, '%i, %i, %i\r\n', j+1,20000,k+N+1);
196 fprintf(fid2, '%i, %i, %i\r\n', j+1001,21000,k);
197 fprintf(fid2, '%i, %i, %i\r\n', j+2001,22000,k+2*N+1);
198 fprintf(fid2, '%i, %i, %i\r\n', j+3001,23000,k+N);
199
200 fclose(fid);true;
201 fclose(fid2);true;
202
203 fid=fopen('elTarnStiff.txt','w');
204 j=24000;
205 fprintf(fid, '%i, %i, %i\r\n', j,k,k+N+1);
206 fprintf(fid, '%i, %i, %i\r\n', j+1,k+N,k+2*N+1);%overst pa tarn
207 c=2*N+4;
208 fprintf(fid, '%i, %i, %i\r\n', j+2,20000+towerHeight-1,c+1);
209 fprintf(fid, '%i, %i, %i\r\n', j+3,21000+towerHeight-1,c);
210 fprintf(fid, '%i, %i, %i\r\n', j+4,22000+towerHeight-1,c+3);
211 fprintf(fid, '%i, %i, %i\r\n', j+5,23000+towerHeight-1,c+2);
212 fprintf(fid, '%i, %i, %i\r\n', j+6,c+1,c);
213 fprintf(fid, '%i, %i, %i\r\n', j+7,c+2,c+3);
214 j=j+6;
215 for i=20070:70:20000+70*4
216     j=j+2;
217     fprintf(fid, '%i, %i, %i\r\n', j,i,i+1000);
218     fprintf(fid, '%i, %i, %i\r\n', j+1,i+2000,i+3000);
219 end
220 fclose(fid);true;
221
222 fid=fopen('cablearea.txt','w');
223 fprintf(fid, '%f, 3.899e-2, 0, 3.899e-2, 1.20e-3 ', A_chosen);
224 fclose(fid);true;

```

Listing C.2: runMultipleAbaqus.m

```

1  %Run Multiple Abaqus
2  input='masterAbaqusScript12';
3  nodes = 139;
4
5  firstFreqList = zeros(4,3,20);
6  %girder =[ A, I_11, I_12, I_22, J, mass per length, I11, I22]
7  girder1=[0.44252, 0.44113, 0.23973, 6.3628, 1.0877, 7734, 8609, 129000];
8  girder2=[0.49860, 0.50781, 0.27691, 7.2541, 1.3028, 8179, 9133, 136145];
9  diff=girder2-girder1;
10 girder3=girder2+diff;
11 girder4=girder3+diff;
12 girder = [girder1;girder2;girder3];
13
14 t=1;
15 d=1;
16 for towerHeight = 300:20:400 %6 stk
17     final_sag=towerHeight-30;
18     d=1;
19     for dist = 7:2:13 %4 stk
20         A_chosen=generateNodes1(dist ,towerHeight ,final_sag);
21
22         fid=fopen('cablearea.txt','w');
23         fprintf(fid, '%f, 3.899e-2, 0, 3.899e-2, 1.20e-3 ', A_chosen);
24         fclose(fid);true;
25
26         for g = 1:size(girder,1) %4 stk
27
28             fid=fopen('girderInput1.txt','w');
29             fid2=fopen('girderInput2.txt','w');
30             fprintf(fid, '%f, %f, %f, %f, %f\r\n',girder(g,1:5));
31             fprintf(fid, '0,1,0 \r\n 210e9, 81e9 \r\n *BEAM ADDED INERTIA \r\n');
32             fprintf(fid, '%f, 0,0,0, %f, %f \r\n',girder(g,6:7));
33             fprintf(fid2, '%f, %f, -%f, %f, %f\r\n',girder(g,1:5));
34             fprintf(fid2, '0,1,0 \r\n 210e9, 81e9 \r\n *BEAM ADDED INERTIA \r\n');
35             fprintf(fid2, '%f, 0,0,0, %f, %f \r\n',girder(g,6:7));
36             fclose(fid);true;
37             fclose(fid2);true;
38             fid=fopen('girderWeight.txt','w');
39             fprintf(fid, 'midtnoder, 3, -%f\r\n',(girder(g,6)*10*20*2));
40             fclose(fid);true;
41             fid=fopen('girderWeightMod.txt','w');
42             fprintf(fid, 'midtnoder, 3, %f\r\n',(-girder(g,6)*10*20*2+125310));
43             fclose(fid);true;
44
45             NodeNumberString=['d' num2str(d, '%02d') 't' num2str(t, '%02d') 'g' num2str(g, '%02d')];
46             JobName=['parametric' NodeNumberString]
47
48             system(['abaqus job=' JobName ' input=' input ' interactive' ' cpus=4'])

```

```
49
50     [Eigenvectors , Eigenvalues]=read_ABAQUS_dat([JobName ' .dat' ], nodes);
51
52     for l =1:20 %de 20 frste frekvensene
53         if g==1
54             firstFreqList1(d,t,l) = Eigenvalues(1,4);
55         elseif g==2
56             firstFreqList2(d,t,l) = Eigenvalues(1,4);
57         elseif g==3
58             firstFreqList3(d,t,l) = Eigenvalues(1,4);
59         elseif g==4
60             firstFreqList4(d,t,l) = Eigenvalues(1,4);
61         end
62     end
63
64     movefile([JobName ' .dat' ],[cd '\parametricDAT' ]);
65     movefile([JobName ' .odb' ],[cd '\parametricODB' ]);
66     delete([JobName ' .stt' ]);
67
68
69     end
70     d=d+1;
71 end
72 t=t+1;
73 end
```